CELLULAR PROTECTION AND TOLERANCE MECHANISMS TO HEAT AND DROUGHT STRESS IN *TRITICUM AESTIVUM*

By

KATHLEEN F. HICKEY

A dissertation submitted in partial fulfilment of
the requirement for the degree of

DOCTOR OF PHILOSOPHY

WASHINGTON STATE UNIVERISTY
Program in Molecular Plant Sciences

DECEMBER 2023

To the Faculty of Washington State University:

The members of the Committee appointed to examine the dissertation of KATHLEEN F. HICKEY find it satisfactory and recommend that it be accepted.

Andrei Smertenko, Ph.D., Chair

Asaph Cousins, Ph.D.

Helmut Kirchhoff, Ph.D.

Karen Sanguinet, Ph.D.

ACKNOWLEDGMENT

I would like to acknowledge my advisor and mentor Andrei Smertenko for his guidance and patience. I am extremely grateful for your guidance and encouragement. I would like to extend my appreciation to my committee members for their advice, constrictive feedback, and for being admirable scientists. This endeavor would not have been possible without the support of the Smertenko lab and of my fellow Molecular Plant Science students. Lastly, I am deeply thankful to my family and friends for their steadfast support and encouragement throughout my Ph.D. And to my father, I am finally out of “college”. I offer my sincerest gratitude to those mentioned above for greatly impacting my growth as a scientist and my personal growth. Thank you to all who have made an impact of my 9 years Pullman.

CELLULAR PROTECTION AND TOLERANCE MECHANISMS TO HEAT AND DROUGHT STRESS IN *TRITICUM AESTIVUM*

Abstract

by Kathleen F. Hickey, Ph.D.
Washington State University
December 2023

Chair: Andrei Smertenko

This dissertation is dedicated to understanding cellular protection mechanism of heat and drought stress resiliency in *Triticum aestivum*. Cellular protection mechanisms include maintaining ROS homeostasis through scavenging ROS and using autophagy to degrade damaged cellular components, were investigated as an adaptive drought and heat tolerance strategy in wheat. Cellular protection mechanisms are underutilized traits in breeding programs due to the complexity of cellular dynamics. Therefore, the development of techniques to phenotype different aspects of cellular protection would impact breeding for heat and drought resiliency. In this dissertation: (1) the growth and development of genetically different wheat varieties through flowering time, root architecture, and yield under drought stress were compared; (2) photosynthetic parameters and ROS homeostasis activity under drought was examined; (3) molecular markers for ROS homeostasis and regulators of peroxisome proliferation were identified; and (4) molecular markers of autophagy were development and characterized, and autophagy under heat and drought was phenotyped in a wheat diversity population. *PEX11C*, *CAT2*, ATG8, ATG7, and NBR1 were identified as

molecular markers for ROS homeostasis and autophagy in wheat. These markers can be used to facilitate breeding heat and drought resilient wheat varieties.

TABLE OF CONTENTS

Page

LIST OF TABLES

Page

LIST OF FIGURES

Page

LIST OF ABBREVIATIONS

Abbreviation	Definition
APX	Ascorbate peroxidase
ATG	AuTophaGy genes and proteins
Autophagy	Refers to macroautophagy
CAT	Catalase
CIMMYT	International Maize and Wheat Improvement Center
CO-A1	CONSTANS A1
DRP	Dynamin-related proteins
FIS	Fission proteins
F_v/F_m	Fluorescence quantum yield
GPX	Guaiacol peroxidase
GS2	Glutamine synthetase 2
GWAS	Genomic-wide association studies
IWGSC	International Wheat Genome Sequencing Consortium
LDRC	Landrace
N-BODIPY	Nitro-BODIPY
NAC	NAM (for no apical meristem), ATAF1 and −2, and CUC2 (for cup-shaped cotyledon) transcription factor family
NAM	Nested-associated mapping
NBR1	NEIGHBOR OF BRCA1
NPQ	Non-photochemical quenching
PEX	Peroxin proteins
PCA	Principle component analysis
PSII	Photosystem II
PSI	Photosystem I
ϕ_{PSII}	Quantum yield of photosystem II photochemistry
ϕ_{PSI}	Quantum yield of photosystem I photochemistry
QA	Primary quinone acceptor (of PSII)
qE	Energy dependent quenching
qI	Photoinhibition
qL	Fraction of open PSII centers
QTL	Quantitative trait loci
ROS	Reactive oxygen species
SOD	Superoxide dismutase
VWC	Volumetric water content
ZIM	Zinc-finger protein expressed in Inflorescence *M*eristem transcription factor family

DEDICATION

Grandma Jo Ann Erickson and Grandpa Kenneth Erickson, Ph.D.

THESIS SUMMARY

This dissertation is dedicated to understanding cellular protection mechanism of abiotic stress resiliency in wheat, *Triticum aestivum.* determining how ROS homeostasis functions as adaptive drought and heat tolerance mechanisms in wheat. ROS production and scavenging was measured in relation to peroxisome dynamics and known physiological mechanisms including photoprotection and autophagy. During this research, molecular markers for ROS homeostasis and autophagy were identified. This study includes the following: (1) To compare the growth and development of genetically different wheat varieties through flowering time and root architecture; (2) To analyse photosynthetic and ROS activity under drought; (3) To identify molecular markers for ROS homeostasis and regulators of peroxisome proliferation; and (4) To analyse autophagy under heat and drought and identify molecular markers of autophagy.

Following the introduction in chapter 1, methods and plant growth conditions are explained in chapter 2. Plant material used for all experiments will be spring wheat varieties or lines from a nested association mapping population, which were provided to this study from the WSU Spring Wheat Breeding Program and by Prof Michael Pumphrey. Techniques used in this research include molecular, biochemical, bioanalytical, and immunology. Chapter 2 will include details about techniques used to measure physiological and morphological difference including root architecture and photosynthesis. This provided information to study many different aspects of stress responses in wheat.

Chapter 3 descriptions the experimental design to monitor root architecture in wheat under drought stress. This chapter included detained description of differences in growth and development between wheat varieties, in addition to effects of drought stress. Classical drought strategies including drought escape and drought avoidance were seen in varieties. A portion of this work was published in *Hickey et al. 2022*.

Chapter 4 describes phenotyping photosynthesis through chlorophyll fluorescence and subsequently measuring ROS scavengers to understand the metabolic modification under drought. 17 varieties were screened for photosynthetic efficiency under drought, and 5 varieties were selected for detailed ROS scavenger characterization. Additionally, 2 varieties with different photosynthetic efficiency, were analysed for PSI kinetics revealing that one sustained oxidative damage to the photosystems. Temporal differences in ROS scavenging and peroxisome abundance between the varieties were found. A portion of this work was published in *Hickey et al. 2022*.

Chapter 5 builds upon chapter 4 through evaluating different genetic regulators of ROS homeostasis and peroxisome proliferation. The ROS scavenging enzyme catalase was characterized by measuring gene transcription. The production and use of a catalase antibody for wheat is also discussed. Genes known to be involved in peroxisome proliferation were measured. This chapter examines the progress made to identify transcriptional regulators of catalase and peroxisome proliferation gene *PEX11-C*. A portion of this work was published in *Hickey et al. 2022*.

Chapter 6 explores the cellular recycling protection mechanism of autophagy. The production of 3 wheat specific autophagy related antibodies is discussed.

Phenotyping autophagy under heat and drought in a wheat diversity population was done and discovered that ATG8 gene expression positively correlates with yield. Identification of 3 molecular markers for autophagy activity was discovered.

Chapter 7 concludes discoveries regarding ROS homeostasis, peroxisome abundance, autophagy, and heat and drought tolerance in wheat. Heat and drought tolerance mechanisms were phenotyped in wheat using molecular, biochemical, physiological, and morphological techniques.

During this dissertation, 3 manuscripts were published:

FIRST AUTHOR PUBLICATION: Hickey, K., Wood, M., Sexton, T., Sahin, Y., Nazarov, T., Fisher, J., Sanguinet, K. A., Cousins, A., Kirchhoff, H., & Smertenko, A. 2022. *Drought Tolerance Strategies and Autophagy in Resilient Wheat Genotypes.* Cells, 11(11), 1765. https://doi.org/10.3390/cells11111765

CO-FIRST AUTHOR PUBLICATION: Hickey, K., Nazarov T., and Smertenko, A. 2023. "*Organellomic Gradients in the Fourth Dimension*." Plant Physiology 193 (1): 98–111. https://doi.org/10.1093/plphys/kiad310

FIRST AUTHOR PUBLICATION: Hickey, K., Sahin, Y., Turner, G., Nazarov, T., Jitkov, V., Pumphrey, M., Smertenko, A. 2023. *Genotype-Specific Activation of Autophagy during Heat Wave in Wheat*. Submitted to Cells.

CHAPTER ONE: INTRODUCTION

Section 1: Wheat Production and Breeding for Stress Tolerance

Wheat is one of the most important crops globally. Wheat, *Triticum aestivum,* is an essential source of protein and calories in our diet (Wheat Initiative, 2013). The domestication of wheat in a Mediterranean environment made the crop well-adapted to dryland environments and provides a potential resource for heat and drought tolerance (Araus et al. 2006). In the US, 93% of wheat is grown without irrigation, using dryland systems that relies on moisture acclimations in the soil throughout the year (*USDA ERS,* 2018). While domestication of wheat resulted in the selection of varieties for arid climates (Araus et al. 2006), recent extreme weather patterns have exposed the vulnerability of dryland farming to drought. Dryland farms are particularly vulnerable to high temperatures and drought. For example, productivity of wheat farms in Washington state dropped by 30-60% due to 30% lower precipitation in 2014 and 2015 (Washington Association of Wheat Growers, 2018).

Climate change will bring higher temperatures, changes to weather patterns, and more extreme weather events which affect plant growth and plant production (ICPP, 2022). Current climate change trends predict drought to be one of the key limiting factors for wheat production globally (Leng & Hall, 2019; NASA Global Climate Change, 2019.). In addition, drought stress often occurs in combination to other stresses including heat and disease, which can exacerbate the yield loss (Zandalinas et al. 2021; Zhao et al. 2017). Breeding heat and drought tolerant varieties is essential to ensure food security.

Complex drought and heat tolerance traits are challenging to breed for**.** Drought and heat tolerance, in terms of maintaining yield, remains an elusive trait, even with the advancement of physiological and genomic breeding. This is due to quantitative genetic control with many small-contributing loci, inconsistent quantitative trait loci (QTL), strong genotype x environment interactions, and low heritability (Sallam et al. 2019; Tricker et al. 2018). Availability of the wheat genome sequencing data, QTL-mapping and genomic-wide association studies (GWAS) can identify and map candidate genes to be used as breeding markers with greater precision (Bilgrami et al. 2020; International Wheat Genome Sequencing Consortium (IWGSC), 2014; Juliana et al. 2021; Verma et al. 2020). Expanding the list of genetic markers for physiological, morphological, and molecular survival mechanisms is essential for breeding drought resilient varieties.

With large and repetitive genome size occurring through multiple hybridization steps, allohexaploid *Triticum aestivum* (2n=6x=AABBDD) is the species that accounts for 95% of the wheat grown worldwide (International Wheat Genome Sequencing Consortium (IWGSC) et al. 2018). The genome structure and size has made it difficult

to use modern genetic and molecule techniques for breeding impeding variety improvement. In 2014, the first sequence for wheat came out mapping chromosome 3B (International Wheat Genome Sequencing Consortium (IWGSC), 2014). In 2018, the International Wheat Genome Sequencing Consortium released an annotated and ordered reference sequence of wheat making it possible to access sequence-level information in the genome impacting breeding efforts (International Wheat Genome Sequencing Consortium (IWGSC) et al. 2018).

However, breeding efficiency relies on genetic diversity. CIMMYT and other international germplasms collections contain approximately 850,000 accessions of *Triticum* species, as well as wild wheat relatives ("Wheat Improvement," 2022). This germplasm provides an excellent source of novel drought tolerance genes for introgression into elite breeding lines, providing new sources for stress tolerance, yield potential, among others (Singh et al. 2018). As behavior of quantitative trait loci could be inconsistent across different environments, identification of robust genetic markers requires mapping populations with high genetic diversity such as wild relatives and landraces (Dempewolf et al. 2017; Sukumaran et al. 2018).

The advancement of genomic sequencing, QTL-mapping, genome-wide associations, and global databases with this information facilitate the mining of tolerance traits (Wen et al. 2017; Blake et al. 2019). The use of nested-associated mapping (NAM) populations aids in breeding efforts by combining the linkage analysis and GWAS to discover novel QTLs and genetic makers that could be used as targets for ingression into elite cultivars (Yu et al. 2007; Kitony, J.K, 2023). Successful identification of the targets relies on sensitive phenotyping tools for the stress resistance

traits. Development of such tools requires information about plant responses to stress on molecular, cellular, organ, and whole-plant levels.

Section 2: Drought and Heat Stress

There are three universal mechanisms of drought survival in plants (Basu et al. 2016). The first is escaping drought by accelerating time to flower (Shavrukov et al. 2017). The second mechanism is drought avoidance via water-use efficiency or increasing soil moisture access through a larger root or stomata closure to reduce transpiration (Basu et al. 2016). The third mechanism is drought tolerance, which focuses on withstanding dehydration through the production of protective molecules (Fang & Xiong, 2015) like preventing accumulation of reactive oxygen species (ROS) and the oxidative damage (Foyer & Noctor, 2016; Voss et al. 2013).

Plants have two types of mechanisms to withstand heat stress: short-term avoidance or long-term tolerance (Yadav et al. 2022). Short-term heat avoidance mechanisms include leaf orientation, leaf rolling, and changes in lipid composition (Higashi et al. 2015; Shiva et al. 2020; Xiang & Rathinasabapathi, 2022). Long-term heat tolerance mechanism prevents extensive damage and include activation of ROS scavenging and stress responsive proteins (Choudhury et al. 2017; J. Zhao et al. 2020).

Section 3: Consequences of drought and heat on wheat plants.

Both heat and drought stress cause morphological, physiological, and biochemical changes. Drought stress causes reduction of plant growth and smaller leaf area. One of the most common drought responses in plants is reducing transpiration

through stomatal closure. Although stomata closure conserves water, the CO_2 uptake becomes reduced leading to inhibition of the photosynthesis and increase in photorespiration, ultimately, yield loss (Reddy et al. 2004; Z. Wang et al. 2018). Heat stress can also lead to inhibition of photosynthesis through chlorophyll biosynthesis and ultrastructure changes (Anderson et al. 2021; Hu et al. 2020). Heat stress decreases the stability of proteins, membranes, and other cellular components and will inactive enzymes essential to cellular function (Akter & Rafiqul Islam, 2017; Fahad et al. 2017; Hasanuzzaman et al. 2013). Wheat is extremely susceptible to heat stress during anthesis, when the cereal is most likely to encounter it, and can cause floret sterility, decrease pollen variability, and reduce grain size (Jacott & Boden, 2020; Stone & Nicolas, 1994).

Drought and heat stress frequently occur simultaneously compounding the impact and damage. Commonly, heat and drought intensify the production of reactive oxygen species (ROS) causing oxidative stress (Caverzan et al. 2016; Miller et al. 2010; Mittler, 2017), which damage proteins, DNA, lipids, RNA, causing cell death and ultimately contributing to overall loss of plant productivity and yield (Demidchik, 2015; Fahad et al. 2017; Møller et al. 2007; Sharma et al. 2012; Waszczak et al. 2018).

Section 4: Reactive Oxygen Species

Reactive oxygen species production. ROS are a product of chemical reactions under normal environmental conditions (Held, 2015; Huang et al. 2019; Voss et al. 2013; Waszczak et al. 2018b), the production of ROS increases under stress (Caverzan et al. 2016; Miller et al. 2010; Mittler, 2017). The main ROS are singlet oxygen ($^1O_2$),

superoxide radical ($O_2^{\cdot -}$), hydroxyl radical ($HO^{\cdot}$), and hydrogen peroxide (H_2O_2). Accumulation of ROS causes oxidative damage to key biological molecules including nucleic acids, lipids, and proteins (Demidchik, 2015; Møller et al. 2007; Waszczak et al. 2018) collectively known as oxidative stress. Oxidative stress compromises stress recovery and can trigger cell death (Choudhury et al. 2017; Demidchik, 2015; Mittler, 2002; You & Chan, 2015). As such, oxidative damage contributes to the overall loss of plant productivity under all stresses including drought (Fahad et al. 2017; Sharma et al. 2012).

Section 5: ROS as signalling molecules.

Increased ROS levels often serve as initiation signals for multiple long distance signalling pathways involved in stress responses and adaptations (Choudhury et al. 2017; Huang et al. 2019; Mittler et al. 2022). ROS, mainly hydrogen peroxide, causes retrograde signalling into nucleus leading to altered gene expression under stress (Exposito-Rodriguez et al. 2017; Maruta et al. 2012). Hydrogen peroxide has been shown to produce spatial specific signals in *Arabidopsis thaliana*. *Sewelam et al. 2014*, showed how *Arabidopsis* can integrate hydrogen peroxide signals from peroxisome and chloroplasts to produce different cellular responses: hydrogen peroxide from the peroxisome induces transcriptions involved in protein repair responses; while chloroplast derived hydrogen peroxide induced early signalling responses, including genes for defence and detoxification (Sewelam et al. 2014). The type of ROS can also influence gene-expression changes, as shown in *Arabidopsis* having singlet oxygen and hydrogen peroxide specific gene-expression changes (op den Camp, 2003). ROS can

initiate programmed cell death through signalling cascades if ROS accumulate (Petrov et al. 2015; Ye et al. 2021). Cellular response to ROS are shown to be derived based on the type, duration and dose of ROS signal, and the site of ROS generation.

One of the main sources of ROS under drought and high temperature is the excess of captured light energy that is not utilized for carbon dioxide fixation. Singlet oxygen can be generated by photosystem II (PSII) due to inefficient energy transfer between chlorophyll and PSII (Foyer & Shigeoka, 2011; op den Camp, 2003; Wagner, 2004; You & Chan, 2015). Superoxide anion radical and hydrogen peroxide can both be generated by the chloroplast electron transport chain (ETC). Superoxide radical can also be generated at multiple sites including photosystem I (PSI) and PSII. Hydrogen peroxide is predominantly produced during photosynthesis and photorespiration (Ślesak et al. 2007; Smirnoff & Arnaud, 2019) of which very high rates are in the peroxisome (Foyer & Noctor, 2003; Smirnoff & Arnaud, 2019).

ROS are scavenged and detoxified. Plants prevent oxidative stress and ROS accumulation using enzymatic ROS scavengers and non-enzymatic antioxidants (Das & Roychoudhury, 2014; Mittler, 2017b; Sharma et al. 2012). Each cellular compartment has a specific set of ROS scavengers (Mignolet-Spruyt et al. 2016; Mittler, 2017; Smirnoff & Arnaud, 2019. Amongst the most common enzymatic scavengers are superoxide dismutase (SOD), catalase (CAT), and peroxidases (Demidchik, 2015; Mhamdi et al., 2012; Sharma et al., 2012; Sofo et al. 2015). The antioxidants group includes carotenoids, tocopherols, flavonoids, polyamides, proline, monosaccharides, ascorbate, and glutathione, amongst others (Agati et al. 2012; Caverzan et al. 2016;

Das & Roychoudhury, 2014; Demidchik, 2015; Hasanuzzaman et al. 2019; Ślesak et al., 2007; Waszczak et al. 2018).

Many studies demonstrate that activity of the ROS scavenging system increases in response to environmental stresses. Superoxide dismutase, catalase, ascorbate peroxidase and glutathione reductase become more active under drought stressed in wheat (Caverzan et al. 2016; Nikolaeva et al. 2010; Tyagi et al. 2021; Wang et al. 2008). Enzymes of the Ascorbate-Glutathione cycle become upregulated in response to drought and salinity in wheat (Hasanuzzaman et al. 2019; Lou et al. 2018; Sairam et al. 2002). Drought activates transcription and translation of genes encoding ROS scavengers including catalase and superoxide dismutase (Ford et al., 2011). Activation of ROS scavenging pathways has been shown to correlate with drought tolerance in wheat (Bowne et al. 2012; Ebeed et al. 2018; Singh et al. 2012; G. Zhang et al. 2017), sorghum (Guo et al. 2018; Nxele et al. 2017; Varoquaux et al. 2019), rice (Duan et al. 2012; Pieters & El Souki, 2005; Xiong et al. 2018; Yin et al. 2015), tomato (Zhou et al. 2019), and maize (Anjum et al. 2017; Chugh et al. 2011; Li et al. 2021; Zheng et al. 2020).

The reactive nature of ROS marks these molecules a serious threat to cell integrity (Kneeshaw et al., 2017). Phenotyping ROS scavenging on a population level remains impossible due to chemical complexity of both ROS and each scavenger (Held, 2015). Superoxide anion, hydrogen peroxide, and hydroxyl radical are produced in almost every subcellular location, therefore there is an overlap between ROS scavenging in the cell encompassing the blanket term “ROS homeostasis”. It is also challenging to due to the extremely short lifetime of many ROS species, for example

superoxide turnover rate is in the range of milliseconds. Lastly, ROS could be entwined into one biochemical pathway, e.g., superoxide is precursor to hydrogen peroxide (Smirnoff & Arnaud, 2019). For this reason, genetic markers of ROS scavenging are unavailable for utilization in breeding programs. Such markers could enable identification of drought-tolerant varieties using genome-sequencing data. This in turn will likely make breeding programs more specific, faster, and cost-efficient.

It has been shown that ROS production in peroxisomes under drought is balanced by higher activity of peroxisomal ROS-scavenging enzymes including catalase, ascorbate peroxidase, and superoxide dismutase (del Río & López-Huertas, 2016; Ebeed et al. 2018; Mhamdi et al. 2012; Sofo et al. 2015; Waszczak et al. 2018b). Peroxisome abundance increases in response to environmental stresses including light (Desai & Hu, 2000, 2008; Goto-Yamada et al. 2015; Schrader et al. 2012), ozone (Oksanen et al. 2004), salt (Fahy et al. 2017; Mitsuya et al. 2010), jasmonic acid (Castillo et al. 2008; Ulloa et al. 2002), heat (Hinojosa et al. 2019), drought (Sanad et al. 2019; Hickey et al. 2022), and heavy metals (McCarthy et al. 2001). Additionally, greater peroxisome abundance correlates negatively with yield under drought in wheat (Sanad et al. 2019) and quinoa (Hinojosa et al. 2019). Thus, maintaining steady ROS levels (robust ROS homeostasis) is an essential drought tolerance trait. Activity of ROS homeostasis could be assessed indirectly by measuring the abundance of peroxisomes (Smertenko, 2017).

Section 6: Peroxisome biogenesis and function.

The peroxisome is a small, single membrane-bound organelle. The peroxisome is considered a microbody and lacks DNA therefore peroxisomal proteins are imported (**Figure 1**). Peroxisomes can form *de novo* from the endoplasmic reticulum or proliferate though fission from existing peroxisomes (J. Hu, 2010; Hu et al. 2012; Koch et al. 2010). The fission occurs in three stages: elongation, constriction, and fission (Koch et al. 2004; Koch et al. 2010; Schrader et al. 2012). PEROXIN11 (PEX11) proteins promote the fission through peroxisome elongation-tubulation (Lingard & Trelease, 2006; Orth et al. 2007). In addition, DYNAMIN-RELATED PROTEIN3 (DRP3) and FISSION1 (FIS1) have been shown to mediate the fission of peroxisomes (Zhang & Hu, 2008, 2009, 2010). Drought (Sanad et al. 2019), heat (Hinojosa et al. 2019), salt stress (Cui et al. 2016; Fahy et al. 2017), hypoxia and biotic stresses (Li & Hu, 2015), wounding and H_2O_2 (Lopez-Huertas et al. 2000) upregulate transcription of peroxisome fission genes in wheat (Sanad et al.

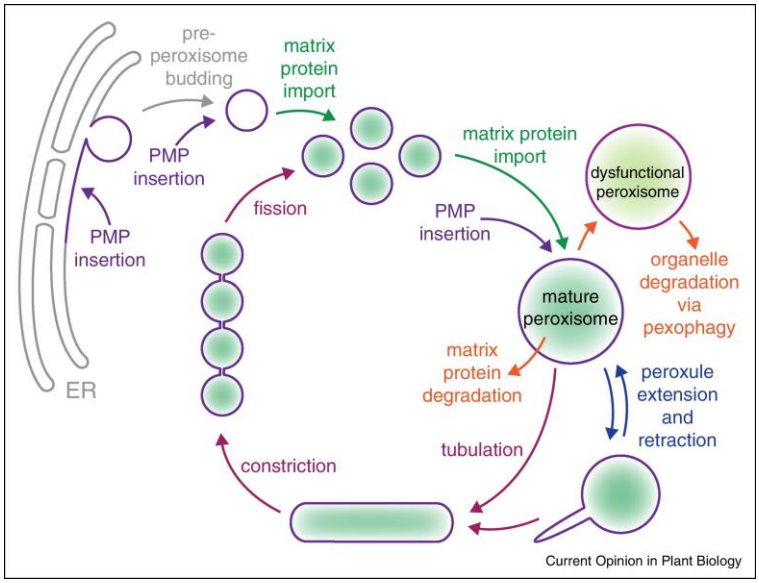

Figure 1.1: Lifecycle of peroxisome**.** Peroxisomes proliferation occurs mainly through tubulation of mature peroxisomes, constriction with the help of *PEX11* proteins and then division by fission with *DRP3* and *FIS1* proteins. Peroxisomes can form de novo from the ER by budding. Peroxisomal quality control includes degrading and eliminating dysfunctional peroxisomes via pexophagy. This figure was original published in *Reumann S, Bartel B. Plant peroxisomes: recent discoveries in functional complexity, organelle homeostasis, and morphological dynamics. Curr Opin Plant Biol. 2016 Dec;34:17-26. Copyright Elsevier.*

2019), quinoa (Hinojosa et al. 2019), and *Arabidopsis* (Cui et al. 2016; Fahy et al. 2017; Li & Hu, 2015; Lopez-Huertas et al. 2000).

Regulation of peroxisome proliferation in response to environmental stresses remains poorly understood with the exception of light pathway. The latter response is mediated through photoreceptor phytochrome A: upon far-red light exposure, phyA moves into nucleus activating transcription factor HYH (Elongated Hypocotyl 5 Homologue). HYH binds directly to Pex11 promotor and up-regulates its transcription (Desai & Hu, 2008).

The peroxisome houses a variety of catabolic and biosynthetic reaction, including reactions for the photorespiratory pathway; β-oxidization of fatty acids; synthesis of hormones auxin, jasmonic acid, and salicylic acid (Kao et al. 2018). Peroxisomes involvement in photorespiration produces large amounts of hydrogen peroxide through the oxidation of glycolate to glyoxylate. Photorespiration derived hydrogen peroxide in the peroxisome accounts for majority of the hydrogen peroxide produced in cells (Queval et al. 2007; Smirnoff & Arnaud, 2019). Because of this, peroxisomes contain ROS-scavenging enzymes including catalase, ascorbate peroxidase, and superoxide dismutase (Waszczak et al. 2018).

Catalase is a key regulator of ROS homeostasis in plant cells. Peroxisomal catalase is a principal ROS-scavenging enzymes in photosynthetic cells. There are three classes of catalase: class I is mainly present in photosynthetic tissues, and its regulation is light dependent; class II is found in the vascular tissues; and class III occurs in young seedlings and reproductive tissues (Tyagi et al. 2021). Catalase is vital

for protecting cells against oxidative damage as it turns hydrogen peroxide into water and oxygen with a high turnover rate (Singh et al. 2018).

ROS accumulation and damaged catalase has been linked to a peroxisome specific type of autophagy, pexophagy (Shibata et al. 2013; Yoshimoto et al. 2014). *Hackenberg et al. 2013* also found a link between ROS, catalase, autophagy, and programmed cell death during plant immunity using *Arabidopsis* knockout mutants *NO CATALASE ACTIVITY 1* and *cat2* (Hackenberg et al. 2013). Catalase function in regulating ROS homeostasis during normal metabolism and under adverse environmental conditions is essential.

During development, peroxisome transition from containing primary enzymes for glyoxylate cycle and β-oxidation to peroxisome containing photorespiration machinery. Peroxisomal protease LON2 plays an important role in the selective degradation of peroxisomal-matrix proteins during the metabolic transition (Lingard and Bartel, 2009; Farmer et al..2013). LON2 is important for the maintenance of peroxisome proteins (Goto-Yamada et al. 2014). LON2 has been shown to inhibit pexophagy, as LON2 deficiency cases enhanced peroxisome degradation by autophagy (Goto-Yamada et al. 2014; Young and Bartel, 2016).

Section 7: Development of method to measure peroxisome abundance with peroxisome-specific fluorescent probe N-BODIPY.

Quantifying the number of peroxisomes in a cell is laborious and technically challenging. Peroxisomes can be detected with electron microscopy, immunocytochemistry with peroxisomal protein antibodies, and live cell imaging with

fluorescent fusion proteins of peroxisome-targeting signal protein. Counting peroxisomes by live-cell imaging is complicated by the fast and constant movement of peroxisomes. These techniques, in addition to being time and resource consuming, can only measure peroxisomes in a limited number of cells and cannot be used in a high-throughput manner. To overcome these limitations, a technique was developed using the small fluorescence dye Nitro-BODIPY (N-BODIPY) that specifically label plant peroxisomes *in vivo* (Landrum et al. 2010). This allows for fluorescence microscopy to be used to image peroxisomes. Additionally, this fluorescence dye was used to develop a technique to quantify peroxisomes in total cell extracts using spectrofluorimetry.

N-BODIPY was first shown to quantify the relative peroxisome abundance in intact tobacco BY-2 suspension cells (**Figure 2A**; Fahy et al. 2017). BY-2 cells were treated with N-BODIPY and imaged using excitation at 488nm and collecting the emitted light at 530nm. Total cell extracts from the BY-2 cells gave an identical emission spectrum. Water did not produce a detectable fluorescence signal when incubated with N-BODIPY. Using total protein extracts from Arabidopsis, the same fluorescence signal was found (**Figure 2B**). This demonstrated that N-BODIPY is activated by the presence of peroxisome in both living cells and total protein extracts. Furthermore, the fluorescence intensity of N-BODIPY was proportional to the amount of total protein in the reaction, meaning that fluorescence values reflected the

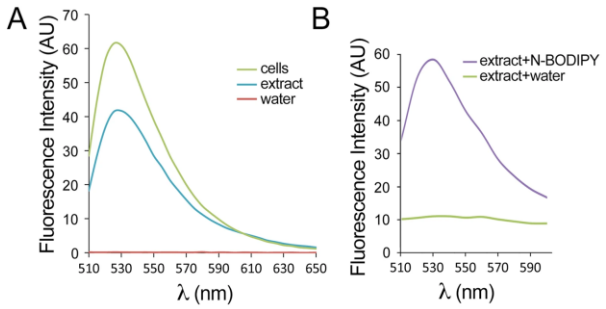

Figure 1.2: N-BODIPY Fluorescence Activation. **A,** Representative chart showing emission spectra of 5 μM N-BODIPY incubated with: i. BY-2 cells (green); ii. total BY-2 protein extracts in water (blue); iii. water (red) at the excitation wavelength 490 nm. **B** Representative chart showing emission spectra of total protein extract from Arabidopsis tissue culture cells incubated with 5 μM N-BODIPY (violet) or with water (green) at 490 nm excitation. This figure was original published in *Fahy et al. 2017*, *Scientific Reports*. *Copyright Springer Nature.*

quantity of peroxisomes in the protein extracts. N-BODIPY does not produce fluorescence until the probe binds yet unidentified peroxisomal protein. The technique was then optimized for high-throughput analysis using 96-well plate format. In addition to *Arabidopsis,* N-BODIPY has been successfully used to measure peroxisome abundance in *Brachypodium distachyon,* rice, *Setaria viridis*, quinoa, grapes, and wheat.

Section 8: Autophagy

Autophagy is an essential regulator of cellular homeostasis. Under environmental stress conditions, the increase of ROS causes damage to cellular components, which triggers a process to degrade and recycle these dysfunctional components called autophagy. Autophagy occurs at basal levels during normal plant growth and development, although is upregulated in response to multiple stresses including oxidative stress/hydrogen peroxide/Methyl viologen (Shin et al. 2009; Xiong et al. 2007); nutrient deficiencies and starvation (Xiong et al. 2005; Guiboileau, et al. 2012; Merkulova et al. 2014); salinity (Lui et al., 2009; Shin et al., 2009); hypoxia (Lin et al. 2021); drought (Bao et al. 2020; Kuzuoglu-Ozturk et al. 2012; Liu et al. 2009; Sun et al. 2018; Wang et al. 2015; Yang et al. 2021); and heat (Zhai et al. 2016; Zhou et al. 2014).

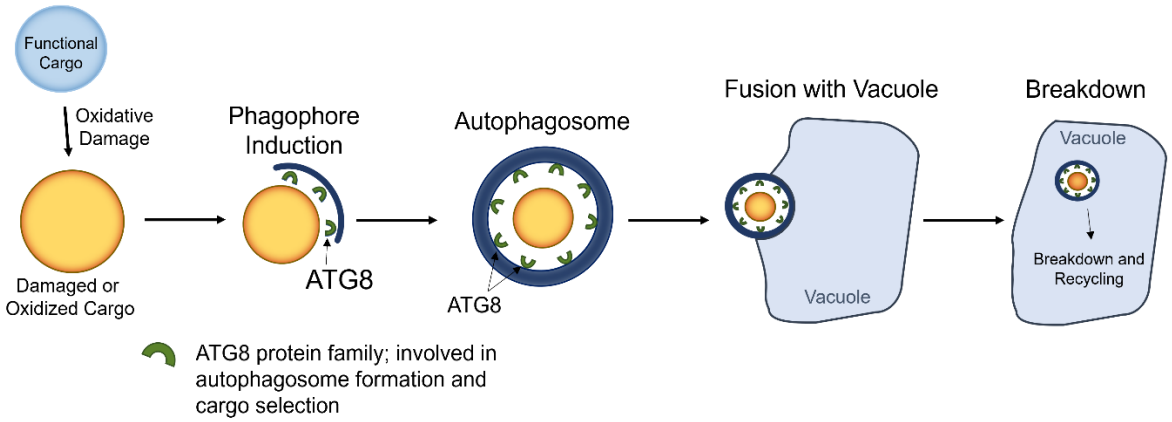

Figure 1.3: Autophagosome and Autophagy Pathway. Upon induction of autophagy, a double-membrane structure called an autophagosome forms around a portion of the cytoplasm (cargo). The autophagosome then transports the cargo to the vacuole. During the fusion process, the outer autophagosome membrane fuses with the vacuole membrane, and the remaining single-membrane structure (termed an autophagic body) is delivered inside the vacuole. The autophagic bodies are then broken down by vacuolar hydrolases, and the products are exported from the vacuole to the cytoplasm for reuse.

Cells can ameliorate the impact of oxidative damage by recycling the damaged cellular components through a highly conserved mechanism called macroautophagy (hereafter referred to as autophagy). Autophagy occurs via the formation of a double membrane vesical on the endoplasmic reticulum, called the autophagosome, which encloses cytoplasmic components and then is trafficked to the vacuole (**Figure 3**; Liu and Bassham, 2012). The autophagy pathway and machinery was first identified in yeast (Matsuura et al. 1997), and several plant orthologs of AuTophaGy (ATG) genes have been identified. There are over 40 autophagy-related genes in Arabidopsis, and 108 putative genes in bread wheat (Yue et al. 2018). Components of the autophagy machinery could be classified into clusters based on their functions: (1) the ATG1-ATG13 kinase complex initiates the formation of autophagosome precursor, phagophore; (2) ATG9, ATG2, and ATG18 mediate lipids delivery for expanding the phagophore; (3) the phosphatidylinositol 3-kinase complex drives vesicle nucleation, autophagosome formation, and trafficking to vacuole; (4) ATG8 covalently bond to

phosphatidylethanolamine (PE) contributes to phagophore membrane expansion and cargo recruitment; (5) ATG5-ATG12-ATG16 complex together with ATG4, ATG7, and ATG3 catalyze conjugation of ATG8 to phosphatidylethanolamine; and (6) ATG10 and ATG7 contribute to assembly of ATG5-ATG12-ATG16 complex (reviewed by Liu and Basshasm, 2012; Marshall and Vierstra, 2018; Liu et al. 2020).

Autophagy is an essential regulator of cellular homeostasis (Marshall and Vierstra, 2018). Previous research has shown that autophagy increases tolerance to oxidative stress/H2O2/Methyl viologen (Xiong et al. 2007; Shin et al. 2009); nutrient deficiencies and starvation (Xiong et al. 2005; Guiboileau et al. 2012; Merkulova et al. 2014); salinity (Liu, Xiong, Bassham, 2009; Shin et al. 2009); hypoxia (Lin et al. 2021); drought (Liu, Xiong, Bassham, 2009; Sun et al. 2018; Bao et al. 2020; Kuzuoglu-Ozturk et al. 2021; Wang et al. 2015; Sun et al. 2018; Yang et al. 2021); and heat (Zhou et al. 2014; Zhai et al. 2016; Zhang et al. 2021). Overexpression of *ATG8* has been shown to increase yield under low nitrogen conditions in Arabidopsis (Chen et al. 2019). Overexpression of *ATG5* and *ATG7* was shown to increase ATG8 lipidation and autophagic activity, leading to greater resistance to pathogens and oxidative stress in Arabidopsis (Minina et al. 2018). Hence, autophagy pathway appears to be an important breeding target for increasing plant stress resistance.

Amongst potential autophagy markers, ATG8 is frequently used to assess the overall activity and track specific stages of the autophagy pathway from the beginning of phagophore formation to the final degradation steps in the vacuole (**Figure 3**; Bassham, D., 2014). ATG8 provides a selective docking platform for autophagy receptors and adapters. Such adapters were identified for plastids (Michaeli et al. 2014; Ishida et al.

2008) and 26S proteasomes (Marshall et al. 2015). Evidence for selective autophagy in plants has been shown for ER (Lui et al. 2012) and peroxisome (Xie et al. 2016; Oikawa et al. 2022).

NBR1 (NEIGHBOR OF BRCA1; also known as *Joka2* in tobacco; Zientara-Rytter et al. 2011) was the first selective autophagy receptor in plants identified through domain organization and homology of two mammalian autophagic adapters p26/SQSTM1 and NBR1 (Svenning et al. 2011). NBR1 plays a role in clearing stress-induced protein aggregates (aggrephagy) and implicated in responses to multiple stresses including heat, drought, and salinity (Zhou et al. 2013; Zhou et al. 2014; Jung et al. 2020). Additionally, *Arabidopsis nbr1* mutants have been shown to accumulate toxic protein aggregates and be hypersensitive to heat, drought, oxidative, and salt stress and (Zhou et al. 2013). NBR1 contributes to stress tolerance through two mechanisms: (i) the recognition and sorting of toxic protein aggregates and (ii) the negative regulation of heat stress memory by mediating the clearance of heat shock related chaperones (Zhou et al. 2013; Zhou et al. 2014; Thirumalaikurmar et al. 2021). Recently, *Arabidopsis* NBR1 was found to function as a microautophagy receptor for photodamaged chloroplasts exposed to high light independently of the ATG7-ATG8 pathway (Lee et al. 2023). Expression level of wheat *TaNBR1* was shown to be induced by drought stress (Chen et al. 2022). Thus, autophagy receptors can be used as markers for isolation of genotypes with more efficient autophagy and identification of corresponding genetic markers.

Peroxisome specific pexophagy autophagy protects cells from ROS derived oxidative damages. Another process that controls peroxisome abundance is

pexophagy**.** Pexophagy is a specific type of autophagy that is responsible for degrading damaged or oxidized peroxisomes (Farmer et al. 2013; Shibata et al. 2013; Young & Bartel, 2016). Autophagy could also contribute to drought tolerance (Bao et al. 2020; Liu et al. 2009; Sun et al. 2018). ATG8 proteins are used as a general marker of autophagy and ATG8 has been implicated in pexophagy (Calero-Muñoz et al., 2019; Shibata et al., 2013).

Recently, the mechanism of pexophagy in Arabidopsis under high light stress was elucidated. *Oikawa et al. 2022*, reports that under light, peroxisomes accumulate ROS, impairing catalase function causing the initiation of selective pexophagy through ATG18 recognition of phosphatidylinositol 3-phosphate on the peroxisome membrane. This causes the classical autophagosome formation pathway and trafficking damaged peroxisome to the vacuole for degradation. However, it remains not clear how ROS generated in the peroxisome matrix induce pexophagy. In yeasts and mammalian systems, pexophagy mechanisms have been demonstrated. Sensor proteins on the peroxisomal membranes recognize ROS accumulation in the peroxisome matrix inducing pexophagy, although orthologs to these proteins have not been identified in plants. It has been postulated that oxidized lipids on the peroxisome membrane may induce pexophagy by functioning as a marker of oxidized peroxisome (Oikawa et al. 2022). Although the exact mechanism of ROS oxidized pexophagy is not fully elucidated, pexophagy is an important mechanism for ameliorating oxidative damage.

CHAPTER 2: EXPERIMENTAL METHODS AND PROCEDURES

Section 1: Plant Growth Conditions

Plants were grown until a specific Zadoks stage in greenhouse, growth chamber, or in field conditions as specified for each experiment below (Zadoks, Chang & Konzak 1974). Drought stress was induced by withholding watering for greenhouse and growth chamber experiments. The volumetric water content (VWC) was measured using ProCheck Soil Moisture Probe with 5TC probe (Decagon now METER environment, Pullman, WA, USA) or HH2 Soil Moisture Meter (Delta-T Devices, Cambridge, UK). Once soil moisture reached below 0.2%, plant material was collected for biochemical assays. Statistical analysis was done using Student T-tests and ANOVA.

The growth conditions following were used for the experiments in Chapter 3. The greenhouse growth conditions were 60% humidity, 16/8hr light/dark cycle, 22°C during the day and 18°C at night. Seeds were germinated on peat plugs for 2 weeks. The seedlings were planted together with the peat plugs into 55 gallons U-line bins filled with Sungro6 peat moss potting soil and watered daily. This type of soil provides the best contrast for root imaging. Fertilizer was not used. The position of bins in the greenhouse

was randomized. Each bin contained one root imaging tube and two soil moisture probe tubes. Each bin was populated with five seedlings of the same genotype. Five bins were setup per each genotype: 2 well-watered controls and 3 drought treatments. The bins were watered for 1 week following transplanting the seedlings and then watering of the drought-stress bins was stopped.

The growth conditions following were used for the experiments in Chapter 4 and Chapter 5. The dynamic impact of drought on photosynthesis was measured in the Phenomics Facility at Washington State University. Seeds were germinated on peat plugs for 2 weeks and then transplanted into 54x38 cm trays filled with Sungro6 Sunshine Mix #1. Five trays were used for drought treatment and two trays were used as watered control. Position of the trays was randomized. Each tray destined for drought stress was populated with 15 seedlings and each watered control trays were populated with 35 seedlings. Seedlings were acclimated in the phenomics chamber for 5 days with daily watering,16/8hr light/dark cycle, 22°C during the day and 18°C at night, 60% humidity, and artificial illumination ~470 µmol/m^2/s. The VWC in soil was measured using Decagon Devices Em-50 soil moisture data-logger probes (Pullman WA). One soil moisture probe connected to a data-logger was used per each tray. Soil volumetric water content values were logged every 6 hours. Drought was induced by withholding watering after seedlings were acclimated in the phenomics chamber for five days. Every day of the drought stress treatment, leaf material was collected from one plant per each drought stress tray making 5 biological replicates per genotype and five randomly selected plants from the watered control. The bottom third part of each leaf

was flash-frozen in liquid nitrogen and stored at -80°C for biochemical assays. The rest of the plant was cut at the below-ground level using scissors and discarded.

The growth conditions following were used for the experiments in Chapter 4. Seeds were planted in 1 gallon pots with Sungro6 Sunshine Mix #1 and grown in a chamber at 16hr/8hr light/dark cycle, 22°C during the day and 18°C at night, 60% humidity, and light intensity ~1000 μmol/m^2/s. Each pot contained 3-4 seedlings. Once plants reached tillering stage (Zadok stage 25), drought was induced by withholding watering. Photosystem I measurements were performed on 4 biological replicates for each genotype and treatment when the VWC in drought-stressed pots reached 0%.

The growth conditions following were used for the experiments in Chapter 6. The 16 spring wheat diversity panel lines (Jordan et al. 2018; Blake et al. 2019) were grown in growth chambers in 16/8hr light/dark cycle, 22°C during the day and 18°C at night, 60% humidity, and artificial illumination ~1000 μmol/m^2/s conditions. To mimic the field setting, 15 seeds were planted in a 1-gallon pot with Sungro6 Sunshine Mix #1 soil supplemented fertilizer, with 2 replicates for well-watered control and 2 for heat+drought stress. Drought stress was induced by withholding water. The volumetric water content (VWC) was measured using ProCheck Soil Moisture Probe with 5TC probe (Decagon now METER environment, Pullman, WA, USA). Once soil moisture reached below 0.2%, drought stressed plants were exposed to 40°C heat stress for 1-hour in a growth chamber. Immediately after, plants were sampled for peroxisome abundance and material was collected for biochemical assays to measure autophagy.

Section 2: Phenotyping

Measuring Root dynamics and Plant Growth

Root images were recorded with a CI-600 In-Situ Root Imager (CID Bio-Sciences, Camas, WA). The images were analyzed using RootSnap! image analysis software (CID Bio-Sciences, Camas, WA). To assess the size of the root system, we measured two parameters: total root length and total root count. Yield parameters including tiller number, grain number, and total yield were collected at maturity. Soil moisture values were recorded twice per week in both tubes at the bottom of the bin (80cm) and 40 cm above the bottom using a PR2 Soil Moisture Profile Probe and HH2 Soil Moisture Meter (Delta-T Devices, Cambridge, UK). Three readings per each depth and each tube were collected and averaged.

Measuring Chlorophyll Fluorescence using phenomics platform

Chlorophyll fluorescence images were collected once per night using combination of 455 nm and 630 nm saturation light and 630 nm measurement pulse using the Fluorcam XYZ system equipped with a Fluorcam 2701 LU camera (PSI Co., Drasov, Czech Republic). For these measurements' plants were illuminated for 300 second with actinic light of 200 °mol quanta m^{-2} s^{-1} prior to taking the meassurments. The images were processed by the Fluorcam 7 software (PSI Co., Drasov, Czech Republic) to derive the following parameters: Fv/Fm (fluorescence quantum yield), ϕ_{PSII} (quantum yield of photosystem II photochemistry) determined after the 300 second light period), non-photochemical quenching (NPQ, determined after the 300 second light period), and NPQ

components: energy dependent quenching *qE*, photoinhibition *qI*, and fraction of open PSII centers *qL* (Nilkens et al. 2010; Ruban 2016).

Measuring Photosystem I

Analysis of photosystem I donor and acceptor sides were performed using a custom-built flash-spectrophotometer (Tietz et al. 2015). Plants were adapted to actinic light (300 µmol quanta·m^{-2}·s^{-1}) for five minutes and then for 60 seconds to each of the following light intensities 50, 100, 200, 300, 500, 800, 1600 µmol/m^{-2}/s^{-1}. The electron flow through photosystem I was measured from saturating multiple turnover light pulse (100 ms) induced redox changes of P700 (determined as the difference between the 810nm and 900nm absorbance change). Efficiency of ϕI was derived from Pm′ − P (Klughammer & Schreiber 2016), where P is $P700^+$ level for a given light intensity; Pm′, $P700^+$ maximal level in the multiple turnover pulse; Pm, maximal $P700^+$ level for the dark-adapted state (determined by a multiple turnover pulse of dark-adapted leaves); and P_0, fully reduced P700 determined in a 0.5-s dark interval followed directly after the multiple turnover pulse. The non-photochemical loss due to oxidized donors and non-photochemical loss due to reduced acceptors were derived using P-P_0 for donor side limitations and P_m-P_m' for acceptor limitations.

Section 3: Molecular Biology

Genetic Analysis

Homoeologs for catalase genes *CAT1* and *CAT2*, and peroxisome biogenesis gene *PEX11-C* were identified using BLAST with the wheat genome database IWGSC

RefSeq v2.1. Homoeologs were classified according to relative homology scores. The 3 homoeologous genes were aligned, and qRT-PCR primers were designed for regions with sufficient number of non-conserved base pairs for capturing specific homoeologs (**Table 2.1**; Sanad et al. 2019).

Homoeologs for ATG8 genes were identified using BLAST with the wheat genome database IWGSC RefSeq v2.1 and clustered based on relative homology scores. Subsequently, we aligned the eleven homoeologous ATG8 genes using Clustal Omega (Siever et al. 2011) and designed qRT-PCR primers to either target individual homeologs or conserved regions of several homoeologous genes (**Table 2.1**).

Total RNA was extracted using RNeasy plant kit (Qiagen) from leaf material. The leaf material was sampled as described above. cDNA was synthesized using Maxima H Minus First Strand cDNA Synthesis Kit (Thermo Fisher Scientific). The primers are listed in **Table 2.1**. qRT-PCR reactions were performed using Fast SYBR™ GreenMaster Mix (Thermo Fisher Scientific) in 96-wells plates on ViiA 7 Real-Time PCR System with default ViiA™ 7 SYBR conditions. Reactions were replicated 3 times and analyzed in QuantStudio™ Real-Time PCR Software v1.3., transcription levels were normalized to housekeeping gene RNase L inhibitor-like protein (Giménez, Pistón & Atienza 2011) or *ADP-ribosylation factor 2* (Paolacci et al. 2009).

Promoter sequences for *PEX11C-7A* and *CAT2-6D* were downloaded from the wheat genome database IWGSC RefSeq v2.1. Primers were designed to amplify ~1,000 base pair regions upstream from the start codon (**Table 2.1**). A biotin-

modification was added to the reverse primer for binding to the streptavidin-agarose affinity chromatography resin (Thermo Scientific).

Phylogenetic analysis and structure prediction

Homoeologs for ATG8 were identified using BLAST with the wheat genome database IWGSC RefSeq v2.1 and clustered based on relative homology scores. Amino acid sequences were downloaded and aligned using ClustalX software package (Thompson et al. 1997). The phylodendrograms were constructed in PAUP using Jackknife method. Bootstrap values were calculated from 1000 iterations. Published ATG8 genes from *Arabidopsis thaliana* and *Oryza sativa* were included for comparing the ATG8 clustering and *Saccharomyces cerevisiae* ATG8 was used as the out group.

Predicted structures of wheat ATG8 homeologs were constructed in AlphaFold Protein Structure Database (Jumper et al. 2021). Amino acid sequences for ATG8c-2A (uniport: Q7XY24), ATG8-6A (uniport: A0A3B6NXU7), ATG8l-6B (uniport: A0A3B6PL31), and ATG8m-6D (uniport: A0A3B6QLC9) were blasted in Uniport and imported in AphlaFold. Protein structures were visualized and superimposed using ChimeraX software (Pettersen et al. 2021).

Section 4: Biochemistry

Measuring peroxisome abundance

Peroxisome abundance was measured using small fluorescent probe Nitro-BODIPY using previously published procedure (Fahy et al. 2017). A 2-cm fragment of the leaf basal part was transferred into deep 96-well plates immersed in a liquid nitrogen bath

and ground to fine powder using a tissue grinder (TissueLyser II, Qiagen, Venlo, Netherlands). Total leaf protein was extracted using 0.8 ml of the extraction buffer A (EBA; 20 mM Tris HCl, pH7.4, 500 mM NaCl, 7M Urea) by rotating the plates for 1 hour. The debris was cleared by centrifugation at 3,000 g for 30 minutes. Then 20 µl of the extract was added to 80 µl of freshly prepared 2 µM solution of N-BODIPY and 100 µl of water in 96-well plates and incubated for 10 min. The fluorescence intensity was measured at 490 nm excitation wavelength and 530 nm emission wavelength using Synergy Neo B spectrofluorometer (Biotek Instrument, Inc). Five biological replicates (individual plants) with three technical replicates were performed per genotype and treatment. The background was measured as (i) 20 µl of each protein extract in 180 µl of water; and (ii) 20 µl of N-BODIPY supplemented with 180 µl of water per each 96-well plate. Both background values were subtracted from the N-BODIPY fluorescence signal value. The fluorescence intensity was normalized by the protein concentration measured with the Bradford Reagent (Biorad Laboratories) using a calibration curve constructed with solutions of known concentration of Bovine Serum Albumin. Fluorescence intensity was calculated in arbitrary units per 1 mg of protein.

Measuring Activity of ROS Scavengers

A 2 cm long fragment at the flag leaf base from three individual plants were sampled and mixed in one tube. One set of three plants constituted a biological replicate. The leaf material was ground in liquid nitrogen using a mortar and pestle. Total protein extract was prepared from 150 mg of the leaf powder in 0.05 M potassium phosphate buffer (pH 7.8) supplemented with following protease inhibitors: 200 µM AEBSF, 100 µM

PMSF, 10 μM leupeptin and 10 μM pepstatin. Protein concentration in the extract was measured using Bradford Reagent (Biorad Laboratories). The enzymatic activity of catalase (CAT) was measured by the rate of hydrogen peroxide decomposition at OD_{240}.

Ascorbate peroxidase (APX) activity was quantified in total protein extract prepared with buffer containing 0.05 M potassium phosphate buffer (pH 7.0), 5 mM EDTA, and 17 mM ascorbic acid. The enzymatic activity was measured by the rate of oxidized ascorbate production at OD_{290}. Guaiacol peroxidase (GPX) activity was quantified by homogenizing total protein extract with 0.05 M potassium phosphate buffer (pH 7.0) containing 1% guaiacol solution. The enzymatic activity was quantified by the rate of tetratguaiacol production at OD_{470}. Superoxide dismutase (SOD) activity was quantified by homogenizing total protein extract in the buffer containing 0.154% (w/v) nitro-blue tetrazolium chloride, 5.82% (w/v) methionine, and 0.0015% (w/v) riboflavin. The reaction was initiated by illuminating the cuvettes with 15 W fluorescent light for ~12 minutes. Absorbance was measured at OD_{560}. One unit of the enzyme activity is equivalent to 50%

Hydrogen peroxide concentration was determined as an indicator of ROS accumulation. 200 mg of tissue was ground under liquid nitrogen conditions using a mortar and pestle. Leaf tissue powder was homogenized with 1% ammonium iron II sulfate (weight/volume) in 0.5 M H_2SO_4. Then, 5% sulfosalicylic acid was added to initiate reaction. Absorbance was measured at OD_{530}. Hydrogen peroxide concentration is determined by a standard curve.

Preparation of antibodies

A fragment of Catalase (GenBank: X94352.1; **Table 2.1**) corresponding to amino acid residues 96 to 385 was amplified using PCR and cloned into pDONR207 (Invitrogen) entry vector using GateWay system. The fragment was verified by sequencing. The fragment was cloned into pGAT4 destination vector and expressed as a recombinant protein with N-terminal His-Tag in *Escherichia coli* stain Rosetta II (Novagen).

A fragment of NBR1 (GenBank: DQ211935.1; **Table 2.1**) corresponding to amino acid residues 20 to 462 was amplified using PCR and cloned into pDONR207 (Invitrogen) entry vector using GateWay system. The fragment was verified by sequencing and cloned into pGAT4 destination vector. The recombinant NBR1 protein was produced with N-terminal His-Tag fusion in *E. coli* stain Rosetta II (Novagen).

A fragment of ATG7 (GenBank: AGW81787.1; **Table 2.1**) corresponding to amino acid residues 31 to 960 was amplified using PCR and cloned into pDONR207 (Invitrogen) entry vector using GateWay system. The fragment was verified by sequencing and cloned into pGAT4 destination vector. The recombinant ATG7 protein was produced with N-terminal His-Tag fusion in *E. coli* stain Rosetta II (Novagen).

A fragment of *ATG8* (GenBank#AK457482.1; **Table 2.1**) corresponding to amino acid residues 1 to 116 was amplified by PCR using forward and reverse primers containing Nhe I and Xho I restriction sites respectively. The PCR fragment was cloned in pGEM-T Easy (Promega, USA) and verified by sequencing. The fragment was

released from the pGEM-T Easy by digesting with Nhe I and Xho I, and cloned into expression vector pET28a cut with NdeI and XhoI.

Recombinant Catalase, NBR1, ATG7, and ATG8 proteins were expressed as N-terminal His-Tag fusions in *E. coli* stain Rosetta II (Novagen). Total bacterial protein was extracted using sonication. Recombinant proteins were purified under denaturing conditions in urea buffers on a nickel-nitrilotriacetic acid agarose column (Qiagen). Antibodies were prepared using our established procedure (Smertenko *et al.* 2004, 2008). Purified protein was dialyzed against PBS supplemented with 20% glycerol overnight at 28°C.

For ATG7, protein concentration was adjusted to 1 mg/mL and 50 µg of recombinant ATG7 were used per each boost. A total of 4 injections were administered over 2 months in mice. The first boost was mixed 1:1 with Freund's complete adjuvant, and the subsequent boosts were mixed 1:1 with Freund's incomplete adjuvant. Antiserum was collected 10 days after final boost and evaluated by immunoblotting.

For catalase, NBR1, and ATG8, protein concentration was adjusted to 1 mg/mL and 500 µg of recombinant protein was used per each boost. A total of 7 injections were administered over 9 months in rabbits. For the first boost, recombinant protein was mixed 1:1 with Freund's compete adjuvant. 25 days after the initial boost was the 1st boost, and antiserum was collected 10 days following the 1st boost. The subsequent six boosts were mixed 1:1 with Freund's incomplete adjuvant. Altogether seven bleeds were collected. Antiserum was collected from all bleeds and evaluated by immunoblotting.

Affinity Purification of Antibody

ATG8 antibody was affinity purified using ATG8 bound to NHS-Activated Agarose Resin (Pierce). Recombinant ATG8 protein was expressed and purified as above and concentrated to 2mg/ml with a spin protein concentrator (Thermo Scientific). ATG8 protein was further purified using a size exclusion column Superdex 200 Increase 10/300GL column (Cytiva) on an AKTA-FPLC in 4M Guanidine-Hydrochloride buffered by phosphate, pH 7.2. Fractions containing pure ATG8 were pooled together and concentrated to 1mg/ml. 300mg of NHS-Activated agarose dry resin was rehydrated with 0.1M sodium phosphate, 0.15M sodium chloride, pH 7.2 buffer, leading to a column of ca. 2mL. 5ml of ATG8 protein (1mg/ml) was then added to the resin and incubated at 30°C for 2 hours. Resin was then quenched using 1M Tris, pH 7.4 and washed in 100mM Tris, 500mM NaCl, pH 7.2.

The ATG8 antisera were pooled together, supplemented with 100 μM PMSF, 25 μM Leupeptin, 100 μM Pepstain A, 50mM Tris, 150mM NaCl, pH 7.4 and then incubated with the ATG8-NHS resin column for 1 hour at 4°C. The resin was washed 3x with 50mM Tris and 150mM NaCl, pH 7.4, and bound anti-ATG8 was eluted from the column in 100mM Glycine-HCl, pH 2.5 supplemented with a pH indicator phenol red at 0.5% (w/v). The eluate was immediately mixed with 1M Tris, pH 9.0 to adjust pH to 7.5. Then bovine serum albumin and sodium azide were added to final concentration of 5% and 0.05%, respectively. Purified Anti-ATG8 serum was concentrated with 10kD spin concentrators, aliquoted, flash-frozen in liquid nitrogen, and stored in -80°C.

Total Protein Extraction Techniques

For the western blotting, total protein was extracted from leaf by crushing the tissue under liquid nitrogen conditions using a mortar and pestle and homogenizing in an extraction buffer containing 50mM Tris (pH 7.2), 10mM EDTA, 10mM Mercaptoethaol 0.2% (v/v) Triton X-100 and proteinase inhibitors: 100 μM PMSF, 25 μM Leupeptin, 10 μM Pepstain A, 1 μM E10, and 1 μM MG132. Total protein extract supernatant was mixed 1:1 with 2x SDS-PAGE buffer and boiled for 3 minutes. As an alternative protocol, leaves were crushed in liquid nitrogen using a mortar and pestle, homogenized in 1:1 with 2x SDS-PAGE sample buffer, and boiled for 3 minutes.

Microsomal fractionation and d*elipidation*

Leaves were ground under liquid nitrogen using a mortar and pestle, and homogenizing with TNIP buffer (50mM Tris-HCl, pH 8.0, 150mM NaCl, 1mM PMSF, and 10mM Iodoacetamide). The homogenate was filtered through cheesecloth and centrifuged at 2,000 x g for 5 minutes. Supernatant was collected and centrifuged at 100,000 x g for 1 hour. The pellet was resuspended in TNIP buffer or 2x SDS-PAGE buffer.

For the delipidation, the microsomal fraction was resuspended in 0.5% triton X-100 in TNIP buffer. Total protein was extracted using the above procedure. A 100μl of total protein extract was incubated with 250 unit/ml^{-1} of *Streptomyces chromofuscus* phospholipase D at 37°C for 1 hour. Reactions were then mixed with 2x SDS-PAGE sample buffer, ran on a 15% SDS-PAGE gel, and transferred to PVDF membrane. Membranes were probed with anti-ATG8 as described above.

Western Blotting

Total protein was extracted from leaf by grinding the tissue in liquid nitrogen using a mortar and pestle followed by homogenizing in an extraction buffer (50mM Tris, pH 7.2, 10mM EDTA, 10mM Mercaptoethaol and proteinase inhibitors 100 µM PMSF, 25 µM Leupeptin, 100 µM Pepstain A, 1 µM E10, and 1 µM MG132). The debris were removed by centrifugation at 13,000 x g for 5 minutes at +4°. The supernatant was collected, mixed 1:1 with 2x SDS-PAGE buffer, and boiled for 3 minutes. The extracts were separated on a 15% SDS-PAGE gel and transferred onto a Polyvinylidene difluoride (PVDF) membrane (Sigma).

To prepare the immuno-depleted anti-ATG8, recombinant ATG8 at final concentration 10 µg/ml was incubated with the primary antibody diluted 1:100 in 1x TBST supplemented with 5% (w/v) fat-free milk powder at room temperature for 30 minutes. Then PVDF membrane with recombinant ATG8 was cut into strips and washed for 20 minutes in same milk-TBST. One strip was incubated with primary antibody diluted 1:100 in the same buffer and another strip was incubated with the depleted primary antibody for 1 hour at room temperature. Both strips were washed 3 times for 10 minutes in TBST and incubated with secondary anti-rabbit horseradish peroxidase conjugates (Jackson ImmunoResearch) diluted to 1:2000 for 35 minutes. Unbound secondary antibody was washed off in TBST three times 10 minutes each. The membranes were developed by ECL reagent (GE Healthcare) and images captured using G:BOX Chemi XT4 Gel Imaging System (Syngene, USA).

The same procedure was used to generate immuno-depleted anti-ATG7 and anti-NBR1. ATG7 or NBR1 recombinant protein was used, and the corresponding antiserum was tested at 1:500 dilution. Anti-mouse horseradish peroxidase conjugate (Jackson ImmunoResearch) diluted to 1:2000 was used as the secondary antibody.

Total protein from leaves of well-watered and heat+drought-stress treated wheat plants was extracted as described above. After removing debris by centrifugation, protein concentration in the extracts was measured using Bradford reagent (Bio-Rad) and adjusted to 1mg/ml. Samples were then mixed 1:1 with 2x SDS-PAGE sample buffer and boiled for 3 minutes. Each gel well was loaded with 25 µg of total protein. The extracts were ran on a 15% SDS-PAGE gel and transferred onto a PVDF membrane. The membrane was washed with 1x TBST supplemented with 5% (w/v) fat-free milk powder for 20 minutes. The membrane was incubated with the primary antibody, either anti-ATG8 diluted 1:100, anti-ATG7, or anti-NBR1 diluted 1:500 in TBST-milk for 1 hr. Membrane was washed, then incubated with secondary antibody (either rabbit-HPR or mouse-HRP) at 1:2000 dilution and imaged as described above.

The membrane was then washed with agitation 3 times for 10 minutes with deionized water then total protein was stained with colloidal silver or amido black. Total protein values on the colloidal silver-stained membrane or amido black and luminescence values on the Western Blotting images were measured using Fiji ImageJ (Schindelin et al. 2012). The luminescence intensity values were normalized by the protein content on the membrane. Statistical differences were analyzed using Student's T Test.

Immunoprecipitation (IP-MS) using anti-ATG8

Affinity-purified anti-ATG8 was incubated with protein A agarose (Pierce) for 1.5hrs on ice, with shaking. The agarose resin was washed with NET-buffer (50mM Tris-HCl, pH 7.5, 150mM NaCl, 1mM EDTA, 0.1% Nonidet P-40, 0.02% sodium azide) and incubated with total protein extract from leaves prepared as described above, for 1.5 hours on ice. Resin was washed with NET-buffer and bound protein was eluted with 100mM Glycine-HCl, pH 2.7. Then, pH of the eluate was immediately adjusted to pH 7.5 with 1M Tris pH 9. The eluate was concentrated down to 100µl, mixed 1:1 with 2x concentrated SDS-PAGE sample buffer, and boiled for 3 minutes. The extracts were run on a 15% SDS-PAGE gel, transferred onto a PVDF membrane, and probed using the protocol above with anti-ATG8. For identification of protein composition, the extracts were separated on 15% SDS-PAGE gel and bands corresponding to specific weight based on the protein ladder were excised. Mass spectrometry analysis was performed by Southern Alberta Mass Spectrometry center (https://cumming.ucalgary.ca/cat/sams). Peptides were identified using *T. aestivum* protein database. Predicted proteins were then analyzed using Scaffold 5 software (Proteome Software, Inc., Portland, Oregon). Resin without antibody was used as a negative control for non-specific interactors.

Affinity-purified anti-ATG8 antibody was incubated with protein A agarose (Pierce) for 1.5hrs on ice, with shaking. The agarose resin was washed with NET-buffer (50mM Tris-HCl pH 7.5, 150mM NaCl, 1mM EDTA, 0.1% Nonidet P-40, 0.02% sodium azide) and incubated with total protein extract using extraction described above, for 1.5 hrs on ice. Resin was washed with NET-buffer. Protein was eluted with 100mM Glycine-HCl pH

2.7, and pH was immediately adjusted with 1M Tris pH 9. Elution was concentrated and mixed with 2x concentrated SDS-PAGE sample buffer and boiled for 3 minutes. The extracts were run on a 15% SDS-PAGE gel and transferred onto a PVDF membrane and probed using the protocol above, with anti-ATG8 as the primary antibody. Protein extracts were loaded on 15% SDS-PAGE gel. Bands corresponding to specific weight based on the protein ladder were excised. Mass spectrometry analysis was performed by Southern Alberta Mass Spectrometry center. Peptides were identified using *Triticum aestivum* genome. Predicted proteins were then analyzed using Scaffold 5 software. Resin without antibody incubation was used to identify non-specific interactors.

Nuclear Fractionation

Nuclei isolation protocol by *Sikorskaite et al. 2013* was optimized for wheat leaves and all steps where performed at +4°C. Briefly, wheat leaves were ground under liquid nitrogen conditions using a mortar and pestle and homogenizing with NIB buffer (10mM MES-KOH, pH 5.4, 10mM NaCl, 10mM KCl, 2.5mM EDTA, 250mM sucrose, 1mM DTT, 100 µM PMSF, 25 µM Leupeptin, 100 µM Pepstatin). The homogenates were filtered through a 20 µM mesh. The leaf material was then homogenised again with NIB buffer and refiltered. Both extracts where combined and filtered through a 10 µM mesh. Trition X-100 was added to a final concentration of 0.5% and the extract was agitated for 20 minutes. Extract was centrifuged at 1000 *x g* for 15 minutes and the supernatant was decanted. Pellet was resuspended in NIB buffer. Supernatant was then loaded on to a 2.5 M sucrose-60% Percoll gradient column. The column was centrifuged for 45 minutes at 1200 *x g.* Nuclei were collected from the 60% Percoll layer and mixed with 5 volumes

of NIB buffer. Nuclei were resuspended in NIB, centrifuged at 1000 *x g* for 10 minutes and resuspended in NIB. To check the quality of the nuclei preparation, the material was stained with DAPI and examined under fluorescence microscope.

Nuclear Protein Extraction with TRIzol

Extracted nuclei were homogenized by vertexing in 1 mL of TRIzol, incubated on ice for 5 minutes, and centrifuged at 12,000 rmp at +4°C for 5 minutes in a table top centrifuge, Supernatant was collected and mixed with chloroform, incubated on ice for 5 minutes, then centrifuged at 12,000 rmp at +4°C for 15 minutes. Aqueous phase was removed. 300 µL of ethanol was added, mixed, and incubated at room temperature for 10 minutes. Extract was then centrifuged at 1000 *x g* at +4°C for 5 minutes. Supernatant was transferred to a fresh tube and mixed with 1.5 mL isopropanol was added. The mixture was incubated at room temperature for 10 minutes. Protein was pelleted by mixing with 2 mL of 100% ethanol and incubating at room temperature for 20 minutes. Then extract was centrifuged 12,000 *x g* at +4°C for 5 minutes. The pellet was washed using ethanol and air dried. The pellet was resuspended in 1% SDS buffer (1% SDS, 10mM Tris, 150mM NaCl, 1mM EDTA) and incubated at 50°C till all protein was dissolved. Solution was diluted to a final concentration of SDS 0.1%.

Streptavidin Affinity Chromatography

DNA-binding proteins were pulled down using Streptavidin Agarose resin (Pierce), following the manufacturer's instructions. Briefly, 100mg of Streptavidin Agarose resin was transferred into a spin-down column. Column was equilibrated with binding buffer (with 0.1M sodium phosphate, 0.15M sodium chloride, pH 7.2 buffer). 500 mL of promoter

DNA was incubated with the resin for 1 hour at room temperature. Nuclear protein extract was incubated with the column for 2 hours at room temperature. The resin was washed with binding buffer. Proteins were eluted from the column in 8M Glycine-HCl (pH 1.5) supplemented with a pH indicator phenol red and immediately mixed with 1M Tris (pH 9.0) to adjust pH to 7.5. Protein elution was concentrated with 10kD spin concentrators and run on SDS-PAGE gel.

Section 5: Buffers

Peroxisome Abundance		
Protein extraction buffer	***200 mL of 1x***	***Stock Solutions***
20 mM Tris-HCl, pH 7.0	4 mL	1M Tris-HCl, pH 7.0
500 mM NaCl	20 mL	5M NaCl
7M Urea	84 g	
2 μM N-Bodipy		10 nM N-Bodipy stock

ROS Scavenging Enzymes		
Protein extraction buffer for Enzymes	***1L of 1x***	
0.05 M potassium phosphate-pH 7.8	7.45 g of potassium phosphate dibasic 986 mg of potassium phosphate monobasic	
	1.5 mL of extraction buffer	
Added at use:		
200 μM AEBSF	15 μL	200 mM AEBSF stock
100 μM PMSF	10 μL	100 mM PMFS stock
10 μM leupeptin	2.5 μL	25 mg/mL leupeptin stock
10 μM pepstatin	1 μL	10 mg/mL pepstain stock

Solution for catalase, ascorbate peroxidase and guaiacol peroxidase	***1L of 1x***
0.05 M potassium phosphate-pH 7.0	4.67 g of potassium phosphate dibasic 3.15 g of potassium phosphate monobasic

Catalase Activity	***2.5 mL reaction***	***Stock Solutions***
0.05 M potassium phosphate-pH 7.0	2.5mL	
3% H_2O_2 solution	3 µL	30% H_2O_2 stock solution

Ascorbate Peroxidase Activity	***2.5 mL reaction***	***Stock Solutions***
0.05 M potassium phosphate-pH 7.0	2.5mL	
0.005 M EDTA	50 µL	5mM EDTA
0.017 M ascorbic acid	20 µL	17 mM ascorbic acid
3% H_2O_2 solution	5 µL	30% H_2O_2

Guaiacol Peroxidase Activity	***3 mL reaction***	***Stock Solutions***
0.05 M potassium phosphate-pH 7.0	2.5mL	
1% guaiacol	600 µL	
H_2O_2	10 µL	30% H_2O_2

Superoxide Dismutase Activity	***3 mL reaction***
0.154% nitro blue tetrazolium chloride (NBT)	1 mL
5.82% methionine solutions	1 mL
0.0015% riboflavin	1 mL

Hydrogen Peroxide Content	***5 mL reaction***
0.5 M H_2SO_4	13.7 mL in 500 mL H_2O
	1x per 200 mg tissue
1% (w/v) ammonium iron (II) sulfate in 0.5M H_2SO_4	5 mL
1.67% sulfosalicylic acid solution	1 mL of 5% (w/v) sulfosalicylic acid

Purification of HIS-Tagged Proteins

Protein extraction buffer	***100 mL of 1x***	***Stock Solution***
50 mM HEPES, pH 7.0	5 mL	1 M HEPES, pH 7.0
300 mM NaCl	6 mL	5 M NaCl
20 mM Imidazole	2 mL	1 M Imidazole, pH 7.0
20 mM β-Mercaptoethanol	35 µL	
8 M Urea	48 g	

Washing buffer 20 mM	***100 mL of 1x***	***Stock Solution***
50 mM HEPES, pH 7.0	5 mL	1 M HEPES, pH 7.0
300 mM NaCl	6 mL	5 M NaCl
20 mM Imidazole	2 mL	1 M Imidazole, pH 7.0
6 M Urea	36 g	

Washing buffer 40 mM		
50 mM HEPES, pH 7.0	5 mL	1 M HEPES, pH 7.0
300 mM NaCl	6 mL	5 M NaCl
40 mM Imidazole	4mL	1 M Imidazole, pH 7.0
4 M Urea	24 g	

Washing buffer 60 mM	***100 mL of 1x***	***Stock Solution***
50 mM HEPES, pH 7.0	5 mL	1 M HEPES, pH 7.0
300 mM NaCl	6 mL	5 M NaCl
60 mM Imidazole	6 mL	1 M Imidazole, pH 7.0
4 M Urea	18 g	

Washing buffer 80 mM	***100 mL of 1x***	***Stock Solution***
50 mM HEPES, pH 7.0	5 mL	1 M HEPES, pH 7.0
300 mM NaCl	6 mL	5 M NaCl
80 mM Imidazole	8 mL	1 M Imidazole, pH 7.0
2 M Urea	12 g	

Elution buffer	***100 mL of 1x***	***Stock Solution***
50 mM HEPES, pH 7.0	5 mL	1 M HEPES, pH 7.0
300 mM NaCl	6 mL	5 M NaCl
250 mM Imidazole	25 mL	1 M Imidazole, pH 7.0
2 M Urea	12 g	

Protein dialysis buffer for Antibodies-pH 7.0	***1L of 1x***
4 mM Na_2HPO_4 X 12 H_2O	1.45 g
1.5 mM KH_2PO_4	212 mg
130 mM NaCl	8 g
20% (v/v) glycerol	200 mL

SDS-PAGE loading buffer	***100 mL of 2X***	***Stock Solution***
ddH_2O	20 mL	
125 mM Tris-HCl, pH 6.8	50 mL	250 mM Tris-HCl, pH 6.8
4% (w/v) SDS	4 g	
20% (v/v) glycerol	20 mL	
10% (v/v) β -mercaptoethanol	10 mL	
0.4% (w/v) Bromophenol Blue	20 mg (several crystals)	

Protein Extraction	***20 mL of 1 x***	***Stock Solution***
50 mM Tris, pH 7.2	1 mL	1 M Tris-HCl, pH 7.2
10 mM EDTA	400 µL	500 mM ETDA
10 mM β -mercaptoethanol	14 µL	
0.2% (v/v) Triton X-100	40 µL	
100 µM PMSF	10 µL	100 mM PMFS stock
25 µM leupeptin	1 µL	25 mg/mL leupeptin stock
10 µM pepstatin	10 µL	10 mg/mL pepstain stock
1 µM E-10	1 µL	1 mM E-10
1 µM MG-132	1 µL	1 mM MG-132

10% Ammonium persulfate (APS)	***10 mL of 1x***
ddH_2O	10 mL
Ammonium persulfate	1 g
*Aliquots 500 µL and store at -20°C. Do not freeze/thaw.	

SDS-PAGE running buffer	***4 L of 10x***
25 mM Tris	120 g Tris
0.19 M Glycine	576 g Glycine
0.1% SDS	40 g SDS

SDS-PAGE resolving gel	***200 mL of 1x***	*See Resolving Gel Mixture Below
0.75 M Tris-HCl, pH. 8.8	18.17g Tris	
0.2% (w/v) SDS	400 mg SDS	

SDS-PAGE stacking gel	200 mL of 1x	*See Stacking Gel Mixture Below
0.25 M Tris-HCl, pH. 8.8	6.06 g Tris	
0.2% (w/v) SDS	400 mg SDS	

Poly Acrylamide Resolving Gel Mixture

	7.5%	10%	12.5%	15%
Total Volume (mL)	28	28	28	28
30% AA (mL)	5.2	8.4	11.6	14
0.75 M Tris (mL)	14	14	14	14
ddH_2O (mL)	8.6	5.4	2.2	-
TEMED (µL)	12	12	12	12
10% APS (µL)	240	240	240	300

Poly Acrylamide Stacking Gel Mixture

	4%
Total Volume (mL)	10
30% AA (mL)	1.3
0.75 M Tris (mL)	5
ddH_2O (mL)	3.6
TEMED (µL)	10
10% APS (µL)	100

Colloidal Coomassie Blue Stain	***1 L of 1x***	
ddH_2O	60 mL	
10% (w/v) Ammonium Sulfate	100 g	*Dissolve fully in water
0.1% (w/v) Coomassie G-250	1 g	*Dissolve fully in water
3% (v/v) Orthophosphoric acid	30 mL	
20% (v/v) Ethanol	200 mL	
*Add each component in order listed above		

Slow Western Blotting

*Run at 12 amps for 12-16 hours/overnight

Transfer buffer	***2 L of 1x***
38 mM glycine	5.8 g
48 mM Tris	11.6 g
0.0037% SDS	0.74 g
	Add to 1x at use:
20% (v/v) methanol	200 mL

Fast Western Blotting

*Run at 90 mV for 60-70 minutes

Transfer buffer	***2 L of 5x***
25 mM Tris	30.3 g Tris
192 mM glycine	144g Glycine
	Add to 1x at use:
1% SDS, pH 8.3	5 mL 10x SDS, pH 8.3
20% methanol	200 mL

TBST washing buffer	***2.5 L of 5x***
20mM Tris HCl, pH 7.4	30.1 g Tris
300mM NaCl	215 g NaCl
0.1% Tween 20	12.5 mL of Tween 20

5% milk-TBST Buffer	***100 mL of 1x***	
5% (w/v) fat-free milk powder	5 g	
TBST	100 mL	*Recipe above

Amido Black Solution	***50 mL of 1 x***
1% Amidoblack	0.5 g Amidoblack
10% methanol	5 mL of methanol

Colloidal Sliver Stain	***20 mL of 1x***	
ddH_2O	18	
40% (w/v) Na_3-citrate	1	*Store at room temperature.
20% (w/v) $FeSO_4x7H_2O$	0.8 mL	*Store in 800 µL aliquots at -20°C. Do not freeze/thaw.
20% (w/v) $AgNO_3$	0.2 mL	*Store in 1 mL aliquots at -20°C. Can freeze/thaw.

*Only use ddH_2O and clean falcon tubes to mix reagents.

Microsomal Fractionation

TNIP buffer	***10 mL of 1x***	***Stock solutions***
50 mM Tris, pH 8.0	1 mL	500 mM Tris, pH 8.0
150 mM NaCl	5 mL	300 mM NaCl
1 mM PMSF	100 µL	100 mM PMSF
10 mM Iodoactaminde	20 mg	

Delipidation Buffer	***5 mL of 1x***	
0.5% (v/v) Triton X-100	2.5 µL (v/v)	
TNIP		*Recipe above

Immunoprecipitation NET buffer	***20 mL of 1x***	***Stock solutions***
50 mM Tris-HCl, pH 7.5	1 mL	1 M Tris-HCl, pH 7.5
150 mM NaCl	3 mL	1 M NaCl
1 mM EDTA	4 µL	0.5 M EDTA
0.1% Nonidet P-40	200 µL	10% (v/v) Nonidet P-40
0.02% NaN_3	10 µL	5% NaN_3

Immunoprecipitation elution and neutralization buffer	***10 mL of 1x***
100 mM Glycine-HCl, pH 2.7	75 mg
1 M Tris pH 9.0	1.21 g

ATG8 Purification FPLC Running Buffer	***1L of 1x***	***Stock solutions***
4M Guanidine-Hydrochloride	382.16 g	
100 mM Phosphate	100 mL	1 M sodium phosphate, pH 7.2

Coupling Buffer	***100 mL of 1x***	***Stock solutions***
100 mM sodium phosphate, pH 7.2	10 mL	1 M sodium phosphate, pH 7.2
150 mM NaCl	15 mL	1 M NaCl

*Buffer needs to be amine-free

Quenching Buffer	***10 mL of 1x***
1 M Tris, pH 7.4	1.21 g

Wash Buffer	***100 mL of 1x***	***Stock solutions***
100 mM Tris-HCl, 7.2	10 mL	1 M Tris-HCl, pH 7.2
500 mM NaCl	50 mL	1 M NaCl

Antisera Wash Buffer	***100 mL of 1x***	***Stock solutions***
50 mM Tris-HCl, 7.2	5 mL	1 M Tris-HCl, pH 7.2
150 mM NaCl	15 mL	1 M NaCl

Elution and Neutralization Buffers	***100 mL of 1x***
100 mM Glycine-HCl, pH 2.5 with 0.5% phenol red	0.75 g
1 M Tris pH 9.0	12.11 g

Column Storage Buffer	***100 mL of 1x***	***Stock solutions***
100 mM Tris-HCl, 7.2	10 mL	1 M Tris-HCl, pH 7.2
500 mM NaCl	50 mL	1 M NaCl
Add at use 10 mL for 1x:		
0.2% NaN_3	10 µL	5% NaN_3

Nuclear Fractionation NIB buffer	***100 mL of 1x***	***Stock solutions***
10 mM MES-KOH, pH 5.4	1 mL	1 M MES-KOH, pH 5.4
10 mM NaCl	1 mL	1 M NaCl
10 mM KCl	1 mL	1 M KCl
2.5 mM EDTA	50 µL	0.5 M EDTA
250 mM Sucrose	2.5 mL	2.5 M sucrose
Add at use:		
1 mM DTT	100 µL	100 mM DTT
100 µM PMSF	10 µL	100 mM PMFS stock
10 µM leupeptin	2.5 µL	25 mg/mL leupeptin stock
10 µM pepstatin	1 µL	10 mg/mL pepstain stock

Percoll Gradient	***10 mL gradient***	
2.5 M Sucrose	5 mL	
60% percoll	5 mL	*Dilute Percoll solution to 60% (v/v) and use for gradient

1% SDS Nuclei Protein Buffer	***10 mL of 1x***	***Stock solutions***
1% (v/v) SDS	100 µL	10% SDS solution
10 mM Tris	100 µL	1 M Tris
150 mM NaCl	150 µL	1 M NaCl
1 mM EDTA	2 µL	0.5 M EDTA

Streptavidin Affinity Chromatography Binding and Wash Buffer	***100 mL of 1x***	***Stock solutions***
100 mM sodium phosphate, pH 7.2	10 mL	1 M sodium phosphate, pH 7.2
150 mM NaCl	15 mL	1 M NaCl

Elution and Neutralization Buffers	***10 mL of 1x***
8M Glycine-HCl, pH 1.5 with 0.5% phenol red	6 g
1 M Tris pH 9.0	1.21 g

Gene Name	Type	5' Mod	Forward	Reverse	References
ATG7	Gateway Cloning		GGGGACAAGTTTGT ACAAAAAAGCAGGC TTCGACCTCCGCCG ACTCAAGCTCGAC	GGGGACCACTTTGTA CAAGAAAGCTGGGTC AGATGCAATGGAGGC CAGTCC	
ATG8	Traditional Cloning		ACATATGAAATCCTT CAAGAAGGAATTCA C	ACTCGAGTCACCCAA ATGTCTTCTCGCTGC	Hickey et al. 2022
NBR1	Gateway Cloning		GGGGACAAGTTTGT ACAAAAAAGCAGGC TTCGATGTTGTTATG CTGGATGATGAC	GGGGACCACTTTGTA CAAGAAAGCTGGGTC TTATCGTGGTGACCT CTCACTGTTATT	
Catalase	Gateway Cloning		GGGGACAAGTTTGT ACAAAAAAGCAGGC TTCGAACGCATACCT GAACGTGTTGTTC	GGGGACCACTTTGTA CAAGAAAGCTGGGTC TCACACATTTTGGAG CATTGACTG	Hickey et al. 2022
Rnase L Inhibitor Like Protein (RLI)	qPCR		CGATTCAGAGCAGC GTATTGTTG	AGTTGGTCGGGTCTC TTCTAAATG	Giménez et al. 2011
APD-ribosylation Factor 2	qPCR		TCTCATGGTTGGTCT CGATG	GGATGGTGGTGACG ATCTCT	Paolacci et al. 2009
ATG8 Universal	qPCR		GGAGATGGCCAAGA CTTGCT	AGCCTTCTCAACGAT CACCG	
ATG8b-2A	qPCR		GGATTGCTCTAGATG GCGCT	ATCCTACGACGAGGC AAACC	
ATG8i-5A	qPCR		CTTCTCCAGCTTCG CCATTGA	ACTTCATCCTCCTCC TCGCT	
NBR1	qPCR		AACGGAACGCACTT CACTTTG	GTCCTCGTCATCATC CAGCAT	
PEX11-A	qPCR		CGCTAGGGGACGTG ACTAA	CAGCGCCGACAGCA ATC	Sanad et al. 2019
PEX11-B	qPCR		CAACCCGTTCTGCA ACCAC	TTCCTATACCACCCA GCCCA	Sanad et al. 2020
PEX11-C	qPCR		GAAGAACGCGATGC TGTCAA	TAAAAGGCAATCCTG CCAAG	Sanad et al. 2021
DRP-3A	qPCR		GACCTGCGGAGACA ATGATAAC	GTTGGTCCTCTCGAA GATAGA	Sanad et al. 2022
DRP-3B	qPCR		TGGACGAGATACCG CTTGAA	CACTGAAAGGTTGTT GCTGC	Sanad et al. 2023
FIS-1A	qPCR		TCCAAGCAGACTGA TGATGTG	TGGGCTGGTGGTTTT ATCAAGA	Sanad et al. 2024
ATG-8.2	qPCR		TCGATCGCAGGTTG GAGATG	TTGATCCTCTTCCGC ACCAC	Hickey et al. 2022
ATG-8.3	qPCR		CTGGAAAGGAGGCA AGCTGA	TTGATCCTCTTCCGC ACCAC	Hickey et al. 2022
ATG-8.4	qPCR		TCTCGCCTCCTCCC TTTACT	TTGAACGAGCTCTTC GCCAT	Hickey et al. 2022
CAT1-5A	qPCR		GGCCGAATTACCTG CTGCT	AAGTAGTCGACCTCC TCGTCG	Hickey et al. 2022

CAT1-4B	qPCR		GGACTATGAGGAGC GGTTCG	GTTGTCGATGTTGCG GTTC	Hickey et al. 2022
CAT1-4D	qPCR		CAGGCTGACAAGTC TCTCGG	TTGGTACGTAATCCT CGCCG	Hickey et al. 2022
CAT2-6A	qPCR		TCAAGAGAGGAAGG ATGGAT	GTAGTCCTCCAGCAA GATCG	Hickey et al. 2022
CAT2-6B	qPCR		CCAGCTTAGCTGAG CTACTT	CTCGTTGTCGTTCCA CACG	Hickey et al. 2022
CAT2-6D	qPCR		GGATGGATCGATCT GCCAT	AGCAGCACAGTATGT AATCGA	Hickey et al. 2022
PEX11-7A	qPCR		CCAGCTTACTACACA GGCA	TGTGACGGTGTCCAA TGAG	Hickey et al. 2022
PEX11-4A	qPCR		TAGCCAGCTTACAC ACACAA	CTCTGACGGTGTCCA CTGA	Hickey et al. 2022
PEX11-7D	qPCR		CCATCCAATAGCCTG GTT	ATGCGAGCCATCACC ATT	Hickey et al. 2022
CAT2-6D Promoter	PCR		CTAGCCGCTCGGAT CTACAC	GCGAGGAAGCAACC TCTAC	
PEX11-7A Promoter	PCR		TCAAGATCCGGTCG GTTTTGGT	GTCGACATTCTGTGC AGG	
Glutamine synthetase 2 (GS2) Promoter	PCR		AGGGCCAAAAGTAC AGGCAG	TCGCCGCTGCTTACT TACTT	He et al. 2015
CAT2-6D Promoter	PCR	Biotin		GCGAGGAAGCAACC TCTAC	
PEX11-7A Promoter	PCR	Biotin		GTCGACATTCTGTGC AGG	
Glutamine synthetase 2 (GS2) Promoter	PCR	Biotin		TCGCCGCTGCTTACT TACTT	He et al. 2015
TaZIM-A1	PCR		GCACAGCACGACGG CAAGCCATA	GGTCACGACCATGGT TCTTCGACA	Liu et al. 2018
TaZIM-A2	Gateway Cloning		GGGGACAAGTTTGT ACAAAAAAGCAGGC TTCGCACAGCACGA CGGCAAGCCATA	GGGGACCACTTTGTA CAAGAAAGCTGGGTC GGTCACGACCATGGT TCTTCGACA	Liu et al. 2019
TaNAC2-5A	PCR		GGGATGCCGGCCGT GAGGAGGAGG	CCGGCGGCATGCCG GCCCCGTTC	He et al. 2015
TaNAC2-5A	Gateway Cloning		GGGGACAAGTTTGT ACAAAAAAGCAGGC TTCGGGATGCCGGC CGTGAGGAGGAGG	GGGGACCACTTTGTA CAAGAAAGCTGGGTC CCGGCGGCATGCCG GCCCCGTTC	He et al. 2016

Table 2.1: Sequences of all primers used.

CHAPTER 3: CAPTURING DROUGHT RESPONSES THROUGH PHENOTYPING ROOT ARCHITECTURE

I completed all the experiments under the guidance of Karen Sanguinet and Andrei Smertenko. A portion of the figures and text was published in *Cells*.

Hickey, K., Sexton, T., Wood, M., Sahin, Y., Nazarov, T., Fisher, J., Sanguinet, K., Kichhoff, H., Cousins, A., Smertenko, A. 2022. Drought tolerance strategies and autophagy in resilient wheat genotypes. Cells, 11, 1765. doi.org/10.3390/cells11111765.

Individual author contributions for the original *Cells* manuscript are listed below:

Conceptualization, A.S., H.K. and K.A.S.; methodology K.A.S.; formal analysis, K.H. and M.W.; investigation, K.H., T.S., T.N., M.W., Y.S. and J.F.; writing—original draft preparation, K.H.; writing—review and editing, T.S., M.W., Y.S., T.N., K.A.S., H.K., A.C. and A.S.; supervision, A.S., H.K., K.A.S. and A.C.; funding acquisition, A.S., H.K., K.A.S. and A.C. All authors have read and agreed to the published version of the manuscript.

Section 1: Introduction and Rational

Section 2: Experimental Setup Overview

Section 3: Root Architecture based on In-Situ Root Imaging

Section 4: Peroxisome Phenotyping

Section 5: Plant Yield and Morphology

Section 6: Correlations of Yield under Drought

Section 7: Discussion and Conclusion

Section 1: Introduction and Rational

There are three universal mechanisms of drought survival in plants (Basu et al. 2016). The first is escaping drought by accelerating reproduction (Shavrukov et al. 2017). The second mechanism is drought avoidance via higher water-use efficiency or increasing soil moisture access. Avoidance uses a range of mechanisms such as longer root system to capture moisture at deeper soil levels or stomata closure to reduce transpiration (Basu et al. 2016). The third mechanism is drought tolerance. This mechanism focuses on withstanding dehydration through the production of protective molecules (Fang & Xiong 2015) which, amongst other roles, contribute to preventing accumulation of reactive oxygen species (ROS; Voss et al. 2013; Foyer & Noctor 2016).

In this chapter a high-throughput technique was used for phenotyping drought avoidance in wheat. Avoidance mechanisms are based on the plant's ability to reach moisture at deep soil layers and offers many benefits in the Pacific Northwest (PNW) where dryland farming practices are commonplace. Additionally, because root phenotyping in large wheat populations is an expensive and time-consuming process,

the use of the high-throughput phenotyping screen by peroxisome abundance was done. We hypothesize that through the phenotyping peroxisome abundance, root morphology traits can be identified and ultimately exploited for breeding more robust varieties for dryland farming.

Section 2: Experimental Setup and Drought Description

Mining soil moisture using longer roots is a known drought avoidance strategy (Manschadi et al. 2006; Fang & Xiong 2015). Roots of wheat plants can reach several meters in depth, hindering the analysis of root architecture in the commonly used greenhouse containers. Analysis of roots in the field situation can provide a more complete approach. However, environments can be significantly different within field locations, between different field locations, and during the growing season limiting the broadness of this approach. Analysis of environmental factors that affect root growth and morophology could not be identified in this situation comprehensively.

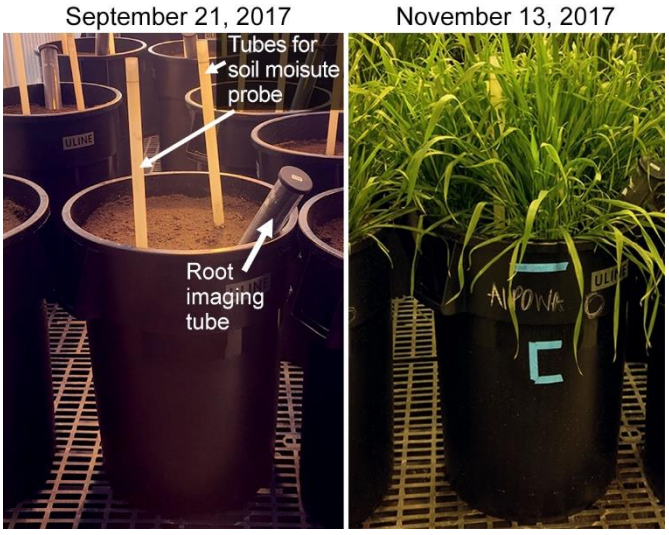

Figure 3.1: A representative photo of a bin set up before trans-planting the seedlings and after 54 days.

Here we developed an approach that would allow comprehensive analysis of root architecture under controllable growth conditions of a greenhouse using 55 gallons bins

and each contained 2 soil moisture probes and one root imaging tube (**Figure 3.1**). The soil moisture probes were used to monitor the VWC at multiple depths. The root imaging tube allowed for continuous imaging of the roots through the soil profile. The root imaging is a non-invasive technique allowing for comparison of environmental conditions on root morphology within the u-bin container. The experimental setup included 7 spring wheat genotypes split into two experimental stress treatments. The first set consisted of genotypes Alpowa, Hollis, Drysdale, and Onas. The second trial included Alpowa, Dharwar Dry, Louise and AUS28451. Alpowa was repeated in both sets.

For the first set, five 2-week-old seedlings of each variety were planted per bin. For the second set, 2-week-old seedlings were vernalized for 9 weeks before transplanting into bins. Seedlings were watered normally until the beginning of tillering

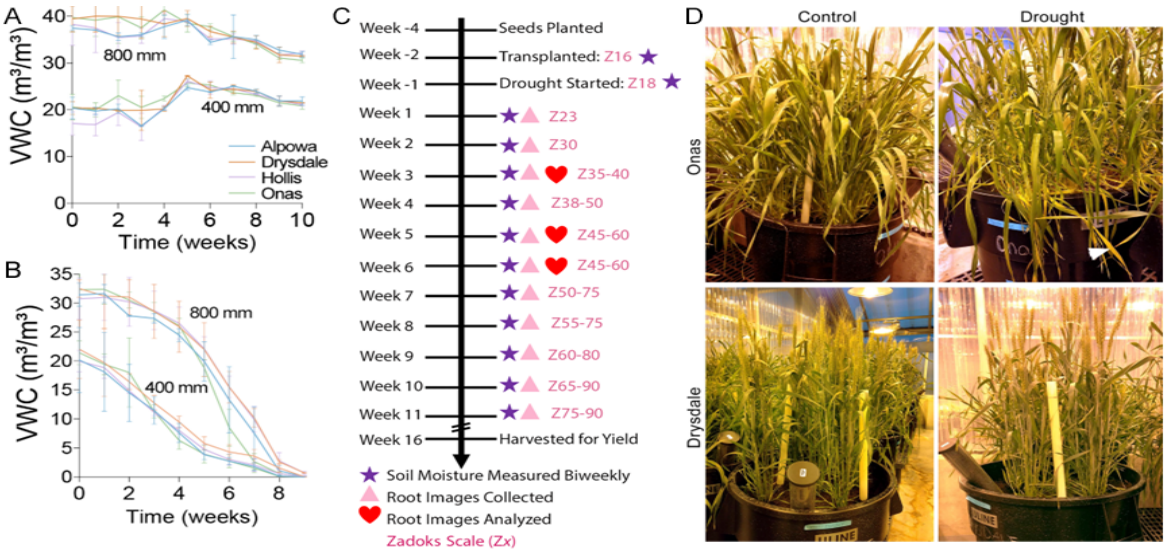

Figure 3.2: Impact of Drought on Growth and Development. **(A)** Representative chart for watered control bins. **(B)** Representative chart for non-watered bins. Watering was stopped at week 0. Error bars represent standard deviation of the mean. Two bins per each genotype were measured for control and three bins were measured for drought-stressed situations. **(C)** The experimental timeline. **(D)** Representative images of genotypic difference to drought. Genotype Onas shows apparent signs of distress: wilting and yellowing of leaves, whereas genotype Drysdale shows no discernible stress symptoms.

stage (Zadoks scale 18-19) and then watering was withheld (**Figure 3.2A**). The soil WVC was measured at 80 cm (bottom of the bin) and at the 40 cm depths. The moisture declined gradually over the 8 weeks of drought treatment at both depths, however the depletion rate was faster at the 40 cm level (**Figure 3.2B**). Overall, the decline of the soil moisture was not significantly different between any of the containers, genotypes, or the two sets.

Root images were taken once a week for 11 weeks, till the plants were in the grain filling stage (**Figure 3.2C**). Representative images were taken during the growth to show that plants were able to growth in the u-bins (**Figure 3.2D**).

Section 3: Root Architecture based on In-Situ Root Imaging

Root images were captured once a week over the course of drought experiment. **Figure 3.3** shows representative images of Alpowa over the course of experiment for both well-water control conditions and drought conditions.

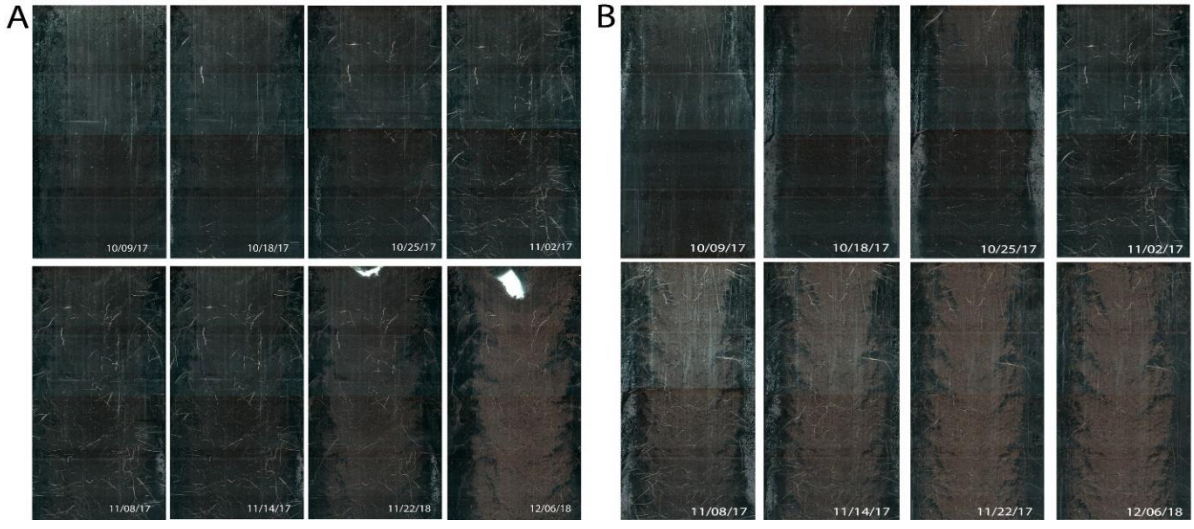

Figure 3.3: Representative root images of Alpowa grown under normal watering (**A**) or drought stress (**B**).

As the drought progressed, the soil dried out, reducing the contrast between roots and soil. Root systems were analysed on images taken at different soil moisture values and developmental stages at week 3, 5 and 6 for set 1 and week 1, 2, 5 for set 2. Representative images are shown in **Figure 3.4A** and examples of how roots images were analysed as shown in **Figure 3.4B**.

At week 3 for set 1, the VWC values at the top section of the bin were 10-28% (27-32% VWC in the watered controls); at week 5, the VWC values were 5-20%; and at week six, the values were 2-10%. Decline of the VWC values at the top of the bin was accompanied by the higher values at the bottom of the bean. Thus, deeper root system in this growth set up provides access to additional water resources. Additionally, week 3 plants were in the vegetative growth phase. Weeks 5 and 6 were right before or immediately after flowering. Later stages were not analysed as wheat roots cease growth past the flowering stage (Ghimire et al. 2020).

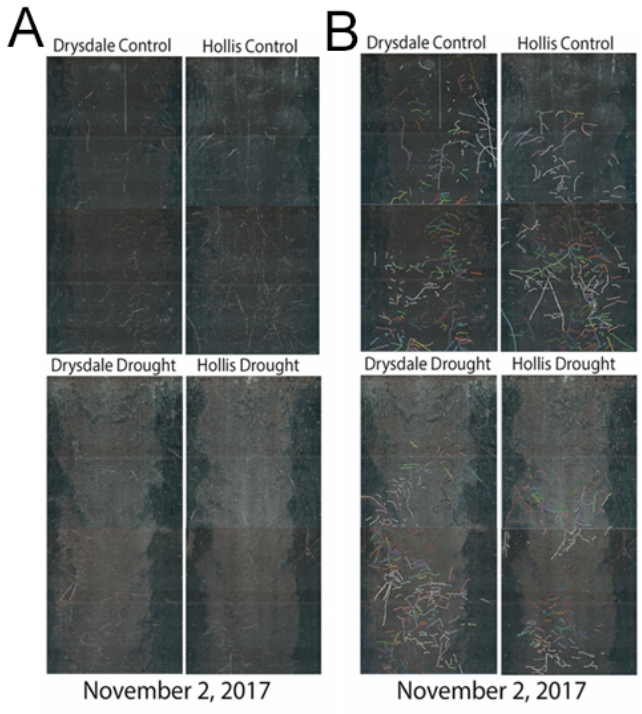

Figure 3.4: Analysis of root growth response to drought stress. **A,** Representative images of roots in control and drought stress bins for Drysdale and Hollis for each of the 1 timepoints analyzed**. B,** Representative images of root analysis using RootSnap! Program for control and drought stress bins.

Root images were used to measure total root length, total root count, total root volume, total root area, and root diameter. Of these measurements, the total root length and total root count were the most

informative because tracking the root thickness in bins with WVC was not possible due to lower image resolution (**Figure 3.3**). Total root length and total root count were used to assess changes of root architecture under drought stress. Both parameters correlated with each other at first, second, and third measurements with R^2=0.92, 0.86, and 0.94 respectively.

Genotype-specific patterns of root growth were observed under both drought and unstressed conditions (**Figure 3.5**). There were three patterns of root response to drought stress: (i) root growth was not affected by drought in Drysdale and Dharwar Dry; (ii) root growth was inhibited by drought in Hollis, Alpowa and Louise; and (iii) root growth was reduced at the later stages of plant development in Onas and AUS28451.

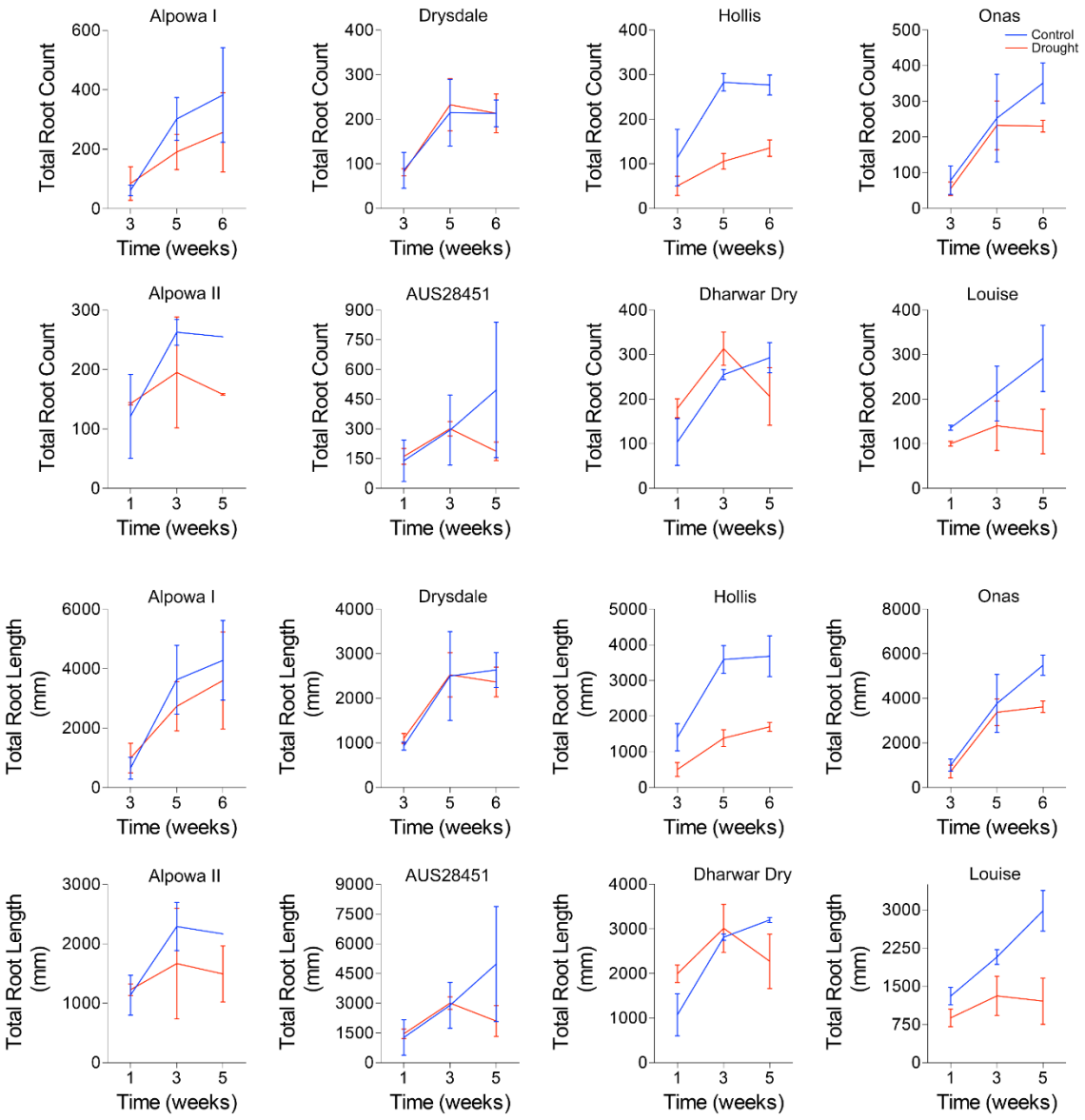

Figure 3.5: Impact of drought stress on total root count and total root length of seven genotypes. Alpowa was measured in two independent experiments shown on separate charts.

Both sets of experiments, on average, had similar number of roots and length of roots at the beginning of the drought stress. There was a proliferation of root growth during the first two time points in all genotypes under both conditions, except for the genotype Hollis. Alpowa was repeated in both sets and the control displayed similar growth patterns, indicating that the conditions were similar. In set 2, under drought,

Alpowa had fewer roots compared to the control, which could be due to the vernalization of seedlings or due to the drought. Alpowa and AUS28451 displayed large variation in root count and root length in unstressed condition, especially at the later time point. This could be due to variation in plant growth, as some plants were entering reproductive stage (Zadoks 35-40 for Alpowa, Zadoks 60 for Hollis). Onas, Drysdale, and Dharwar Dry root growth was not affected by drought as severely as in case of other genotypes. Onas maintained root growth until the last time point (under 8% VWC). Drysdale did not have any significant differences in root count and root growth between the control and the drought stress, indicating that Drysdale does not respond to drought stress through altering root architecture. Although, the number of roots based on root count is lower in Drysdale than other genotypes for the unstressed conditions. Dharwar Dry was the only genotype to have more roots and longer roots under drought stress compared to the unstressed conditions until the last point.

Hollis, under drought stress, showed increased root number (root count) and root length, relative to the unstressed control. Louise also showed root growth under drought, although lower than in Hollis, until the last time point of the drought stress. Roots in Louise under control conditions continued growing in almost linear fashion, whereas under drought the roots grow as in the control the VWC reached 8%. Generally, the drought inhibited root growth in all genotypes between the last two time points.

Section 4: Peroxisome Phenotyping

During the drought stress leaf material was sampled for analysis of peroxisome abundance. For set 1, the leaf material was sampled twice corresponding to weeks 6 and 7 (**Figure 3.6**). While collected, the material for the second appeared unreliable and was not included in the analysis. The material for the second set was harvested when the plants have started reproductive phase, during or after anthesis (Zadoks 60+) and the plants were under a severe drought. These factors make the peroxisome abundance for set 2 inaccurate as once the plants reach or finish anthesis, leaves start senescence (Xie et al. 2016). Generally, drought stress caused higher peroxisome abundance in all genotypes at least at one time point with exception of Drysdale. Statistically significant differences were observed in Alpowa at 6 weeks and Hollis both time points. Hollis root growth was inhibited by drought. Drysdale's root growth and peroxisome abundance was unaffected by drought stress.

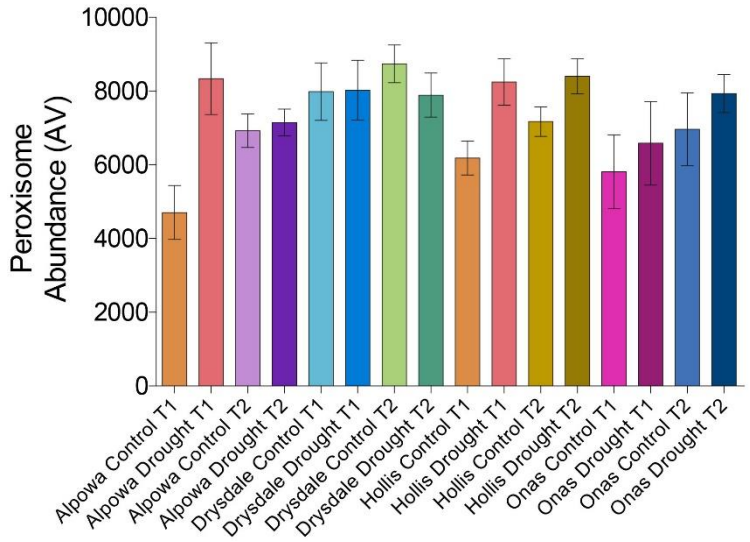

Figure 3.6: Impact of drought on peroxisome abundance.

Section 5: Plant Yield and Morphology

We collected the following yield parameters at maturity: height, spike number per plant, grain yield per spike, and total yield per plant (**Figure 3.7**). Total grain yield was significantly reduced in all genotypes, whereas plant height was lower in genotypes with exception of Dharwar Dry. In the first set, the number of spikes was counted per plant in each pot (5 plants), while in the second set the number of spikes was counted per pot (2 pots for controls and 3 for drought) therefore the comparison for spikes will be within each individual set.

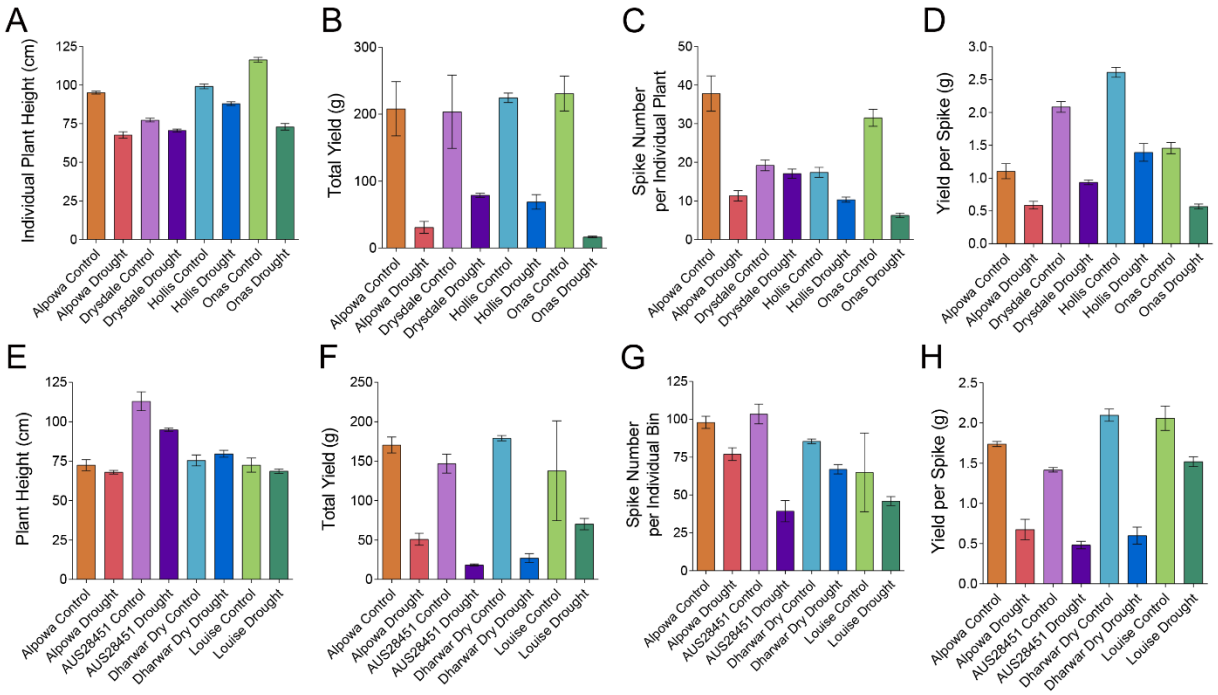

Figure 3.7: Impact of drought on yield. **A, E,** Plant height (cm). **B**, **F**, Yield (g). **C,** Number of spikes per plant. **D**, **H,** Yield per spike (g). **G,** Number of spikes per bin.

In set 1, all genotypes had similar total yield (g) under unstressed conditions that was reduced under drought. Hollis and Drysdale showed similar total yield (g) under drought stress, higher than total yield (g) of Alpowa and Onas (**Figure 3.7B**). The

number of spikes per plant in Drysdale was not affected by drought (**Figure 3.7C**), whereas the number of spikes per plant was reduced in all other genotypes. Although, Hollis and Drysdale had the highest yield per spikes under control conditions, Alpowa and Onas had more spikes (**Figure 3.7C-D**). Hollis under drought conditions had a higher grain yield per spike similar to that of Onas under control conditions. Drysdale and Hollis sustained higher yield under drought stress relative to Alpowa and Onas; however, the structure of the yield was different: the number of spikes per plant was significantly lower in Hollis than in the Drysdale, whereas the grain weight per spike was greater in Hollis. Hollis also had the highest yield per spike under control conditions in both sets, meaning this genotype can increase the size and weight of the grain in each spike or produce more seeds in each spike compared to the others.

In set 2, total yield and yield per spike were radically reduced in AUS28451 compared to other genotypes (**Figure 3.7F, H**). Louise total yield (g) under unstressed conditions was variable due to unexplainable reduction of yield in one bin. Additionally, Louise sustained the yield per bin while the yield per bind in other 3 genotypes was significantly reduced.

Section 6: Correlation of Yield under Drought

The relationship between the experimental parameters was examined using principal component analysis (**Figure 3.8**). Volumetric soil moisture content at all three time points correlated positively with the yield (R^2=0.66, 0.68, 0.79 respectively). Interestingly, both Total Root Count and Total Root Length at time point 3 correlated

negatively with yield (R^2=0.49 and 0.61 respectively) under drought conditions. Under normal watering we also observed negative correlation between these parameters (R^2=0.41 and 0.64). It indicates that a bigger root system at the later stages of plant development imposes yield costs regardless of the soil moisture content.

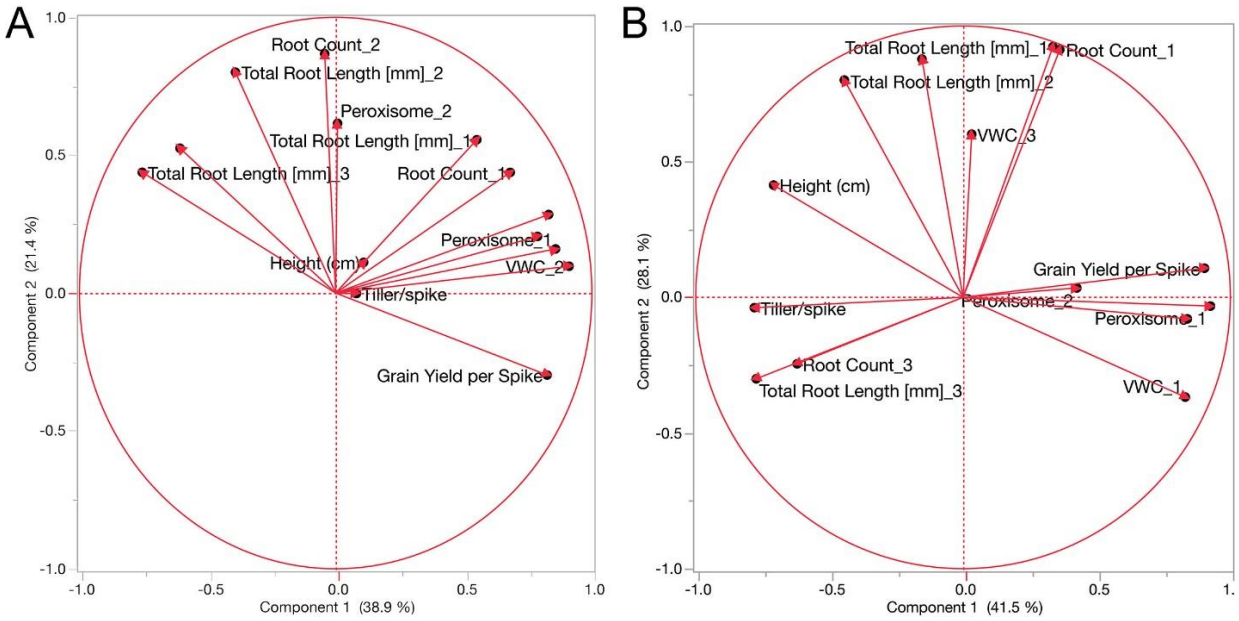

Figure 3.8: Principal component analysis of the relationships between yield, root parameters, and peroxisomes in our experiments under drought conditions (**A**) or normal watering (**B**).

Peroxisome abundance in leaves was measured at two time points and root architecture was measured at three time points. First peroxisomal measurement (Peroxisome_1) coincided with the third root measurement (Total Root Lentgh_3 and Root Count_3). At this time, there was a strong negative correlation between total root length or total root count and peroxisome abundance values in drought-stressed plants (R^2=-0.54 and -0.48 respectively). We observed no correlation between the second peroxisome measurement (Peroxisome_2) and root parameters, most likely because these parameters were collected at different time points. There also was a strong positive correlation between peroxisome abundance at the early stress point

(Peroxisome_1) and yield (Grain Yield Per Spike; R^2=0.75), but negative correlation between peroxisome abundance at the later drought stress (Peroxisome_2) and stress (R^2=-0.55). This is consistent with the fact that increase of peroxisome abundance under drought is the consequence of oxidative stress, which causes oxidative damage and lower yield. It also indicates that drought avoidance by increasing root architecture may not be as efficient as tolerance through ROS scavenging.

Section 7: Discussion and Conclusions

Using large 55-gallon containers, in-situ soil cameras, and soil moisture probes, morphological responses roots of wheat plants to reduction of soil moisture were captured over the growth season. This set up resembles the field situation where moisture can be accessed at a deeper soil level, which is a common drought avoidance mechanism. Root growth was monitored in seven wheat genotypes under well-watering and drought stressed conditions, revealing different root strategies to overcome the drought stress.

Comparison of the wheat genotypes demonstrated different strategies for drought tolerance. On the developmental level, Hollis relies on the drought escape to a greater extent than the other genotypes. First, Hollis enters flowering stage one week before Drysdale, and 3-4 weeks before Onas or Alpowa. Onas and Alpowa displayed slower transition to flowering stage in comparison with Hollis and Drysdale, which could explain the significant differences in yield. Many spikes in Onas under drought stress did not form seeds. Reduction of grain yield due to reproductive defects including pollen

sterility, carbohydrate deprivation, and sucrose importation into the seeds has been reported in other crops under drought stress (Al-Ghzawi et al. 2009; Anderson et al. 2002; Farooq et al. 2015). All genotypes displayed significant yield loses under drought conditions, which is consistent with previous research on the effects of drought during grain filling.

Second, vegetative growth was reduced in Hollis as evident from reduced size of root system and lower tiller number. Onas and Alpowa exhibited the greatest decline in vegetative growth under drought stress. Longer time to heading has been reported to correlated with increased root proliferation (number of roots and root length; Ghimire et al. 2020). This could explain the smaller root system in Hollis compared to Drysdale, although time to heading was not included in the PCA analysis. Third, Hollis had larger grains and more grains per spike than the other genotypes. The latter could be due to greater grain sink strength and capacity, which is determined during the early stages of grain development. In previous studies Drysdale was found to be a water usage efficient variety (Condon et al. 2006) and showed that Drysdale had a constitutive advantage in a range of environments for most yield components except single seed weight (Parent et al. 2017). Alpowa and Onas in set 1, have higher vegetative growth under well-watered conditions (based on plant height) than Hollis and Drysdale. Both genotypes exhibited severe effects of reproduction as manifested by decline of total yield (g), spike number per plant, and yield pre spike.

Classical drought escape traits include early flowering and high metabolic rates (Basu et al. 2016; Shavrukov et al. 2017). Earlier transition to flowering may extend the

period of grain filling. High metabolic rates facilitate rapid development and accumulation of photoassimilates which could be used during grain filling stage. Grain weight is largely determined by starch accumulation (Ji et al. 2010; Rivera-Amado et al. 2020). Grain sink strength may influence biomass allocation from vegetative growth (roots) to reproductive (grain) (Schapendonk et al. 2007; Asseng et al. 2017; Rivera-Amado et al. 2020). Larger grain size is known to correlate with drought tolerance in rice (Uga et al. 2013) and wheat (Ji et al. 2010; Rivera-Amado et al. 2020).

Root system architecture is another source of drought resistance. Studies in rice (Henry et al. 2011; Uga et al. 2013), maize (Lynch 2013; Burton et al. 2014; Sebastian et al. 2016; Al-Naggar, Shafik & Elsheikh 2019), and wheat (Manschadi et al. 2006; Manschadi et al. 2008; Saradadevi et al. 2015; Ghimire et al. 2020) indicate that longer roots and sharper branching angle can reduce the yield loses by improving access to both soil moisture and nutrients. In our study, root length and root number under drought were significantly lower in Hollis than in the other genotypes. However, Drysdale and Alpowa do not have any significant differences in root length or root count under drought. This suggests Drysdale and Alpowa use drought avoidance mechanisms to maintain access to soil moisture in deeper soil profiles.

Production of longer roots in response to reduction of the soil moisture content contributes to drought avoidance by providing greater access to soil moisture. Root growth under low water potential was reported as a drought avoidance trait in wheat (Dalal et al. 2018), Arabidopsis (van der Weele et al. 2000), soybean (Yamaguchi et al. 2010; Yamaguchi & Sharp 2010; Song et al. 2016), and maize (Sharp, Silk & Hsiao

1988; Lynch 2013; Al-Naggar et al. 2019). Consistent with these reports, Drysdale root growth continues during period of drought. However, despite a larger root system, the reduction in soil moisture content in containers with Drysdale was similar to that in Hollis. This outcome is consistent with reductions in stomatal conductance in both varieties. Furthermore, reduced stomatal conductance in Drysdale occurs even when roots have access to soil moisture (Schoppach & Sadok 2012). It means, genotypes with efficient water usage can take advantage of the bigger and deeper root system in deep soils.

We found that under drought conditions, root system size correlated negatively with peroxisome abundance at the later wheat development stages (after Zadoks stage 49). This means that: (i) plants with smaller root system exhibited higher peroxisome abundance and plants with bigger root system exhibited lower peroxisome abundance; and (ii) peroxisomes can inform on the size of root system under drought. We also found that yield correlated negatively with the root system size. In terms of wheat breeding practice, it means that longer and more branched root system does not guarantee higher yield under drought. One explanation for this outcome is that smaller root system could be more efficient in extracting soil moisture.

Phenotyping root architecture under different environmental conditions remains challenging, which in turn limits the knowledge about desired root traits that could be exploited for breeding new varieties with advanced performance in arid climates. Phenotyping roots of wheat plants in field setting is complicated by the environmental factors, and complexity of soil medium and profiles. Traditional greenhouse containers

are too shallow to capture the full growth of wheat roots. Therefore, this experiment looked to develop a better technique for phenotyping roots under greenhouse conditions. Using in-situ cameras, we found that root count and root length are indicators of drought tolerance mechanisms. Drought escape through arresting root growth, drought avoidance through increasing root system size, and drought tolerance through ROS scavenging have comparable contributions to sustaining the yield.

CHAPTER 4: ANALYSIS OF PHOTOSYNTHESIS AND REACTIVE OXYGEN SPECIES UNDER DROUGHT STRESS

A portion of the figures and text was published in *Cells*. Magnus Wood performed the photosystem I analysis and helped with setting up the phenomic chamber used for chlorophyll fluorescence measurements. Jessica Fisher aided in analysis of ROS scavengers.

Hickey, K., Sexton, T., Wood, M., Sahin, Y., Nazarov, T., Fisher, J., Sanguinet, K., Kichhoff, H., Cousins, A., Smertenko, A. 2022. Drought tolerance strategies and autophagy in resilient wheat genotypes. Cells, 11, 1765. doi.org/10.3390/cells11111765.

Individual author contributions for the original *Cells* manuscript are listed below:

Conceptualization, A.S., H.K. and K.A.S.; methodology K.A.S.; formal analysis, K.H. and M.W.; investigation, K.H., T.S., T.N., M.W., Y.S. and J.F.; writing—original draft preparation, K.H.; writing—review and editing, T.S., M.W., Y.S., T.N., K.A.S., H.K., A.C. and A.S.; supervision, A.S., H.K., K.A.S. and A.C.; funding acquisition, A.S., H.K., K.A.S. and A.C. All authors have read and agreed to the published version of the manuscript.

Section 1: Introduction and Rational

Section 2: Wheat Variety Selection

Section 3: Environmental Profiling of Phenomic Chamber

Section 4: Photosynthetic and Biochemical Profiling of 5 wheat genotypes

Section 5: Discussion and Conclusions

Section 1: Introduction and Rationale

The goal of this project was to understand the effects of drought on photosynthesis and ROS homeostasis. The project started with 17 genotypes of varying drought-tolerance and 5 genotypes were ultimately selected for in-depth characterization. The objectives of this project were: (1) to identify genotypes that exhibit drought tolerance; (2) to understand how duration and severity of drought effects photosynthesis, ROS homeostasis, and peroxisome dynamics; (3) to identify when peroxisomes respond to water-deficiency; and (4) to understand how photosynthetic and peroxisomal responses lead to difference in drought tolerance. The hypothesis is: drought-tolerant genotypes will be able to maintain the same level of photosynthesis under severe drought conditions. The level of peroxisomes will increase to stabilize ROS homeostasis and ensure that the intracellular effects of drought do not overwhelm the plant's cells.

Section 2: Wheat Variety Selection

To accomplish these goals 17 genotypes were phenotyped using phenomic platform: 3 reference lines (Alpowa, Berkut, and Onas); 10 AFRI grant lines (Agawam, Drysdale, Dayn, Hollis, IDO686, Lolo, McNeal, Otis, Patwin515, and WA8910); and 4 landraces from a spring wheat genetic diversity panel (LDRC5, 16, 33, 37; Jordan et al. 2019; Blake et al. 2019). These lines were exposed to a drought stress through withholding watering and monitored for photosynthetic parameters using a phenomics platform. The drought stress was monitored by collecting volumetric water content. Peroxisome abundance was tested once the plants VWC decreased under 0.2%. Chlorophyll fluorescence images were captured twice per day, once in the day and once at night. The imaging data was used to measure the following photosynthetic parameters: Fv/Fm (fluorescence quantum yield), ϕ_{PSII} (quantum yield of photosystem II photochemistry) determined after the 300 second light period), non-photochemical quenching (NPQ, determined after the 300 second light period), and NPQ components: energy dependent quenching *qE*, photoinhibition *qI*, and fraction of open PSII centers *qL.*

The 17 genotypes were split into 2 groups for testing because of the limited room size. The first group comprised Alpowa, Berkut, Onas, Agawam, Drysdale, Dayn, Hollis, IDO686, Lolo, McNeal. The second set included: Alpowa, Berkut, Onas, Otis, Patwin515, WA8910, LDRC 5, LDRC 16, LDRC 33, LDRC 37. Alpowa and Onas were included in both sets as the reference controls to measure the difference between both sets.

Each genotype was transplanted after sprouting into two 21” x 15” trays with 8 replicates, and the trays were randomized in the chamber room. Every tray had a soil moisture probe to monitor volumetric water content. One tray was watered regularly through the experiment, the other tray was watered until the start of the drought stress. Plants were left for 5 days to acclimate in the growth chamber before the drought stress. Drought stress was induced by withholding the watering until the volumetric water content was under 0.2% for most of the trays. The plants were between Zadok’s 22-24 stages and the drought stress lasted for 17 days.

On the last day of the drought stress (day 17), each genotype was sampled for peroxisome abundance. The base of the flag leaf was collected. Peroxisome abundance was assayed as described in the Method section. The chlorophyll fluorescence images were collected during the night and analyzed manually.

Both rounds of phenomics experiments had variation in the drying time of the trays. For trays in set 1, the dry down stage was reached after 14 to 17 days of drought. For set 2, the dry down was reached after 11 to 17 days, though, majority of the trays reached dry down point after 14 days to 17 days. The pattern of dry down was similar in both sets, although faster in set 2 compared to set 1. The trays in set 2 started at a higher soil moisture and lost soil moisture faster than set 1. In set 1, genotypes either had minimal responses to the drought compared to the well-watered, or the

photosynthetic responses declined (**Figure 4.1**). Drysdale, Hollis, IDO686, and Lolo showed decline of the fluorescence quantum yield (**Figure 4.1A**), ϕ_{PSII} (quantum yield of photosystem II photochemistry; **Figure 4.1B**) and non-photochemical quenching (**Figure 4.1C**). Except for Drysdale, these genotypes also lacked a peroxisomal response to the drought (**Figure 4.1D**). In set 2, the changes in photosynthetic parameters were not as pronounced. The quantum yield of all the genotypes had an insignificant decline. There was a decline in photosynthetic parameters under drought stress in both sets (**Figure 4.1**).

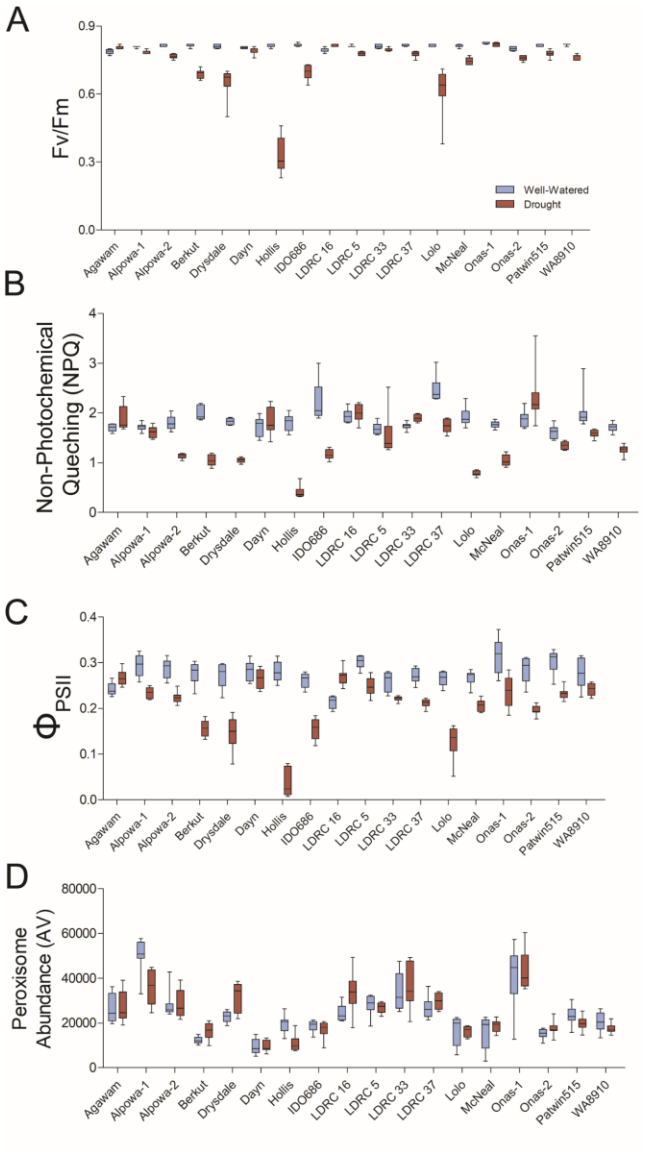

Figure 4.1: Impact of drought on the photosynthetic parameters and peroxisome abundance in 17 genotypes. **A,** The quantum efficiency of open photosystem II centers (F_v/F_m). **B,** Quantum yield of photosystem II photochemistry (ϕ_{PSII}). **C,** Non-photochemical quenching (NPQ). **D,** peroxisome abundance. The values represent the mean±SD of 5 biological replicates for both control and drought treatments.

There were limitations in this experiment. First, the phenomics imaging platform did not capture images every day of the drought due to mechanical failures. This did not affect the overall results, as the mechanical issues were able to be fixed leading to one- or two-day gaps during the middle drought stress. Second, the main limitation of this experiment was the chamber environment. When the repeated genotypes (Alpowa and Onas) were analyzed, there was high variability in photosynthetic parameters (**Figure 4.2**). The second set had significant changes in photosynthetic parameters in Aplowa and Onas, indicating that the drought stress was more severe than in the first set (**Figure 4.2**). The VWC in the second set decreased at a faster rate for the two genotypes and reached >0.2% 2-3 days earlier than in the first set. Although the genotypes in the second set took 11-17 days to reach the severe drought, the overall trend was a sharper decrease of VWC in the second set than in the first, which occurred over a range of 14-17 days.

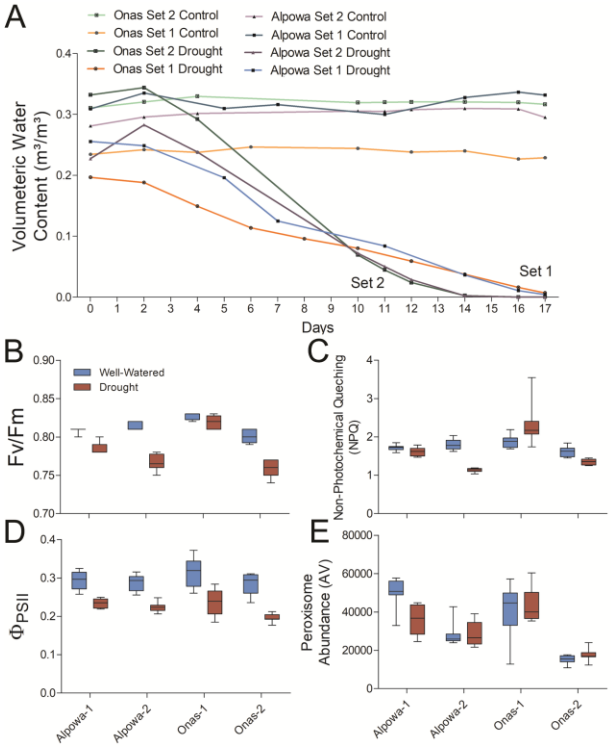

Figure 4.2: Impact of drought on the photosynthetic parameters and peroxisome abundance in Alpowa and Onas in both sets of experiments. **A,** Volumetric water content (VWC) at the corresponding time points for both sets of experiments. **B,** The quantum efficiency of open photosystem II centers (F_v/F_m). **C,** Quantum yield of photosystem II photochemistry (ϕ_{PSII}). **D,** Non-photochemical quenching (NPQ). **E,** Peroxisome abundance. The values represent the mean±SD of 5 biological replicates for both control and drought treatments.

In addition to the variation in VWC, there were differences in photosynthetic parameters. Decline of F_v/F_m (fluorescence quantum yield) in set 1 indicated severe

inhibition of photosynthesis, whereas there were almost no changes of F_v/F_m due to drought in set 2. Peroxisome abundance was sampled at the end of the 17 days, when VWC reached >0.2% all the trays. No significant changes of peroxisome abundance could be due the sampling was performed too late in the drought stress.

Section 3: Environmental Profiling of Phenomic Chamber

This variability between the two sets indicated that the room environment was a significant factor that affected the dynamics of response to the drought stress in all genotypes. To test the role of environment in the different kinetics of drought, the following experiment examined regions in the room subjected to the highest environmental fluctuations. Once identified, that region could be avoided or controlled during subsequent experiments. For this experiment, 6 genotypes were selected from the original 18: Agawam, Drysdale, Hollis, Lolo, Onas, and Patwin515. These genotypes were selected based in the photosynthetic parameters of F_v/F_m (fluorescence quantum yield), ϕ_{PSII} (quantum yield of photosystem II photochemistry), and non-photochemical quenching (NPQ). Using yield under drought as a criterion, we selected three high-yielding genotypes (Agawam, Drysdale, and Hollis) and two low-yielding genotypes (Patwin 515 and IDO686). Onas was included in both sets for normalization. Furthermore, Onas displayed low proliferation of peroxisomes to drought which could provide a baseline in this experiment.

The 6 genotypes were then germinated and transplanted in 21” x 15” trays. Each tray contained one plant for each genotype located in the place of every tray. Ten trays

were used as watered controls, and 10 trays were exposed to drought stress. The trays were oriented in the same direction in the chamber and randomized to reduce the variation between the replicates. All drought trays and 5 well-watered trays (15 trays in total) were monitored with soil moisture loggers. 5 well-watered trays were monitored manually with a soil moisture probe every day to ensure the soil moisture was maintained. The drought stress was imposed by withholding water. Drought stress lasted 11 days, then the watering was resumed to analyse plant responses during the recovery phase. Fluorescence images were acquired once during the day and during the night. The images collected during the night were analysed for photosynthetic parameters described above. Leaf material for peroxisome abundance was collected when the VWC reached ca. 0.2% for all trays under drought. All leaf material was collected during the same sampling period.

We found some variability of the photosynthetic parameters in different room locations (**Figure 4.3**). Most of the variation was in the first two days of drought. Patwin515 had a steady F_v/F_m even at the end of the drought treatment, with small variation meaning that the drought stress was not as severe as in previous experiments (**Figure 4.3A**). All genotypes had a decline in ϕ_{PSII} that the plants experienced drought stress ((**Figure 4.3B**). Lolo and Patwin515 also had similar patterns. Patwin515 and Drysdale showing higher NPQ under severe drought compared to Lolo and Hollis (**Figure 4.3C)** which indicated Hollis and Drysdale had similar patterns for all photosynthetic parameters with exception of NPQ. Peroxisome abundance was assayed following the procedure described above. Three genotypes, Agawam, Hollis, and Lolo showed a significant decline of peroxisome abundance whereas Drysdale,

Patwin515, and Onas had no significant difference between stressed and well-watered samples (**Figure 4.3D**). Taken together, the drought responses in the first set of experiments were weak due to the mild drought stress caused by tray position in the room. In the second set of experiments the stress response was more consistent though timing peroxisome abundance could be better optimized.

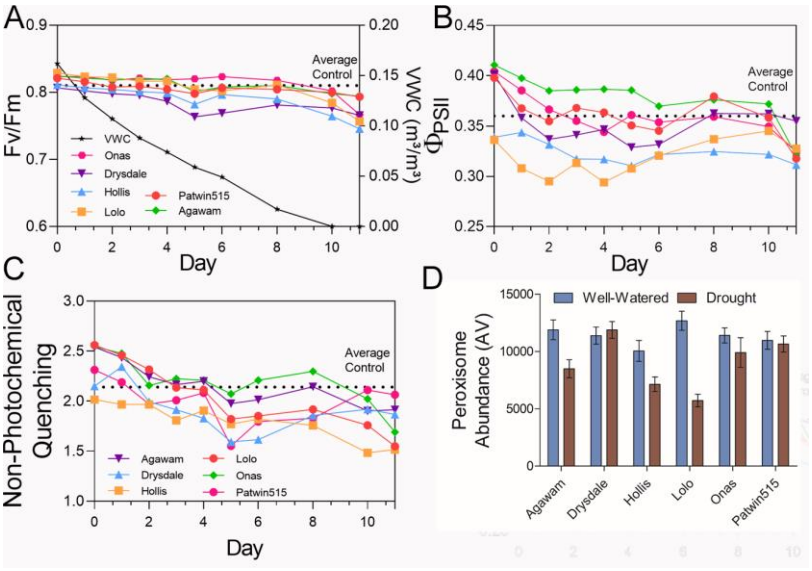

Figure 4.3: Impact of location on photosynthetic parameters and peroxisome abundance in phenomic chamber. Charts are depicting drought responses only. **A,** The quantum efficiency of open photosystem II centers (F_v/F_m). The right Y-axis shows volumetric water content (VWC) at the corresponding time points. **B,** Quantum yield of photosystem II photochemistry (ϕ_{PSII}) **C,** Non-photochemical quenching (NPQ). **D,** peroxisome abundance. The values represent the mean±SD of 8 biological replicates for and drought treatments.

Section 4: Photosynthetic and Biochemical Profiling of 5 wheat genotypes

Based on the previous experiments, 5 genotypes with different drought tolerance in the field and photosynthetic dynamics under drought were selected. Two drought tolerant genotypes based on Washington State University Wheat and Small Grains Variety Selection and Testing database (http://variety.wsu.edu/2013/index.htm) were selected: Drysdale and Hollis. Drysdale is a hard white spring wheat that was bred for water use efficiency under drought conditions (Condon, Richards, Rebetzke & Farquhar 2004). Hollis is a hard red spring wheat (Kidwell *et al.* 2004) selected for maintaining high yield (29 bushels per acre) in locations with annual precipitation below 12"

(http://smallgrains.wsu.edu/variety/). The 3 other genotypes have low yield under drought and are Lolo (Souza E, Guttieri M and McLean R, 2003), IDO686, and Patwin515. For this experiment, the 5 genotypes were split into 2 groups (Drysdale, Hollis, and Patwin515; Lolo and IDO686) and exposed to a nine-day drought or an eleven-day drought, respectively.

The experimental design reproduced the previous round with the major change being in the number of seedlings per tray. Five trays destined for drought stress were populated with 15 seedlings each and two trays for watered control trays were populated with 35 seedlings each. The growth conditions and drought treatment were as described above. After the onset of drought, leaf material was collected daily from one plant per each drought stress tray making 5 biological replicates per genotype and five randomly selected plants from the watered control. The bottom third part of each leaf was flash-frozen in liquid nitrogen and stored at -80°C for biochemical assays. The rest of the plant was cut at the below-ground level using scissors and discarded.

The drought stress caused a decline in photosynthesis in all genotypes, which was assessed by measuring chlorophyll fluorescence. These measurements revealed that photosynthesis is unaffected until the VWC decreases below 1%. The F_v/F_m (quantum yield) and ϕ_{PSII} declined in all genotypes with exception of Drysdale where the decline was mild (**Figure 4.4**). All chlorophyll fluorescence values decline significantly for Lolo and IDO686 when the VWC dropped below 1%. Lolo and IDO686 both exhibit stable NPQ values under drought compared to the well-watered control but had a higher high-energy quenching (qE) values throughout the drought stress, which could be the

mechanism that both genotypes use to overcome the drought stress pressure on photosynthesis (**Figure 4.4**). The NPQ values were significantly lower at all time points in Hollis and in particular at VWC values below 1% (**Figure 4.4**). Analysis of two NPQ components, high-energy quenching (qE) and photoinhibitory-dependent quenching (qI) showed similar qE for all genotypes in set 1, but significantly higher qI values in Drysdale (**Figure 4.4**). Patwin515 had a similar response as Drysdale compared to Hollis, although Patwin515 showed a steady decline for all the parameters.

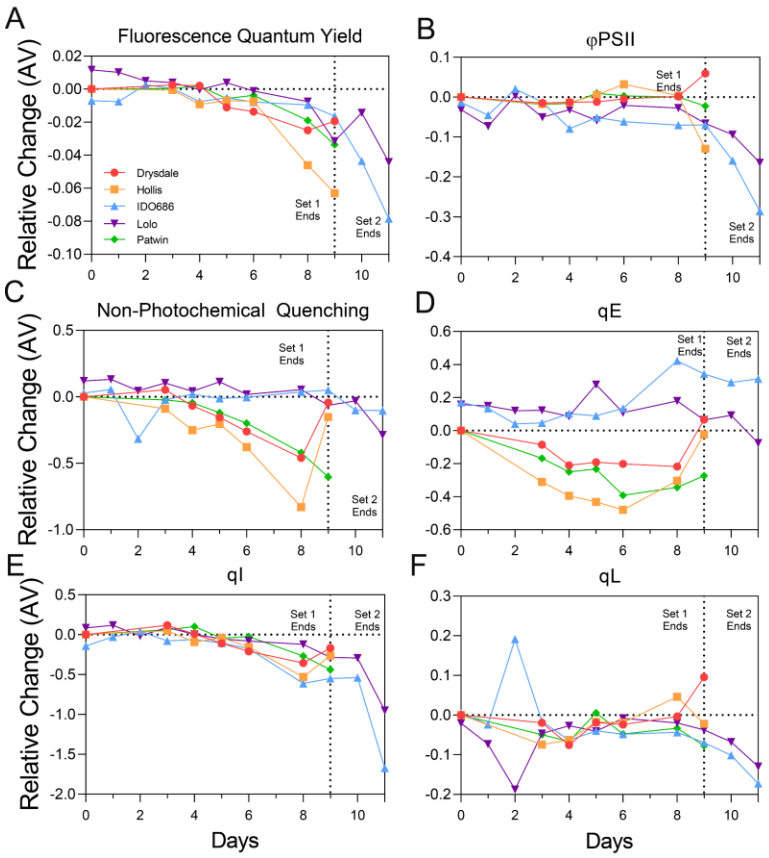

Figure 4.4: Impact of drought on photosynthetic parameters. **A,** Quantum yield of photosystem II photochemistry (ϕ_{PSII}). The right Y-axis shows volumetric water content (VWC) at the corresponding time points. **B,** The quantum efficiency of open photosystem II centers (F_v/F_m). **C,** Non-photochemical quenching (NPQ). **D,** Energy-dependent quenching (qE). **E**, Photoinhibitory quenching (qI). **F,** Open photosystem II centers (qL). The values represent the mean±SD of 5 biological replicates for both control and drought treatments.

There were two genotypes that had different photosynthetic responses within one set, Drysdale and Hollis. The two genotypes had similar F_v/F_m and ϕ_{PSII} until VWC decreased below 1%, when Hollis both parameters declined significantly indicating damages of photosystem II (**Figure 4.4**). Lower ϕ_{PSII} values in Hollis under these conditions denote lower linear electron transport rate. However, the fraction of photosystem II centers in open

(oxidized) state (qL) remained similar in both varieties under drought. Thus, the electron pressure on photosystem II in Hollis and Drysdale was similar.

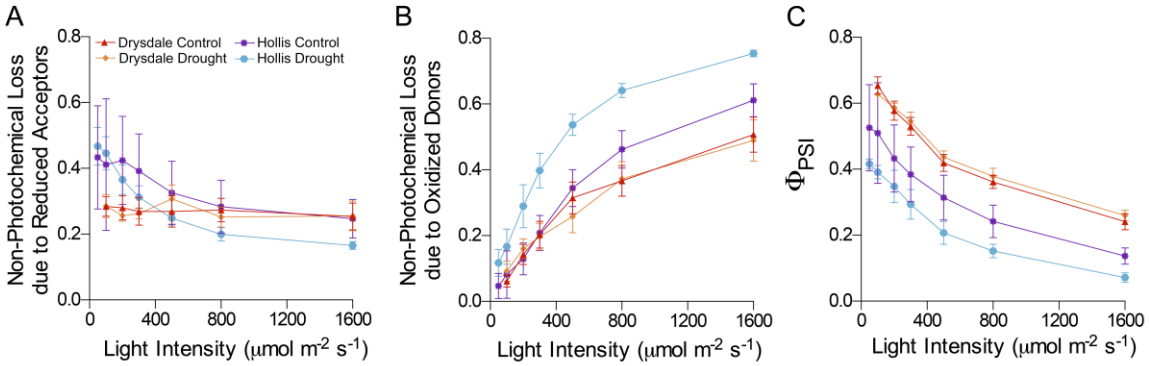

Figure 4.5: Photochemical analysis of photosystem I. **A,** Y(NA), non-photochemical loss due to reduced acceptors. **B,** Y(ND), non-photochemical loss due to oxidized donors. **C,** Y(I), photoefficiency of photosystem I. The values represent the mean values ±SEM of 5 biological replicates for both control and drought conditions. This figure was original published in *Hickey et al. 2022, Cells*

To further compare the electron flow in Hollis and Drysdale, we analysed photosystem I under 1% VWC (**Figure 4.5**). The quantum yield of photosystem I photochemistry (ϕ_{PSI}) values were significantly lower in Hollis under normal watering and further decreased under drought. We examined the reason for this difference by measuring the non-photochemical loss due to oxidized electron donors and reduced electron acceptors. According to this analysis, reduction of ϕ_{PSI} in Hollis under drought is mostly caused by the donor site limitation rather than the acceptor site limitation, whereas ϕ_{PSI} in Drysdale was not affected. This implies that electron transport between photosystem I and II is limited to a greater extend in Hollis than in Drysdale in line with the more reduced primary quinone, QA of PSII (lower qL parameter).

Complexity of the reactions responsible for maintenance for ROS homeostasis can be assessed using peroxisome abundance (Smertenko 2017). All 5 genotypes were assayed for the peroxisome abundance at different time points of the drought stress (**Figure 4.6A**). We found that there was a general increase in peroxisome abundance in all genotypes for at least one time point, but Hollis and Lolo showed higher values when the VWC decreased below 4% and remained high relatively to control until the last day of the treatment (**Figure 4.6A**). Peroxisomes abundance in Drysdale and Patwin515 was not significantly affected throughout the drought time course. IDO686 peroxisome abundance was not affected till the VWC decreased below 2%.

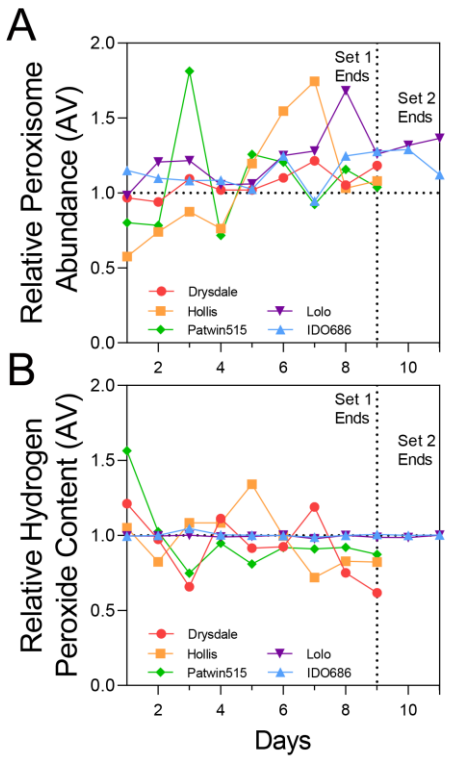

Figure 4.6: Relative Peroxisome abundance and hydrogen peroxide content. The charts show fold change of the peroxisome abundance and hydrogen peroxide in the drought-stressed samples relatively to the control. **A**, Peroxisome abundance. **B,** hydrogen peroxide content.

Next, all genotypes were assayed for hydrogen peroxide content. Lolo and IDO686 did not have any change in hydrogen peroxide content throughout the stress (**Figure17B**). Patwin515 had no significant increase compared to the control even during severe drought. Hollis and Drysdale both had peaks of hydrogen peroxide content, which coincided with the increase of peroxisome abundance. Therefore, Hollis and Drysdale were used to measure activity of ROS scavengers.

Analysis of ROS scavenging activity in leaf material collected during drought stress time course was used to measure superoxide dismutase (SOD), catalase (CAT), guaiacol peroxidase (GPX) and ascorbate peroxidase (APX) activity (**Figure 4.7**). SOD was more active in Hollis during beginning of drought and in Drysdale during later stages of drought compared to the well-watered control (**Figure 4.7A**). Catalase and guaiacol peroxidase were more active during later stages of drought in both genotypes (**Figure 4.7B, C**). Activity of ascorbate peroxidase in Drysdale was higher in the middle of the stress whereas in Hollis the activity was higher toward the later drought stages (**Figure 4.7D**). These results demonstrate that both genotypes use different components of the hydrogen peroxide scavenging throughout the drought stress in a dynamic fashion.

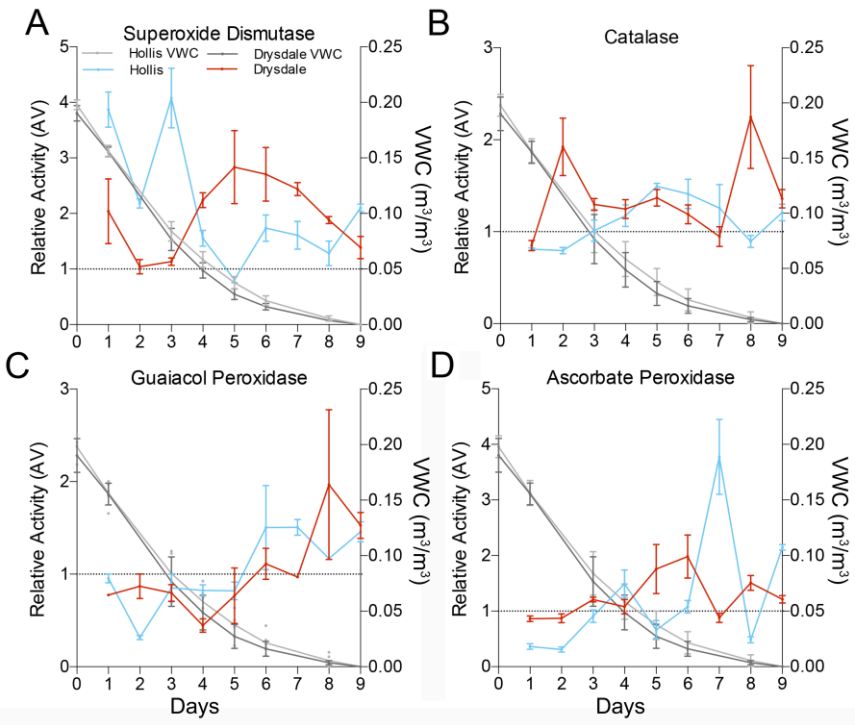

Figure 4.7: Relative activity of ROS scavenging enzymes during drought stress. The charts show fold change of the enzyme activity in the drought-stressed samples relatively to the control for genotypes Hollis and Drysdale. The right Y-axis shows volumetric water content (VWC) at the corresponding time points. **A**, Superoxide dismutase. **B**, Catalase. **C**, Guaiacol peroxidase. **D**, Ascorbate peroxidase. This figure was original published in *Hickey et al. 2022, Cells*.

Section 5: Discussion and Conclusions

This study profiled photosynthetic efficiency under drought stress by measuring chlorophyll fluorescence in a time-dependent manner. This approach has been applied to many crops including barley, bean, and rice. Maintaining photosynthetic efficiency was shown to be an essential drought tolerance mechanism in all plants examined thus far including rice, maize, wheat, and barley (Guo et al. 2008; Murchie & Lawson 2013; Eisenhut et al. 2017). Seventeen genotypes of varying drought tolerance were selected to identify how photosynthesis and ROS homeostasis contribute to drought tolerance. Subsequently, 5 genotypes were selected for in-depth profiling of ROS metabolism and peroxisome response. Out of these 5 genotypes, Drysdale and Hollis were selected for a more detailed profiling of photosynthetic parameters including PS1 kinetics and activity of ROS scavenging system.

One of the biggest limitations of this study was the environmental variability in different parts of the phenomics chamber. Uneven dry down within the same experiment and between experimental sets, made interpretation of the data challenging. To overcome this problem, photosynthetic changes and ROS responses were compared based on the soil VWC and not on the number of days. It was found that majority of drought responses can be seen when soil VWC declined below 2%, and significant responses are seen when VWC was below 1%, indicating that selected genotypes have a robust general response to drought stress. This outcome suggests that domestication of wheat in arid climates involved mechanisms of robust ROS homeostasis.

Out of the 5 genotypes, Drysdale and Hollis are classified as high yielding in climate zones with very rainfall (drought tolerant) and the other 3, Lolo, IDO686, and Patwin515 are classified as low yielding under water limiting conditions (drought sensitive). In our experiment, all genotypes maintained F_v/F_m and ϕPSII at the VWC above 1%. The decline in F_v/F_m at severe drought in Hollis and IDO686 provides evidence for a photooxidative damage to photosystem II (**Figure 15**). Consequently, the decrease in linear electron transport rates (indicated by ϕPSII, seen in both genotypes) could be the consequence of a slower electron injection by PSII into the electron transfer chain (Long et al. 1994; Murata et al, 2007).

Slower electron injection could lead to excess of energy which can be dissipated through NPQ. Higher NPQ were reported in drought tolerant tomato (Mishra et al. 2012), maize (Efeoğlu et al. 2009), rice (Pieters & El Souki 2005; Faseela et al. 2020) and barley (Li, Guo, Michael, Stefania & Salvatore 2006; Guo et al. 2008). Consistent with these findings, we observed similar NPQ values in all genotypes at VWC>1%. However, there were differences in NPQ between the two sets, and Drysdale, Hollis, and Patwin515 exhibited decline in NPQ values below 1% (**Figure 4.4**).

Analysis of two NPQ components demonstrates similar patterns for fast relaxing component of the NPQ, qE, in both sets (set 2 is higher than set 1) but lower slower-relaxing component of NPQ, qI, under drought in all genotypes (**Figure 4.4**). Lolo and IDO686 showed significant photoinhibition at VWC values below 1%. A part of the slower-relaxing component could be zeaxanthin-dependent quenching (Nilkens et al. 2010).

The observed increase in NPQ in Drysdale relative to Hollis under severe drought is likely to be responsible for reducing the photodamage to photosystem II and maintaining higher Fv/Fm. Whereas Fv/Fm decline in Hollis is indicative of photodamage to photosystem II. Although, another reason for reduced Fv/Fm and ϕPSII in response to drought could be limitations of the electron flux through PSI (Tietz et al. 2015; Klughammer & Schreiber 2016). The ϕPSI values were significantly lower in Hollis under normal watering and further decreased under drought (**Figure 4.5C**). This suggests that drought causes reduction of the photosystem I donor sites (**Figure 4.5B**) ultimately leading to reduction of electron transport between photosystem II and I. This limitation could be caused by damage of the cytochrome b_6f complex by ROS (Kohzuma et al. 2009; Baniulis et al. 2013; Hura et al. 2018; Wada et al.2019) and indicates that Hollis is more likely to experience oxidative stress.

Accumulation of ROS in the chloroplast under drought inhibits photosynthesis by causing peroxidation of lipids and oxidative damages to the components of electron transfer chain (Foyer & Noctor 2000, 2003; Miller et al. 2010). Plants ameliorate oxidative damages by upregulating transcription of genes encoding ROS scavenging enzymes *SOD*, *CAT*, and peroxidases (Luna et al. 2005; Wang et al. 2008; Nikolaeva et al. 2010; Caverzan et al. 2016; Tyagi et al. 2021). Activity of ROS scavengers including catalase, SOD, ascorbate peroxidase, and glutathione reductase is upregulated in wheat leaves under drought stress (Sairam et al. 2002; Luna et al. 2004; Wang et al. 2008; Nikolaeva et al. 2010; Lou et al. 2018; Hasanuzzaman et al. 2019; Tyagi et al. 2021).

ROS homeostasis could be assessed indirectly by measuring the abundance of peroxisomes (Smertenko 2017). It has been shown that ROS production in peroxisomes under drought is balanced by higher activity of peroxisomal ROS-scavenging enzymes including catalase, ascorbate peroxidase, and superoxide dismutase (Mhamdi et al. 2012; Sofo et al. 2015; del Río & López-Huertas 2016; Waszczak et al. 2018; Ebeed et al. 2018). Patwin515, Hollis, and Lolo showed higher peroxisome abundance under drought. IDO686 and Drysdale marinated a steady level of peroxisomes under drought suggesting that these genotypes maintain ROS homeostasis using different mechanisms.

Hydrogen peroxide content in leaves was measured in all genotypes (**Figure 4.6A**). Drysdale and Hollis showed peaks of hydrogen peroxide content at about 1% VWC. Patwin515 had high hydrogen peroxide content in the beginning and maintaining lower content during the drought. However, Lolo and IDO686 did not show any changes in hydrogen peroxide content indicating: (1) the technical assay for hydrogen peroxide is not sensitive; (2) well-watered control was experiencing stress, therefore producing hydrogen peroxide at the same rates as the drought stressed plants; or (3) these genotypes are capable of decomposing the hydrogen peroxide at fast rate.

As Hollis and Drysdale displayed peaks of hydrogen peroxide content, both were expected to up-regulate ROS scavenging enzymes. Additionally, differences in the NPQ, F_v/F_m, and ϕ_{PSII} taken together with different electron flux through PSI indicate different strategies for handling the excess of ROS production. Therefore, these two genotypes were selected for a characterization of ROS scavengers. We found that Hollis mostly

relies on ROS scavenging to prevent oxidative damages, whereas Drysdale combines efficient NPQ and ROS scavenging.

Drysdale showed two peaks of catalase activity at the beginning and the end of the drought (**Figure 4.7B**). While Hollis catalase activity coincided with the peroxisome abundance peak towards the end of drought treatment. SOD activity increased in both genotypes, but to a greater degree in Hollis. SOD activity in Drysdale peaked during the middle of the drought (**Figure 4.7A**). Early activity of SOD could be a result of ROS production during photosynthesis. Reduction of SOD activity during early stages of drought stress in Hollis could leave the photosystems vulnerable to oxidative damages. This could explain the decline in F_v/F_m and ϕ_{PSII} discussed above.

Although, the overall activity of the ROS scavenging system was consistently elevated under drought stress in Hollis relative to Drysdale, activity of individual enzymes varied amongst independent experiments. For example, SOD activity was greater in Drysdale than in Hollis under VWC 0-1% (**Figure 4.7A**), whereas under comparable drought conditions SOD activity was somewhat higher in Drysdale than in Hollis. This variability reflects the non-linear nature of drought responses and some functional redundancy amongst the individual components of the redox system. Hence, measuring activity of ROS scavenging system with a limited set of enzymatic assays is prone to misinterpretation. Introducing integrative parameters, such as peroxisome abundance, provides more accurate means of assessing the status of the ROS scavenging system under drought stress.

Drysdale relies more on NPQ mechanisms for maintaining high photosynthetic rates under drought. Dynamic responses of ROS scavengers were found in both varieties. Hollis, though, exploits peroxisome abundance to combat stress-derived ROS and oxidative damages more efficiently than Drysdale. Peroxisomes appear to be an essential component of drought adaptation.

CHAPTER 5: GENETIC REGULATORS OF ROS HOMEOSTASIS AND PEROXISOME PROLIFERATION

A portion of the figures and text was published in *Cells*. Dr. Andrei Smertenko did the imaging of peroxisome staining in leaves. The RNA-Seq Analysis was done in collaboration with Dr. Yunus Sahin. qRT-PCR for *PEX11C* and *CAT* homoeologs was performed by Dr. Taras Nazarov.

Hickey, K., Sexton, T., Wood, M., Sahin, Y., Nazarov, T., Fisher, J., Sanguinet, K., Kichhoff, H., Cousins, A., Smertenko, A. 2022. Drought tolerance strategies and autophagy in resilient wheat genotypes. Cells, 11, 1765. doi.org/10.3390/cells11111765.

Individual author contributions for the original *Cells* manuscript are listed below:

Conceptualization, A.S., H.K. and K.A.S.; methodology K.A.S.; formal analysis, K.H. and M.W.; investigation, K.H., T.S., T.N., M.W., Y.S. and J.F.; writing—original draft preparation, K.H.; writing—review and editing, T.S., M.W., Y.S., T.N., K.A.S., H.K., A.C. and A.S.; supervision, A.S., H.K., K.A.S. and A.C.; funding acquisition, A.S., H.K., K.A.S. and A.C. All authors have read and agreed to the published version of the manuscript.

Section 1: Introduction and Rational

Section 2: Brief Overview of Methods

Section 3: Peroxisome Proliferation Gene Expression

Section 4: Catalase Dynamics

Section 5: Peroxisome Genetic Regulators

Section 6: Discussion and Future Direction

Section 1: Introduction and Rational

Cellular protection mechanisms including ROS scavenging and peroxisome proliferation provide a source of novel traits for advancing plant resilience. However, as measuring ROS homeostasis is challenging these traits remain underutilized in the breeding programs. Experiments described in Chapter 4 show that peroxisome abundance can be used as a proxy for the activity of ROS scavenging system. This chapter described analysis of genes responsible for peroxisome proliferation and the production of antibody and characterization of ROS-scavenging enzyme catalase. Additionally, the progress towards identifying genetic regulators of peroxisome proliferation will be discussed. Identification of genetic markers of peroxisome proliferation is essential for breeding wheat with greater stress resiliency.

Section 2: Brief Overview of Methods

This chapter will focus on using the same wheat varieties and material collected and described in Chapter 4. The techniques used in this chapter include peroxisome

abundance quantification, qRT-PCR of peroxisome fission and autophagy genes, protein quantification by western blotting using anti-ATG8 and anti-catalase, *in silico* RNA-seq analysis of peroxisome fission genes, DNA-affinity chromatography using nuclear proteins. Detailed description of the methods used in this chapter can be found in Chapter 2.

Section 3: Peroxisome Proliferation Gene Expression

As reported in Chapter 4, Hollis was found to increase peroxisome abundance in response to drought stress. Peroxisome abundance was found not significantly affected throughout the drought time course. This was also confirmed through imaging peroxisomes in leaf epidermis cells using N-BODIPY (**Figure 5.1A**) and calculated the density of peroxisomes. The average density of peroxisome was significantly higher in drought-stressed Hollis leaves (p=0.0144), whereas there were no significant differences in leaves in Drysdale under drought stress (**Figure 5.1B**).

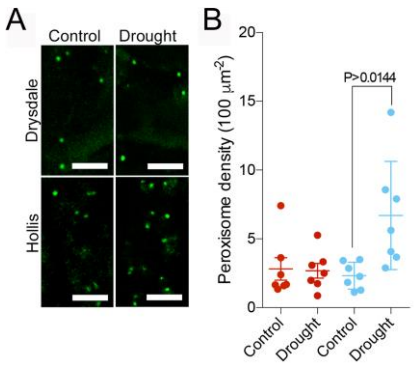

Figure 5.1: Peroxisome imaging in leaves. **A**, Representative images of peroxisomes in leaf epidermis cells of watered and drought-stressed Drysdale and Hollis plants. Scale bar, 5 mm. **B**, Average density of peroxisomes per 100 mm^2 of leaf surface in leaf epidermis cells. This figure was original published in *Hickey et al. 2022. Cells*.

Peroxisome abundance depends on the balance of peroxisome proliferation/biogenesis and degradation. Peroxisomes can proliferate through fission driven by *PEX11*, *FIS1A*, *DRP3A*, *DRP3B*, and *DRP5B*. There are three *PEX11* genes in the wheat genome: *PEX11A*, *PEX11B*, *PEX11C*. We analyzed gene transcription of these genes by qRT-PCR in leaves from day 7 of the drought stress time course for

Hollis and Drysdale. We found that out of the 7 peroxisome fission genes, only *PEX11C* was up-regulated by drought in both genotypes (**Figure 5.2A**). Although peroxisome abundance under drought stress was greater in Hollis than in Drysdale, transcription of *PEX11C* was equally up-regulated in both genotypes. Wheat genome has three *PEX11-C* homoeologs on chromosomes 7A, 7D, and 4A (Ma et al. 2013; Zhou et al. 2020). qRT-PCR analysis demonstrated that only *PEX11C*-7A was expressed under both control and stress conditions, whereas PCR with primers for the other two homoeologs did not yield a fragment. Transcription of *PEX11C-7A* was upregulated in responses to drought in Hollis but not in Drysdale (**Figure 5.2B**). The difference between the generic and homoeologs-specific primers suggests that the generic *PEX11C* primers could have off-targets.

To find out why peroxisome abundance was different in these genotypes, we assessed the activity of the pexophagy pathway that is responsible for peroxisome degradation. As a type of autophagy, the activity of pexophagy depends on the autophagic flux, which could be determined by the transcription level of *ATG8* (Ustun et al. 2018). The wheat genome contains 13 putative *ATG8* genes, and six *ATG8* genes were shown to respond to heat and drought stress (Yue et al. 2018).

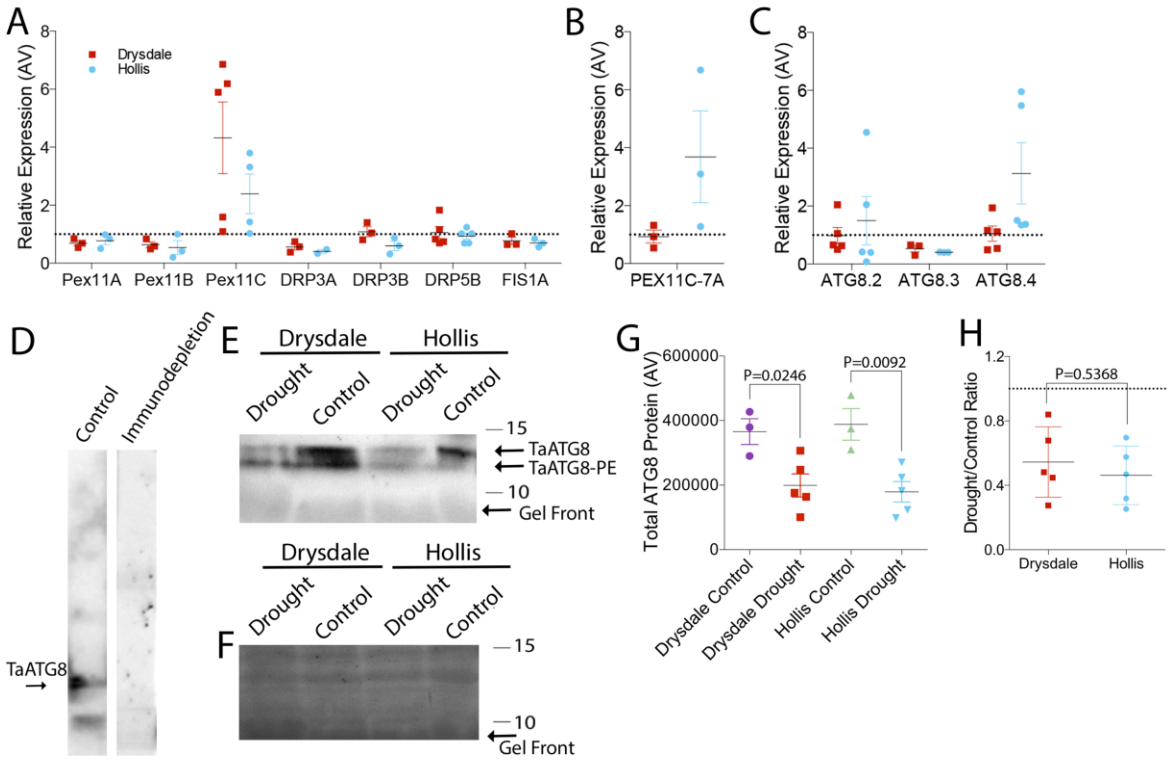

Figure 5.2: Drought response of peroxisome biogenesis and autophagy markers. **A, B, C**, Transcription level of peroxisome fission genes, peroxisome fission gene PEX11-C homoeologs from chromosome 7A and autophagy flux marker ATG8. qRT-PCR transcription levels were normalized to housekeeping gene RNase L inhibitor-like protein (Giménez, Pistón & Atienza 2011). **D,** Western blotting with ATG8 antibody or following immunodepletion of the antibody with the ATG8 protein. Pre-incubation of the antibody with the antigen abrogates recognition of ATG8 in leaf total protein extract. **E**, Western blotting with anti-ATG8 of total protein extracts from leaves of control and drought stressed Drysdale and Hollis plants. Bars and number indicate position and corresponding size of molecular weight markers. **F**, Colloidal Silver staining of the corresponding western blotting membrane showing total protein. Bars and number indicate position and corresponding size of molecular weight markers. **G**, Quantification of ATG8 protein abundance on the western blotting membranes. P-values represent student T-Test results of three technical replicates of extracts from three biological replicates (individual plants). **H**, The ratio of ATG8 protein in extracts from drought-stressed leaves to that in control leaves. P-values represent student T-Test results of three technical replicates of extracts from three biological replicates (individual plants). This figure was original published in *Hickey et al. 2022, Cells*.

Our pilot tests demonstrated that of these six genes, transcription of three genes was upregulated under our drought stress conditions. We found only *ATG8.4* was significantly upregulated in Hollis in response to drought (**Figure 5.2C**). The transcriptional analysis was complemented by measuring the ATG8 protein abundance under normal and stress conditions using Western blotting with anti-ATG8. The specificity of the antibody was verified using an immuno-depletion assay (**Figure 5.2D**).

ATG8 abundance under drought decreased in both genotypes relative to the watered control (**Figure 5.2G**), though the decrease of ATG8 abundance was somewhat greater in Hollis than in Drysdale (**Figure 5.2H**).

Peroxisomes are known to contain ca. 300 different proteins (Reumann et al. 2007; Bussell et al. 2013). Plausibly, other peroxisome biogenesis genes could be transcriptionally up regulated in response to drought. Dr. Yunus Sahin, in collaboration with our laboratory, analyzed transcription of all annotated peroxisomal genes in response to drought using 19 published RNA-Seq datasets from *Zea mays*, *Oryza sativa*, *Sorghum bicolor*, and *Arabidopsis thaliana*. To verify the impact of stress on global gene transcription, we compared the GO term enrichment in the stressed versus control datasets. Genes involved in response to abiotic stimuli including drought and stress-induced regulation of gene expression were enriched in the all RNA-Seq

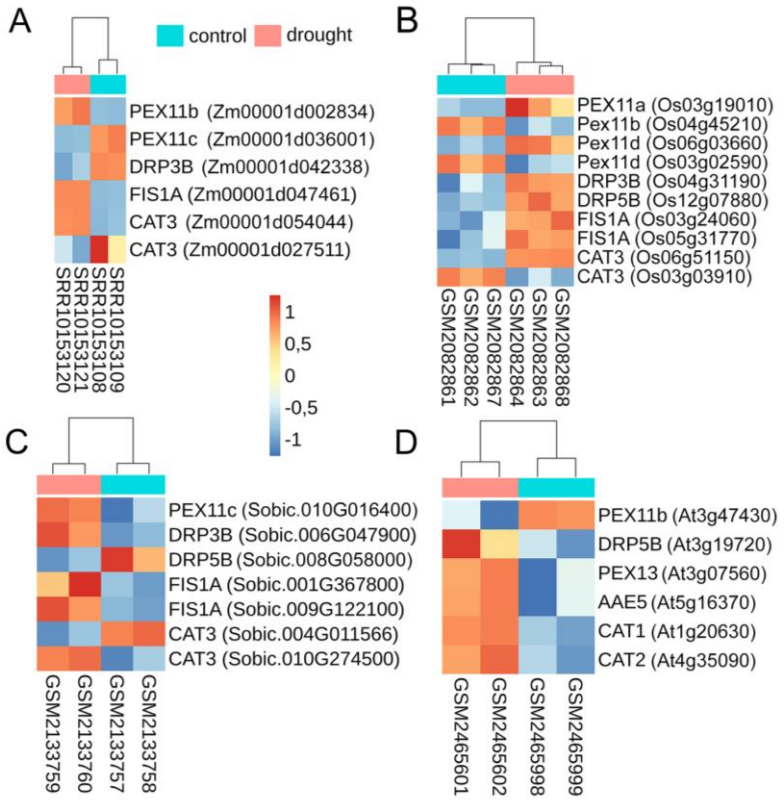

Figure 5.3: Expression of peroxisome biogenesis genes in response to drought stress. **A-D**, Heatmaps of peroxisome fission genes that are differentially expressed in response to drought stress in *Z. mays* (**A**), *O. sativa* (**B**), *S. bicolor* (**C**), *A. thaliana* (**D**). The figure was generated with the R pheatmap package using VarianceStabilizedTransformation -vst() function- built in DESEq2 package. Vst values were represented based on the z-score transformation. Samples were clustered according to Pearson correlation analysis. Loci name of orthologs that were mapped to peroxisome fission genes are included next to the gene names. This figure was original published in *Hickey et al. 2022, Cells*.

datasets for the stress samples relatively to control. Hence, drought treatment in all experiments induced a stress response.

Analysis of the peroxisome genes in these datasets showed that 75 to 120 genes encoding peroxisome proteins were differentially expressed across the species. However, only catalase (*CAT*) and *PEX11* were upregulated in all experiments (**Figure 5.3**). Interestingly, some members of *CAT* and *PEX11* gene families were downregulated in response to drought. It means there is functional specialization amongst these gene families under stress.

Section 4: Catalase Dynamics

We verified outcomes of the RNA-Seq analysis by measuring transcription of *CAT* genes in leaves on the 7th day of drought. *CAT1* is mostly expressed in leaves, *CAT2* is expressed in vascular tissues, and *CAT3* is expressed in reproductive tissues and roots (Mhamdi et al. 2012; Tyagi et al. 2021). Based on this information, we analyzed transcription of CAT1 and CAT2. CAT1 homoeologs are located on chromosomes 5A, 4B, and 4D (Ma et al. 2013; Zhou et al. 2020) and *CAT2* homoeologs locate on chromosomes 6A, 6B, and 6D. Transcription of all three *CAT1* homoeologs under drought was higher in Drysdale than in Hollis, whereas transcription of all three *CAT2* homoeologs was higher under drought in Hollis than in Drysdale with the greatest upregulation of *CAT2-6D* (**Figure 5.4A-B**).

As transcription of CAT genes was unregulated under drought in both genotypes, we measured abundance of catalase using western blotting. Anti-catalase was produced in mice as described in the Chapter 2 Methods. Specificity of the anti-catalase antibody was verified using immuno-depletion assay (**Figure 5.4C**). Analysis of the extracts from control and drought-stressed plants demonstrated greater catalase protein

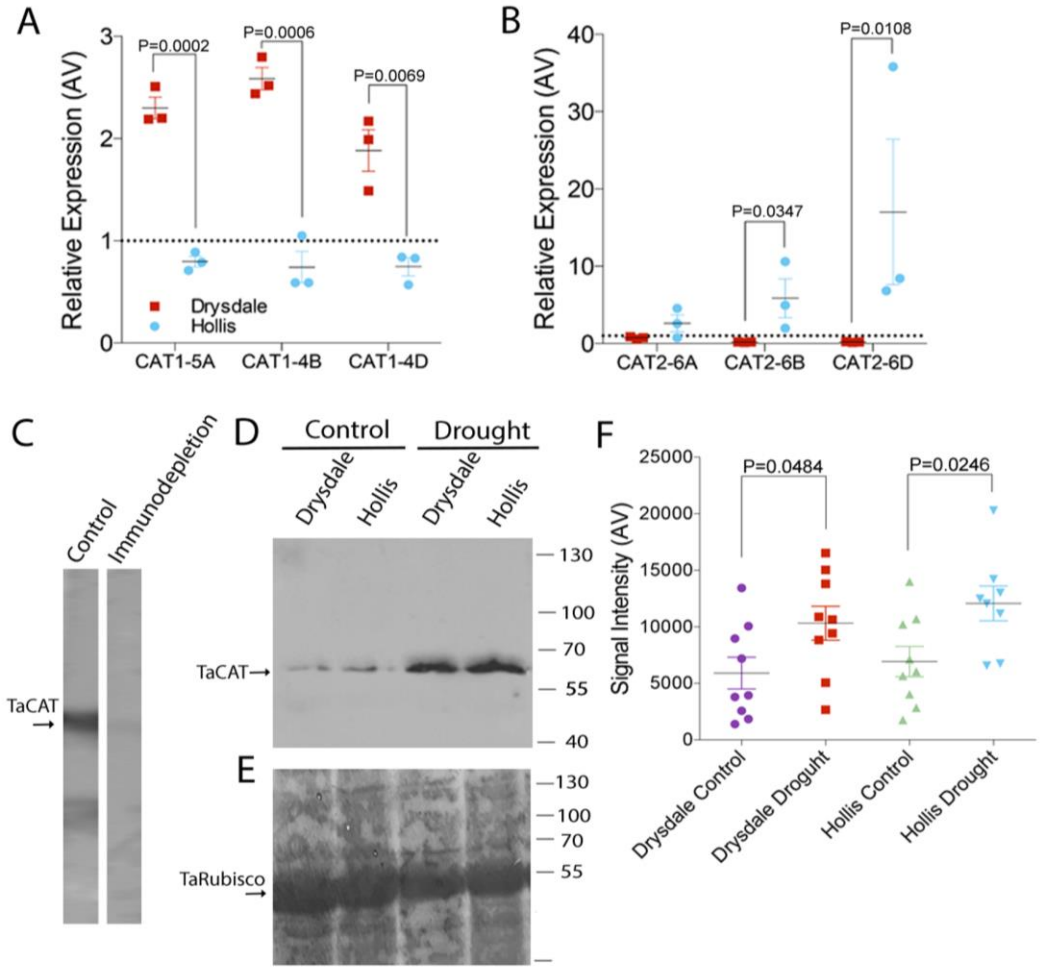

Figure 5.4: Characterization of Catalase in response to drought stress**. A**, Transcription of CAT1 homoeologs in leaves of control and drought-stressed Hollis and Drysdale plants. P-values were calculated using student T-Test (n=3). **B**, Transcription of CAT2 homoeologs in leaves of control and drought-stressed Hollis and Drysdale plants. P-values were calculated using student T-Test (n=3). **C**, Western blotting with catalase antibody or following immunodepletion of the antibody with the catalase protein. **D**, Western blotting of total protein extracts from leaves of control and drought stressed Drysdale and Hollis plants. **E**, Colloidal silver staining of the western blotting membrane showing total protein in the corresponding extracts. Bars and number indicate position and corresponding size of molecular weight markers. **F**, Quantification of CAT protein levels on the western blotting membranes. P-values represent student T-Test results of three technical replicates of extracts from three biological replicates (individual plants). This figure was original published in *Hickey et al. 2022, Cells*.

abundance under drought relative to the watered control (**Figure 5.4D**). The average signal was greater in Hollis than in Drysdale indicating higher abundance of catalase enzyme in the former genotype (**Figure 5.4F**).

Section 5: Peroxisome Genetic Regulators

Peroxisome abundance increases and peroxisome biogenesis genes are upregulated in response to drought stress. Peroxisome proliferation in response to light stress has been elucidated. Upon limitation in *Arabidopsis*, the transcription factor HYH binds to the promoter of *PEX11B*, significantly upregulating *AtPEX11B* expression and increasing the number of peroxisomes within 4-hours (Desai and Hu, 2008). During drought stress, *TaPEX11B* is not upregulated, suggesting a different mechanism of transcriptional regulation. It is currently unknown how peroxisome proliferate in response to stresses, including drought stress. To elucidate the molecular mechanism for the upregulation of peroxisome proliferation, a DNA-protein affinity chromatography approach was taken. This section will discuss the progress made towards performing the affinity chromatography pull-down, however, is project was not completed.

As transcriptional up-regulation of *PEX11C-7A* and *CAT2-6D* in response to drought stress coincided with higher peroxisome abundance in Hollis, we assumed that promoters of these genes interact with transcriptional factors that drive peroxisome fission. Therefore, promoters of *PEX11C-7A* and *CAT2-6D* were used as the “DNA bait” in the affinity chromatography experiment to identify transcription factors that regulate peroxisome abundance under drought stress. First, a fragment of wheat genomic

sequence located ~3,000 base pairs upstream of the start codon of each gene was downloaded from the wheat genome database IWGSC RefSeq v2.1. This region of the *PEX11C-7A* promotor sequence was not sequenced completely and therefore we selected a region within the sequenced part of this regions which was 1,000 base pairs upstream of the start codon (**Figure 5.5A-B**).

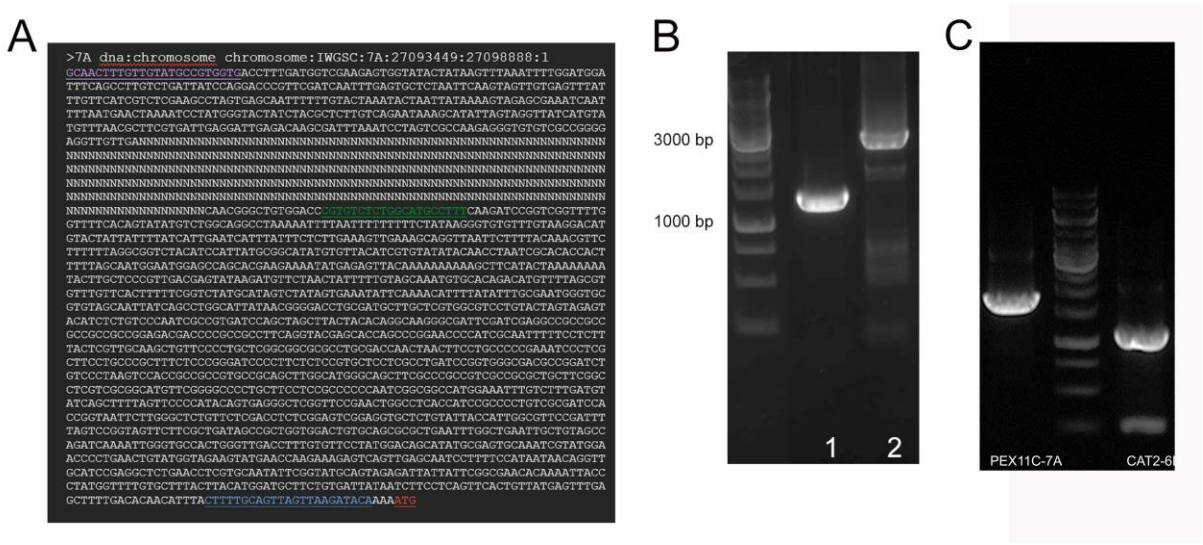

Figure 5.5: *PEX11C-7A* and *CAT2-6D* promoter amplification**. A**, 2339 bp fragment upstream of PEX11C-7A was used for primer design to amplify PEX11C-7A promotor region. Two forward primers were used corresponding to 2336 bp upstream (based on N=bp) and a 1561 bp fragment after the missing fragment. **B,** Agarose gel image of *PEX11C-7A* promotor regions amplification. Line 1 is 1561 bp fragment corresponding the sequence amplified below the missing section of the promotor. Line 2 is 3000 bp fragment corresponding to an amplified section of 2239, meaning the sequenced region contains at least 1000 bp. **C,** Agarose gel image of *PEX11C-7A* and *CAT2-6D* promotor regions amplification with biotin-tagged primers. A 1561bp fragment corresponding to 1564-3bp upstream of the start codon corresponding to *PEX11C-7A* and 1081 bp fragment corresponding to *CAT2-6D* 1189-46bp upstream of the start codon

Primers were designed for each sequence and a biotin-modification was added to the reverse primer for binding to the streptavidin-agarose affinity chromatography resin (Thermo Scientific). Promoter regions of *PEX11C-7A* and *CAT2-6D* were amplified with un-biotinylated primers. Fragments were visualized by agarose gel. Unmodified promotor fragments were cloned into pGEM-T Easy Vector (Promega). Promoter

fragments are GC-rich fragments making the PCR challenging. Cloning fragments into vectors aided the subsequent modification PCR.

pGEM-t vectors containing promoter fragments were used as a template for biotinylation using an unmodified forward primer and a biotinylated reverse primer.

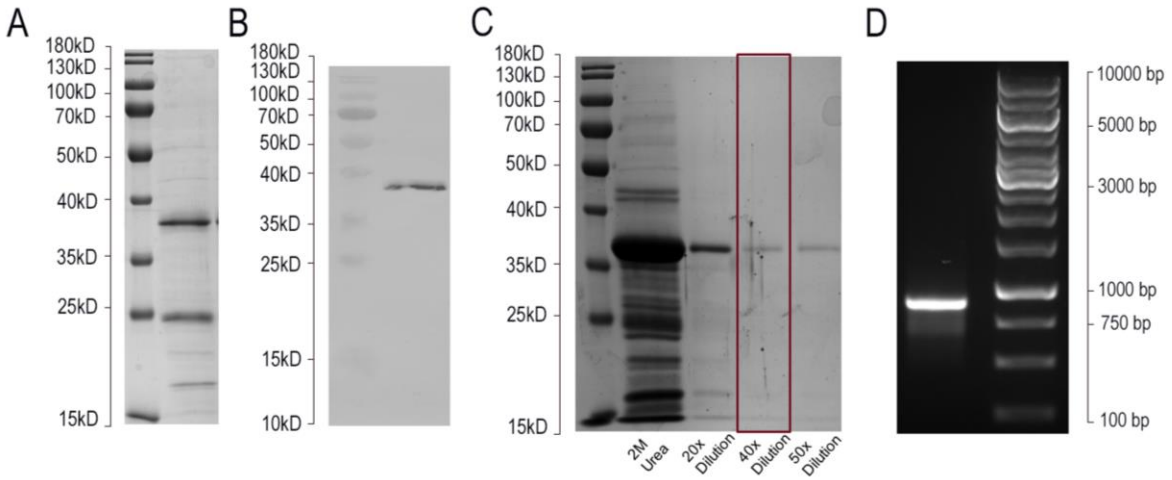

Figure 5.6: Expression of TaNAC2-5A protein and biotin amplification of promotor region of *TaGS2-2A*. **A**, SDS-PAGE gel of TaNAC2-5A transcription factor protein after recombinant protein expression and purification. NAC2-5A is ~38kD. **B**, Western blot with anti-HISTAG of TaNAC2-5A recombinant protein. **C,** SDS-PAGE gel of TaNAC2-5A dilution. NAC2-5A protein was eluted off nickel-column in 2M urea buffer and subsequently diluted 20x, 40x, and 50x. Dilution of 40x was selected for downstream applications, denoted with red box. **D,** Amplification and biotinylation of *TaGS2-2A* promotor, 865 bp fragment upstream of the start codon. Bars and number indicate position and corresponding size of molecular weight markers.

Biotinylated fragments were visualized by agarose gel, pooled and gel purified (**Figure 5.5C**). Pooled fragments were loaded to an agarose gel and excised based on molecular weight. Fragments were gel purified using a PCR clean up kit (Qiagen). Promotor DNA was then purified and pooled for subsequent assays.

For exclusion of unspecific interactors during the affinity chromatography, a known wheat specific gene and binding transcription factor was needed that was known to not be involved in drought stress. Two different genes and their transcription factors were identified in the literature: TaNAC2-5A and the promoter of gene *TaGS2-2A* (He et

al. 2012), and TaZIM-A1 and the promoter of gene *TaCO-A1* (Lui et al. 2018). The genes encoding both transcription factors were amplified, however the promoter regions could not be amplified. To overcome this problem, we synthesized genes encoding both transcription factors with a His-Tag was added to the N-terminus of each gene for subsequent purification by metal-affinity chromatography. TaNAC2-*5* and TaZIM-A1 were expressed in *E.coli*, however TaZIM-A1 could not be expressed under our laboratory conditions. Therefore TaNAC2-5A and promoter of *TaGS2-2A* were selected as the control for the affinity chromatography experiment (**Figure 5.6**).

To increase specification of the DNA-affinity chromatography, nuclear proteins were isolated. Published protocol for isolation of nuclei (Sikorskaite et al. 2013) was optimized for wheat leaves. The optimization for wheat included the use of different inhibitors, no treatment using diethyl ether, increasing the first centrifugation step from 10 minutes to 15 minutes at 1000 *x g*, increasing the step centrifugation step in the percoll gradient from 30 minutes to 45 minutes. The nuclear proteins were then extracted using TRIzol method.

Each promoter DNA was bound to the streptavidin resin following the manufacturer's instructions. However, during optimization, it was found that TaNAC2-*5A* transcription factor could bind to both promoter region of *TaGS2-2A*, and the promoter region of *CAT2-6D*. *TaNAC2-5A* was shown to be nitrate inducible and could bind to promoter regions of three wheat genes: *TaNRT2.1-6B*, *TaNPF7.1-6D*, and *TaGS2-2A* (He et al. 2015). TaNAC2-5A functions in multiple tissue types including roots, old leaves, and flag leaves (He et, 2015). The promiscuous behavior of TaNAC2-5A

complicates use of TaNAC2-5A as a control of our affinity-chromatography assay. The NAC transcription factor family is known to be involved in both biotic and abiotic stress responses, including drought stress (Nuruzzaman et al. 2013; Vranic et al. 2022). Therefore, TaNAC2-5A is not suitable as a use of a negative control protein. Hence, this project ended without the identification of genetic regulators of peroxisome proliferation.

Section 6: Discussion and Future Direction

We observed a significant increase of peroxisome abundance under drought only in Hollis. This suggests that both genotypes maintain ROS homeostasis using different mechanisms; one of which is an increase of peroxisome abundance. Peroxisomal proliferation is driven by a set of genes including *PEX11* (Orth *et al.* 2007; Koch *et al.* 2010). Of three wheat *PEX11* genes, transcription of only *PEX11C* was upregulated under drought in both genotypes under our experimental conditions (**Figure 5.2A**). Analysis of RNA-Seq data from rice, maize, sorghum, and *Arabidopsis* revealed that a member of *PEX11* gene family was upregulated under drought stress in all species. Interestingly, some members of *PEX11* gene families were downregulated in response to drought as *PEX11A* and *PEX11B* in this work. In *Arabidopsis,* PEX11A was implicated in formation of peroxisome extensions known as peroxules under cadmium stress (Rodríguez-Serrano et al. 2016), while PEX11B is involved in light-induced peroxisome proliferation (Desai & Hu 2000). This indicates differences in peroxisome proliferation process under drought and in other situations.

Dysfunctional peroxisomes are degraded through pexophagy (Voitsekhovskaja et al.2014; Young & Bartel 2016; Calero-Muñoz *et al.* 2019). Activity of autophagy (the

autophagic flux) can be assessed by measuring transcription level *ATG8* (Bassham 2015; Ustun et al. 2018). One of three wheat *ATG8* measured, *ATG8.4* was upregulated in both genotypes (**Figure 5.2C**). The average level of *ATG8.4* transcription was 3-folds higher in Hollis than in Drysdale. Another characteristic of the elevated autophagic flux is degradation of ATG8 protein (Klionsky et al. 2021). We compared relative abundance of ATG8 in total leaf protein extracts from control and drought stressed plants. This showed reduced protein content in both genotypes indicating activation of autophagy (**Figure 5.2G**). However, higher transcription level of *ATG8* accompanied by somewhat lower ATG8 protein abundance in Hollis relative to Drysdale suggests greater autophagic flux under drought stress in Hollis. ROS could modulate or act as a regulator of autophagic responses during abiotic stress (Zhou *et al.* 2014; Signorelli et. 2019; Su et al. 2020).

RNA-seq analysis demonstrated that of all peroxisomal genes only *PEX11* and *CAT* were upregulated in response to drought. Of two *CAT1* and *CAT2* genes, *CAT1* transcription in response to drought was upregulated by 2 folds in both Drysdale and Hollis, whereas *CAT2* expression was 5-fold higher in Drysdale under drought (**Figure 5.4A-B**). CAT2 has been identified as the enzyme responsible for detoxifying photorespiratory-derived hydrogen peroxide (Mhamdi *et al.* 2012). Overall, both *CAT* transcription and CAT protein appear to be good markers of peroxisome abundance.

Recently, it has been reported that CAT3 can be transnitrosylated and targeted for selective autophagy (Sandalio et al. 2019; Chen et al. 2020). Ubiquitinated CAT accumulates in a pexophagy adaptor mutant *nbr-1* in *A. thaliana* (Zhou et al. 2013). CAT has also been shown to co-localize with ATG8 and NBR1 in the electron dense

peroxisomal core in response to cadmium stress (Calero-Muñoz et al. 2019). It is plausible that catalase functions as a pexophagy receptor and higher protein level of catalase in Hollis is linked to greater rejuvenation of the peroxisome population in the stressed cells through pexophagy.

Peroxisome abundance and catalase activity patterns overlap in Hollis under drought. This is consistent with higher transcription of *CAT1*, *CAT2* and *PEX11C.* Higher catalase activity and up-regulation of *CAT1*, *CAT2*, and *PEX11B* transcription in Drysdale is accompanied by a relatively steady peroxisome abundance. Both varieties had significant increase in CAT protein. Catalase undergoes multiple post-translational modification including carbonylation, S-nitrosylation, and phosphorylation (reviewed by Sandalio et al. 2019). PEX11 is also a target of post-translational modifications including phosphorylation, acetylation, and S-nitrosylation (Sandalio *et al.* 2019). Post-translational modifications could be responsible for fine-tuning the activity of peroxisome fission and degradation processes.

PEX11C-7A and *CAT2-6D* were identified as peroxisomal drought responsive genes. To identify the genetic regulation of stress induced peroxisome proliferation, we performed a Streptavidin Affinity Chromatography pull down. This project was not completed, and interactions were not identified. The methods and experimental setup was optimized in promoter cloning and amplification, nuclear protein extraction, and streptavidin resin column usage.

Completion of DNA-affinity chromatography would facilitate the discovery of regulations of peroxisome proliferation. To complete this assay, the first step would be identification of a suitable control transcription factor. The cloning of a secondary

characterized transcription factor has been complete (TaZIM-A1). The expression of TaZIM-A1 protein would need to be optimized through optimization of expression timing and temperature. Another approach would be to identify a different characterized wheat-specific transcription factor to be used. The steps for collection of nuclear proteins and the optimization of the chromatography technique have been done. Once the DNA-affinity chromatography is complete, the next steps would be proteomics and identification of potential regulators. Characterization of potential regulations would include localization and confirming interactors through techniques such as biomolecular florescence complementation.

Peroxisomes appear to be an essential component of drought adaptation. Peroxisome abundance increases in response to drought stress. *CAT* and *PEX11* gene families are upregulated under drought stress. Identification of genetic regulators of *CAT* and *PEX11* gene would provide targets for increasing cellular protection under stress. Future identification and characterization of genetic markers of peroxisome proliferation is essential for breeding wheat with greater stress resiliency.

CHAPTER 6: ROLE OF AUTOPHAGY UNDER HEAT AND DROUGHT STRESS

The figures and text of this Chapter were submitted for publication at *Cells* with co-authors Yunus Sahin, Glenn Turner, Taras Nazarov, Vadim Jitkov, Mike Pumphery, and Andrei Smertenko titled *Genotype-Specific Activation of Autophagy during Heat Wave in Wheat*. The RNA-Seq Analysis was done by Dr. Yunus Sahin, Dr. Glenn Turner processed the material for microscopy, Andrei Smertenko performed the microscopy imaging. Taras Nazarov and Vadim Jitkov coordinated the field experiments.

Section 1: Introduction and Rational

Recycling of dysfunctional cellular components plays a key role in both development and stress (Marshall and Viestra, 2018; Tang and Bassham, 2018; Wang et al. 2021). Therefore, cellular mechanisms of adaptation to harsh environmental conditions rely on autophagy. Autophagy occurs via the formation of a double membrane vesicle on the endoplasmic reticulum, called the autophagosome, which encloses cytoplasmic components and then delivers them to the vacuole (Lui and Bassham, 2012).

Autophagy plays a role in tolerance to many stresses including oxidative stress/H_2O_2/Methyl viologen (Xiong et al. 2007; Shin et al. 2009); nutrient deficiencies and starvation (Xiong, et al. 2005; Guiboileau et al. 2012; Merkulova et al. 2014); salinity (Liu, Xiong, Bassham, 2009; Shin et al. 2009); hypoxia (Lin et al. 2021); drought (Liu, Xiong, Bassham, 2009; Sun et al. 2018; Bao et al. 2020; Kuzuoglu-Ozturk et al.

2021; Wang et al. 2015; Sun et al. 2018; Yang et al. 2021); and heat (Zhou et al. 2014; Zhai et al. 2016; Zhang, et al. 2021). We have previously shown that reduction of ATG8 abundance in two tolerant spring wheat genotypes under drought stress was accompanied by up-regulation of *ATG8* genes (Hickey et al. 2022). Hence, autophagy pathway appears to be an important breeding target for advancing stress resilience.

ATG8 is frequently used as a marker for assessing the overall activity and tracking progression of the autophagy pathway (Bassham, D., 2014). ATG8 provides a selective docking platform for autophagy receptors and adapters. NBR1 (NEIGHBOR OF BRCA1; also known as *Joka2* in tobacco; Zientara-Rytter et al. 2011) was the first selective autophagy receptor in plants identified through domain organization and homology of two mammalian autophagic adapters p26/SQSTM1 and NBR1 (Svenning et al. 2011). NBR1 plays a role in clearing stress-induced protein aggregates (aggrephagy) and implicated in responses to multiple stresses including heat, drought, and salinity (Zhou et al. 2013; Zhou et al. 2014; Jung et al. 2020). Thus, autophagy receptors can be used as markers for isolation of genotypes with active autophagy and identification of corresponding genetic markers.

This Chapter aims at developing phenotyping tools and assessing the activity of autophagy in response to heat and drought stress across a panel of 16 phylogenetically distant wheat genotypes adapted to different geographical regions. The stress was applied under greenhouse conditions. As the output of autophagic activity we measured protein and transcript abundance for three makers: ATG8, ATG7, and NBR1. The response of these markers was correlated with yield collected in the field trials under

heat and drought stress. We found that all three markers were affected by the stress and changes of ATG8 and NBR1 protein abundance correlated negatively with yield, and changes of *ATG8* gene transcription correlated positively with yield. Thus, ATG8, ATG7, and NBR1 informs on the heat and drought stress resiliency and can be exploited for developing varieties for arid and hot environments.

Section 2: Overview of methods

This chapter characterizes 3 wheat specific autophagy markers: ATG8, ATG7, and NBR1. The antibodies for the autophagy markers were developed and used to phenotype autophagy under heat and drought stress in a wheat diversity panel. The yield data is collected from field trails located in Lind and Othello, WA. Plant material for technical assays was collected from 2 sets of heat and drought experiments in the greenhouse. Techniques used in this Chapter include ATG8 antibody affinity purification, western blotting with anti-ATG8, anti-ATG7, and anti-NBR1, qRT-PCR, *in silico* RNA-seq analysis of autophagy genes. Detailed descriptions of the methods are in Chapter 2.

Section 3: Characterization of ATG8 protein heterogeneity

Probing the total leaf extract from the spring wheat variety Berkut grown under normal conditions with polyclonal anti-ATG8 resulted in detecting two bands of molecular weight 12 and 14 kD (**Figure 6.1A**). In addition, multiple bands of higher molecular weight were observed in seven bleeds from two rabbits. To examine the nature of these bands, we performed an immuno-depletion assay. The ATG8 antigen was incubated with the antibody prior to probing the membrane with total protein extract. Although the immunodepleted serum failed to recognize the lower molecular weight bands, the higher molecular weight bands persisted (**Figure 6.1A**). This outcome demonstrates that the anti-serum in addition to ATG8 recognizes other proteins.

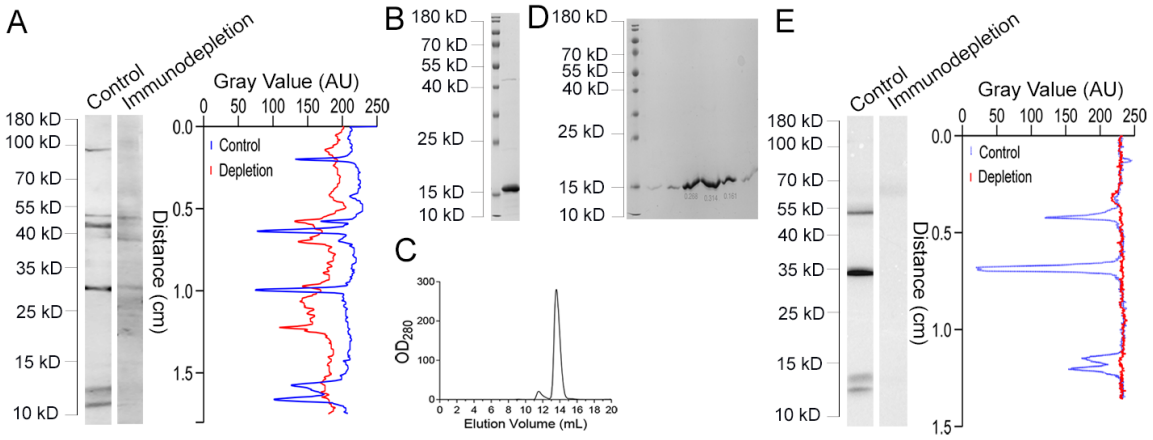

Figure 6.1: Characterization of anti-ATG8**. A**, Western blotting images and corresponding densitometric scans of the total leaf extract from Berkut with anti-ATG8 or immunodepleted anti-ATG8. Pre-incubation of the serum with ATG8 protein depletes only some bands. In this experiment bleed 5 was used. **B**, SDS-PAGE gel of recombinant ATG8 protein expressed in E. coli after purification by Ni-affinity chromatography. **C**, Elution profile of ATG8 from the size-exclusion column in 4M Guanidine-HCl buffer. **D**, SDS-PAGE gel of fractions 11-16 corresponding to the peaks on the elution profile in panel **C**. **E**, Western blotting images and corresponding densitometric scans of total leaf extract from Berkut probed with purified ATG8 antibody or with the immunodepleted antibody. Immunodepleted with ATG8 abrogates the signal.

To eliminate the non-specific reactivity of the antiserum we isolated anti-ATG8 by immuno-affinity chromatography. First, ATG8 recombinant protein was purified using nickel affinity chromatography, followed by a second purification step on a gel-filtration column (**Figure 6.1B-D**). Purified ATG8 protein was covalently bound to the NHS-

agarose resin and the resin was used for isolation of anti-ATG8. The purified antibody cross-reacted with the lower-molecular weight bands and still recognized several higher-molecular weight bands. The specificity of the purified antibody was tested using the immuno-depletion assay. This time, all bands disappeared following the immuno-depletion (**Figure 6.1B-D**). Thus, all bands detected with anti-ATG8 contain ATG8 antigen. This outcome demonstrates heterogeneity of ATG8 proteins under normal growth conditions.

Next, we examined the probability that ATG8 heterogeneity originates from cross-reactivity of anti-ATG8 with paralogs or proteins harboring ATG8-like motifs. Wheat genome has 12 putative ATG8 proteins and no proteins contained ATG8-like motifs longer than seven amino-acids. Phylogenetic analysis under stringent conditions (clades were retained in the phylodendrogram if the bootstrap value was above 70%) produce only on clade containing wheat, rice, and Arabidopsis proteins (**Figure 25A**). Two wheat paralogs ATG8-6A and ATG8m-6D form a distinct clade. Other genes remain unclustered. At a lower stringency more clades could be identified. Next, wheat ATG8 proteins were analyzed for conserved regions. Only one 7-amino acid long peptide was conserved in 10 of the 12 TaATG8 proteins and no other protein in the NCBI gene bank contained this motif. Thus additional bans could result from antibody recognizing ATG8 paralogs, but not from cross-reactivity with other proteins.

Sequences of ATG8-6A and ATG8m-6D showed conservation with ATG8-6B but lacked the highly conserved ubiquitin-like fold. We visualized the predicted protein structures for all TaATG8 homoeologs on chromosome 6 (**Figure 6.2C-E**) and superimposed each of them over predicted structure of ATG8c-2A (**Figure 6.2B**). The alignment demonstrated structural difference in the predicted ubiquitin fold meaning that ATG8-6A and ATG8m-6D are not canonical ATG8. The predicted size of these proteins ranges between 22 and 26 kD, whereas other predicted size of other ATG8 proteins is ~12 kD.

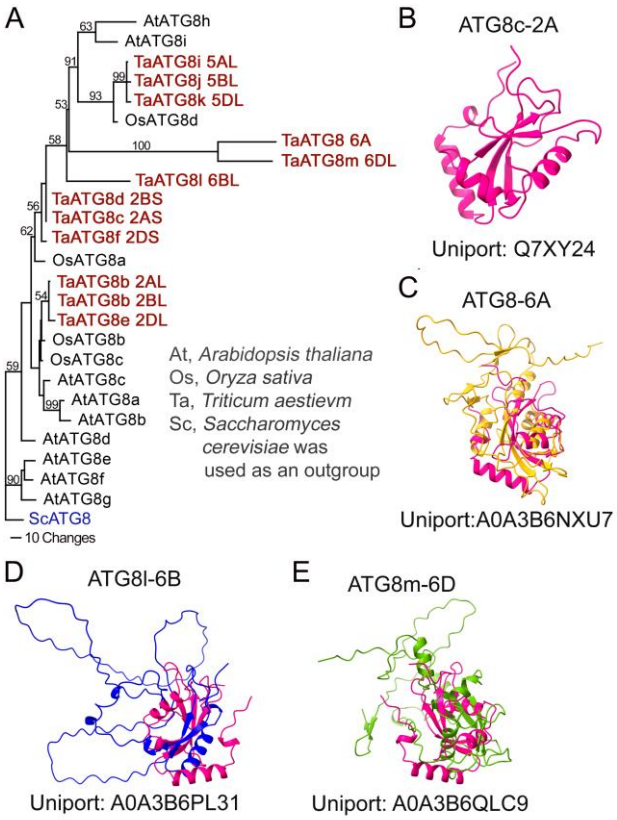

Figure 6.2: Phylogeny and predicted structure of ATG8 in wheat**. A**, Phylogenetic tree of ATG8 proteins from *T. aestivum* (Ta), *A. thaliana* (At), *O.sativa* (Os). *S. cerevisiae* ATG8 was used as the outgroup. **B**, Structure of ATG8c-2A (uniport: Q7XY24) based on Alphafold prediction. **C-E**, Alphafold predicted structures of ATG8 homeologs on chromosome 6 superimposed with ATG8c-2A (pink). (**C**) ATG8-6A (uniport: A0A3B6NXU7). (**D**) ATG8l-6B (uniport: A0A3B6PL31). (**E**) ATG8m-6D (uniport: A0A3B6QLC9).

To test conservation of ATG8 heterogeneity in other monocot species, we performed Western blotting with total protein extracts from *Arabidopsis thaliana, Brachypodium distachyon,* and *Oryza sativa* grown under normal conditions (**Figure 6.3A**). The 17 and 90 kD species were detected in all species, 12, 14, and 27 kDa species occurred in all monocots, and other bands were not conserved.

Conservation of ATG8 heterogeneity in different species prompted us to get a deeper insight into the nature of high-molecular weight bands. It was possible to immunoprecipitate ATG8 bands from total leaf extract of variety Berkut (**Figure 6.3B**). We analyzed the presence of ATG8 in gel slices corresponding to different ATG8 species by proteomics analysis. The excised gel slices correspond to areas highlighted by red boxes in **Figure 6.3B**. ATG8 was found in gel slices corresponding to size 10-17kD, 30-38kD, and 65-85kD. But not in the slice corresponding to 95-110kD.

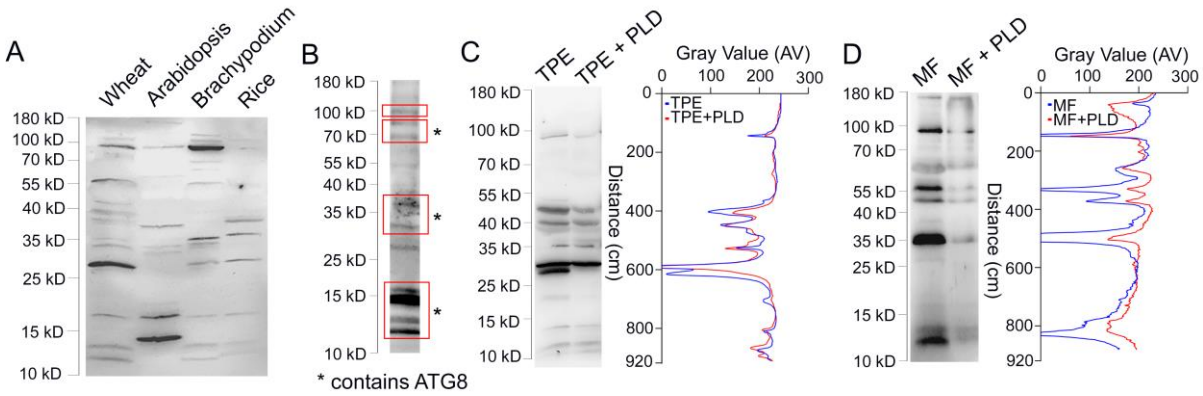

Figure 6.3: Characterization of ATG8 heterogeneity**. A**, Western blot of total protein extract from *Triticum aestivum*, *Arabidopsis thaliana*, *Brachypodium distachyon*, and *Oryza sativa* using anti-ATG8. **B**, Western blot of proteins that were immunoprecipitated from total protein extract of Berkut probed with anti-ATG8. Red boxes indicate gel slices that were excised and sent for proteomics analysis. Asterisks (*) denote slices in which ATG8 was detected. **C-D**, Delipidation assay of ATG8. Western blotting and corresponding desitometric plots of total protein extracts (**C**) or microsomal fractions (**D**) from leaves of var. Berkut before and after incubation with Phospholipase D with anti-ATG8. Arrows point peaks that disappear after the delipidation. Bars and numbers indicate position and corresponding size of molecular weight markers.

It has been shown that lipidation with phosphatidylethanolamine contributes to ATG8 heterogeneity (Yoshimoto et al. 2004). To examine this possibility, we incubated the total protein extract and microsomal fraction with Phospholipase D. After the delipidation reaction, the intensity of two bands was significantly reduced in both samples (**Figure 6.3C,D**). Thus, immuno-affinity purified ATG8 antibody captures heterogeneity of ATG8 states some of which is generated through lipidation.

Section 4: Impact of heat and drought on ATG8 protein levels

Autophagic responses to heat and drought stress were measured in sixteen genotypes from the spring wheat diversity panel “Elite” of 30 genotypes (**Figure 6.4**; Blake et al., 2019). The lines were selected according to their yield in field trials during 2023 growth season. The trials were performed at the WSU Lind Dryland Research Station located in Lind, Washington where the average precipitation in the 2023 season was 0.006” and the average temperature was 86°F/30°C (**Figure 6.A**). The trials were performed at the WSU Irrigated Agricultural Research and Extension Center located in Othello, Washington where the average precipitation in the 2023 season was 0.009” and the average temperature was 84°F/29°C (**Figure 6.5B**). Using yield as criteria, we selected low-yielding genotypes LDRC2, LDRC10, LDRC33, LDRC42, and LDRC65; medium yielding LDRC5, LDRC15, LDRC16, LDRC81, and Berkut; and high-yielding LDRC9, LDRC19, LDRC37, LDRC43, LDRC48, and LDRC74. Selected lines were subjected to heat and drought stress under greenhouse conditions. The experiment was repeated twice. In each experiment we collected leaf material from two different plants and all subsequent experiments were performed with this leaf material.

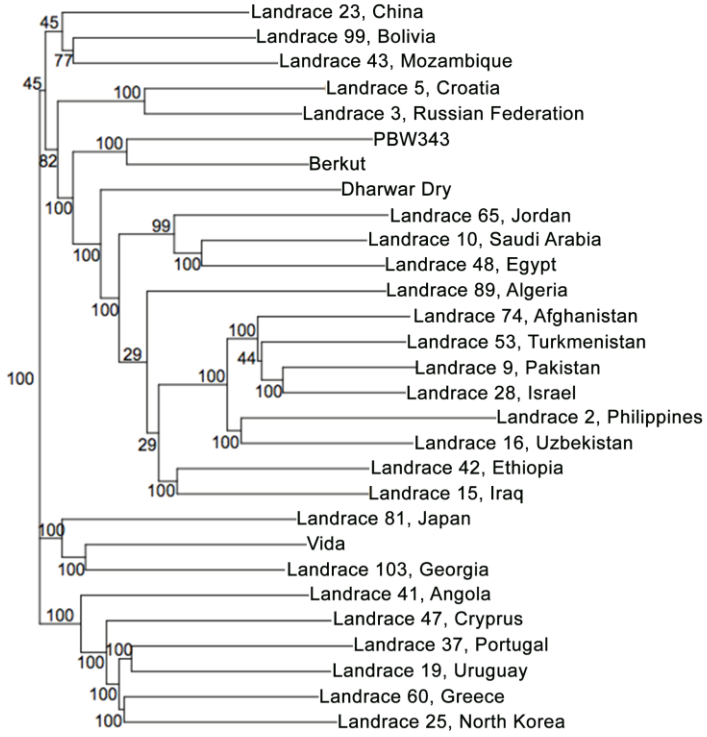

Figure 6.4*:* Phylogenetic analysis of wheat varieties and origin of varieties from the spring wheat diversity panel “Elite.

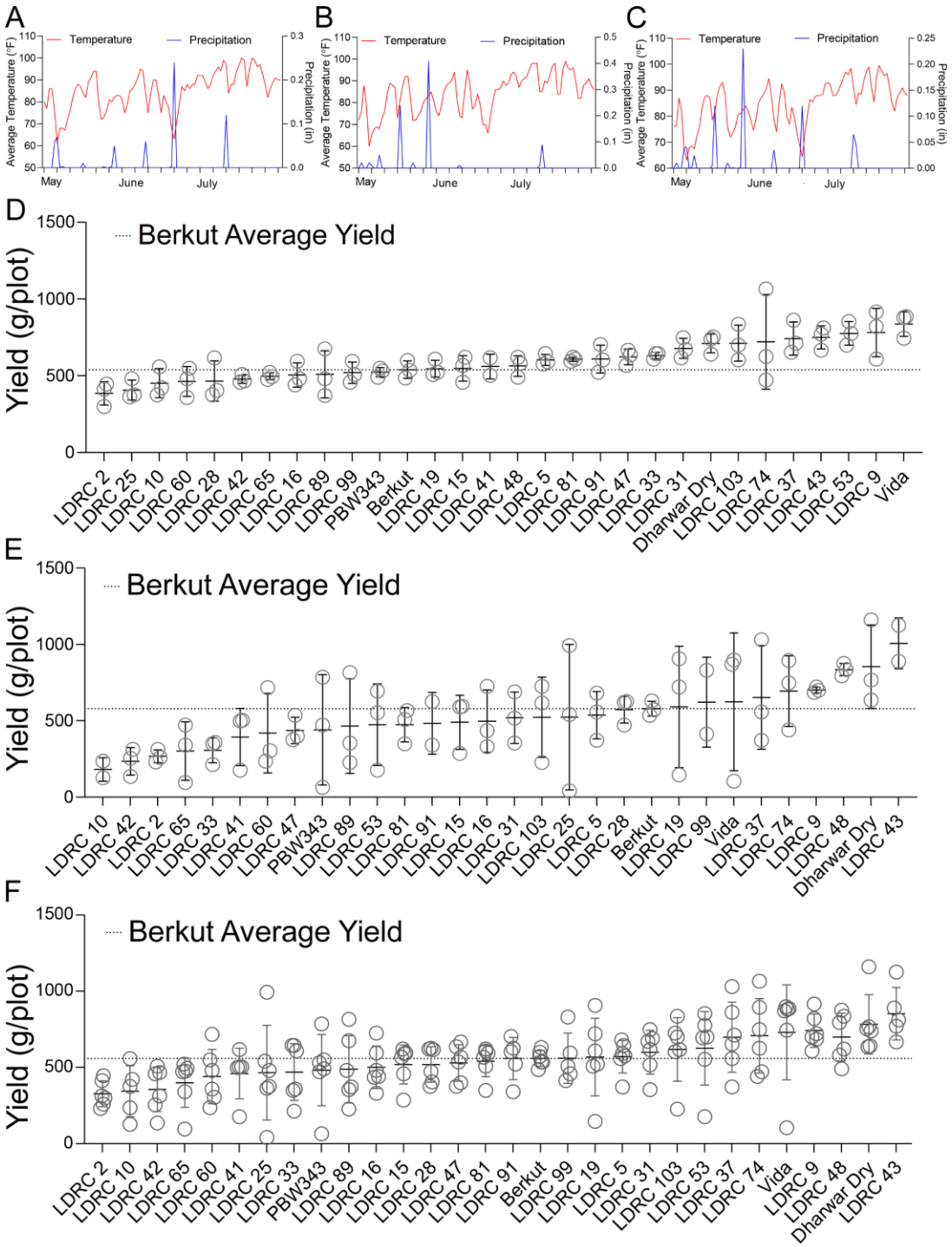

Figure 6.5: Field trials weather patterns and yield. Temperature and precipitation accumulation in Lind, WA (**A**), Othello, WA (**B**) and the average of both sites (**C**) during May-July, 2023. Yield of lines from the spring wheat genetic diversity panel, grown in Lind, WA (**D**)and Othello, WA (**E**), and the average from both sites (**F**) during May-July, 2023.

Probing total extracts from control and heat+drought stressed plants with anti-ATG8 revealed genotype-specific patterns of ATG8 bands that were seemingly different under stress treatment (**Figure 6.6A-F**). Quantification of the cumulative intensity of all bands in each lane of the heat+drought stress extracts relative to the control revealed 3 patterns (**Figure 6.6G**): (1) no change of relative ATG8 abundance (Berkut, LDRC2, LDRC19, LDRC37, LDRC42); (2) increase of ATG8 abundance (LDRC9, LDRC16, LDRC48, LDRC65); and (3) decrease of ATG8 abundance (LDRC 5, LDRC10, LDRC15, LDRC33, LDRC43, LDRC74, LDRC81). The intensity of Rubisco band was used for normalization of protein loading.

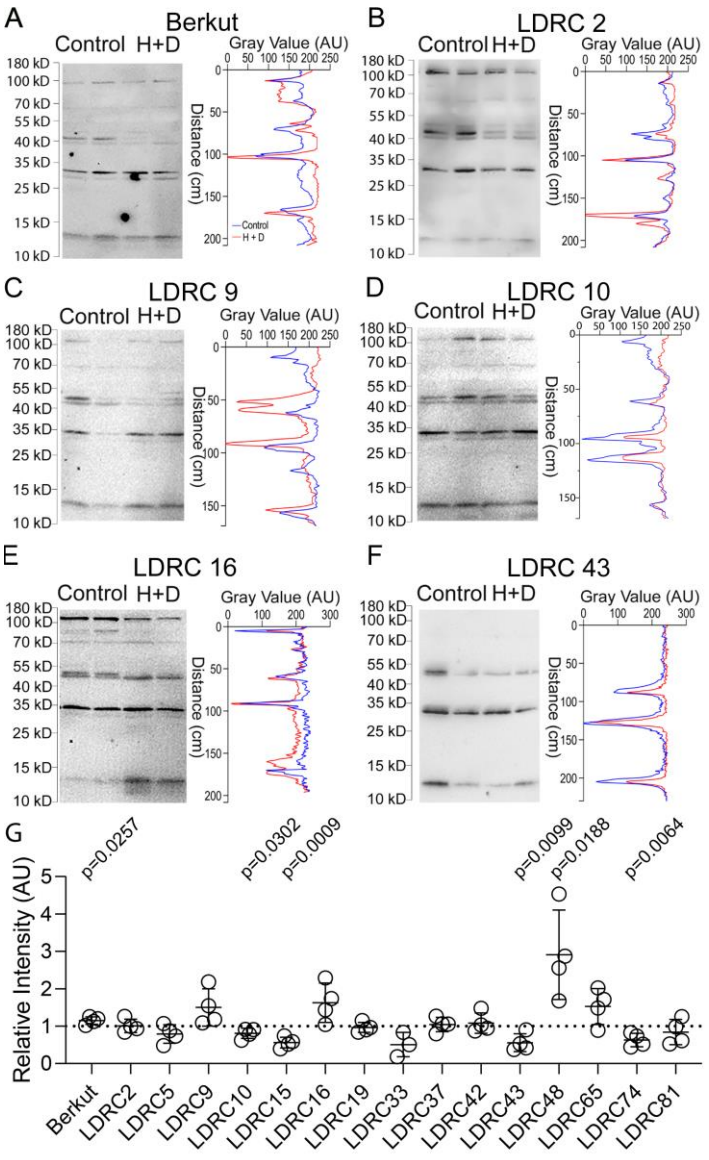

Figure 6.6: Response to ATG8 to heat and drought**. A-F**, Representative images of western blotting with anti-ATG8 and corresponding densitometric scans of total protein extracts from leaves of control and heat + drought stressed (H+D) Berkut plants (**A**), LDRC2 (**B**), LDRC9 (**C**), LDRC10 (**D**), LDRC16 (**E**), LDRC43 (**F**). Bars and numbers indicate position and size of molecular weight markers. **G**, Fold change of cumulative ATG8 bands intensity in extracts from heat and drought stress material relative to the control. P-values represent statical differences for Student's T-Test at 95% confidence.

Next, we measured abundance of 12-15 kD ATG8 band under control and heat and drought stress (**Figure 6.7A-F**). Generally, there were three types of responses (**Figure 6.7G**): (1) increase of relative ATG8 abundance (Berkut, LDRC2, LDRC9, LDRC16, LDRC48, LDRC74); (2) decrease of relative ATG8 abundance (LDRC 43); (3) no change (LDRC10, LDRC42, LDRC81). In LDRC5, LDRC15, LDRC19, LDRC33, LDRC37, LDRC65 the response was inconsistent. To test the correlation between ATG8 abundance and formation of autophagosome, we stained autophagosomes on the transverse sections through leaf of LDRC48 under control and heat and drought stress with anti-ATG8 (**Figure 6.7H**). Under heat and drought stress,

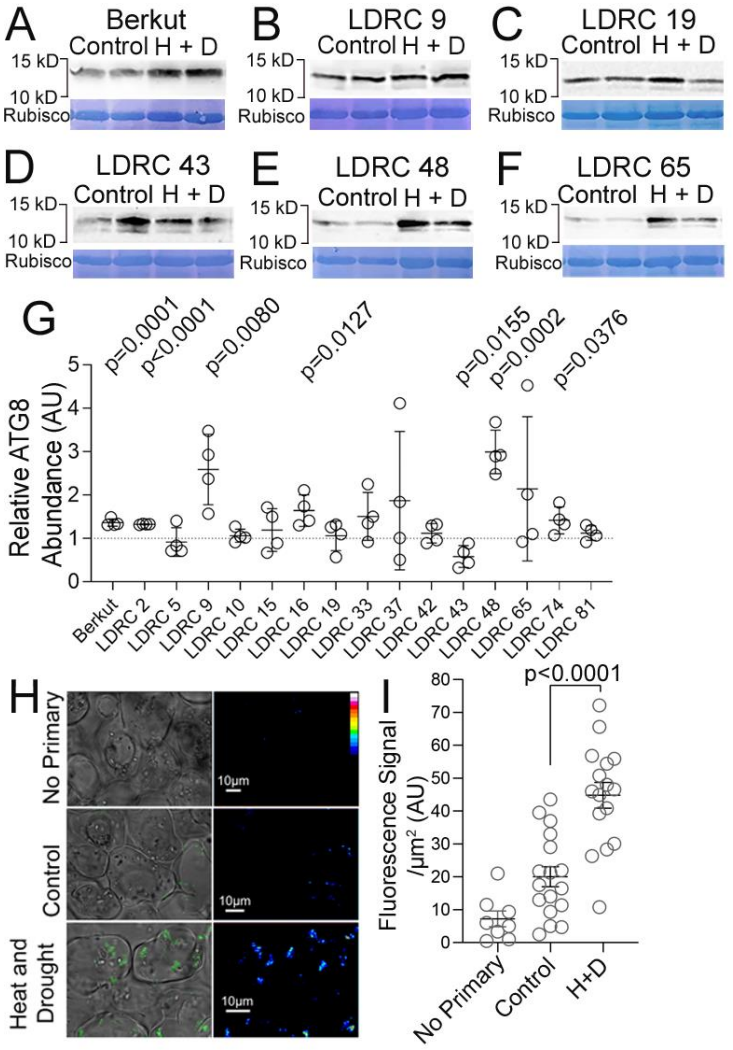

Figure 6.7: Impact of heat and drought stress on abundance of ATG8. **A-F**, Western blotting with anti-ATG8 of total protein extracts from leaves of control and heat + drought stressed (H+D) plants of Berkut (**A**), LDRC9 (**B**), LDRC 19 (**C**), LDRC 43 (**D**), LDRC 48 (**F**), LDRC 65 (**F**). Bars and number indicate position and corresponding size of molecular weight markers. Amido black staining of the corresponding western blotting membrane showing Rubisco protein. **G**, Fold change of ATG8 protein abundance in response to heat and drought stress relative to the control. P-values represent statistical differences between control and stress treatments for Student's T-Test at 95% confidence (n=4, two different plants in two independent experiments). **H,** Representative images showing immunostaining of ATG8 in control or heat and drought treated leaves of LDRC48. Each image is a single 1 mm thick optical section. Scale bar, 10 mm. **I**, Average florescence signal per µm^2 in control or heat and drought treated leaves.

LDRC48 had a significant (p<0.0001) increase in autophagosome (**Figure 6.7I**).

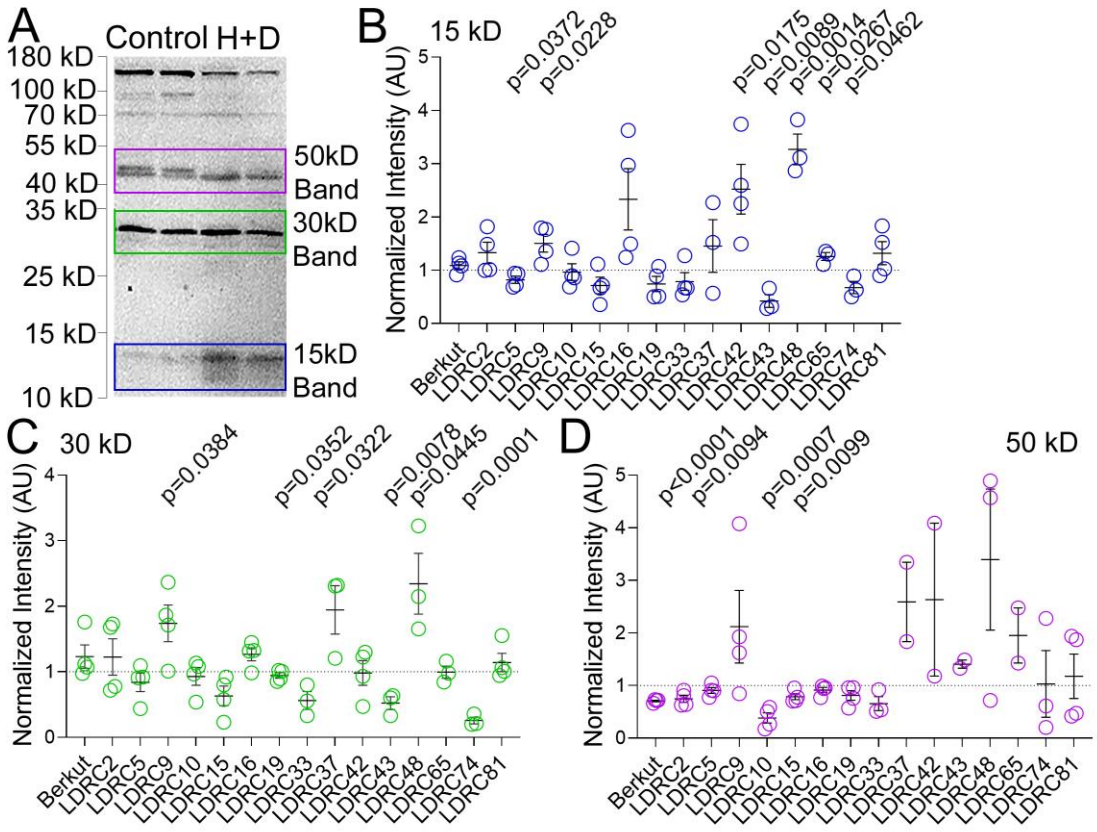

Figure 6.8: Impact of heat and drought stress on different ATG8 bands. **A**, A representative western blot membrane of total protein extract from leaves of control and stressed LDRC16 with anti-ATG8. The intensity of bands corresponding to approximately 15kD, 30kD, and 50kD denoted by the rectangles were used for quantification in panels **B-D**. Bars and numbers indicate position and corresponding size of molecular weight markers. **B-D**, Fold change of 15 kD (**B**), 30 kD (**C**), or 50 kD (**D**) ATG8 bands abundance in the heat + drought stressed plants relative to the control. P-values represent statical differences for Student's T-Test at 95% confidence. (n=4, two different plants in two independent experiments).

As ATG8 protein was also detected in the gel slices corresponding to ~30kD, and ~50kD bands, we compared impact of heat stress on the abundance of these bands with the abundance of 15 kDa band (**Figure 6.8**). The regions used for measuring the intensity of bands are shown in **Figure 6.8A**. In most genotypes the response of the bands was synchronous. The intensity of all bands increased or was not affected in LDRC9, LDRC37, LDRC42, LDRC48, LDRC65, and LDRC81. In other group of

varieties, the intensity of all bands decreased: LDRC5, LDRC10, LDRC15, LDRC19, LDRC33, and LDRC74. In four varieties, Berkut, LDRC2, LDRC16, and LDRC43 the changes of bands varied. For example, in LDRC16 the intensity of the 15 and 30 kD bands increased whereas the intensity of the 50 kD decreased. We found that variability of the 30kD band between biological replicates was lower than variability of the 15kD and 50kD bands. The 30kD band was on average lower in intensity in the population compared to 15kD and 50kD.

To measure impact of heat and drought stress on transcription of *ATG8* genes we designed a pair of universal primers capable of simultaneous amplification of *ATG8d-2B*, *ATG8c-2A*, *ATG8f-2D*, and *ATG8l-6B2* and two pairs of homoeolog-specific primers for

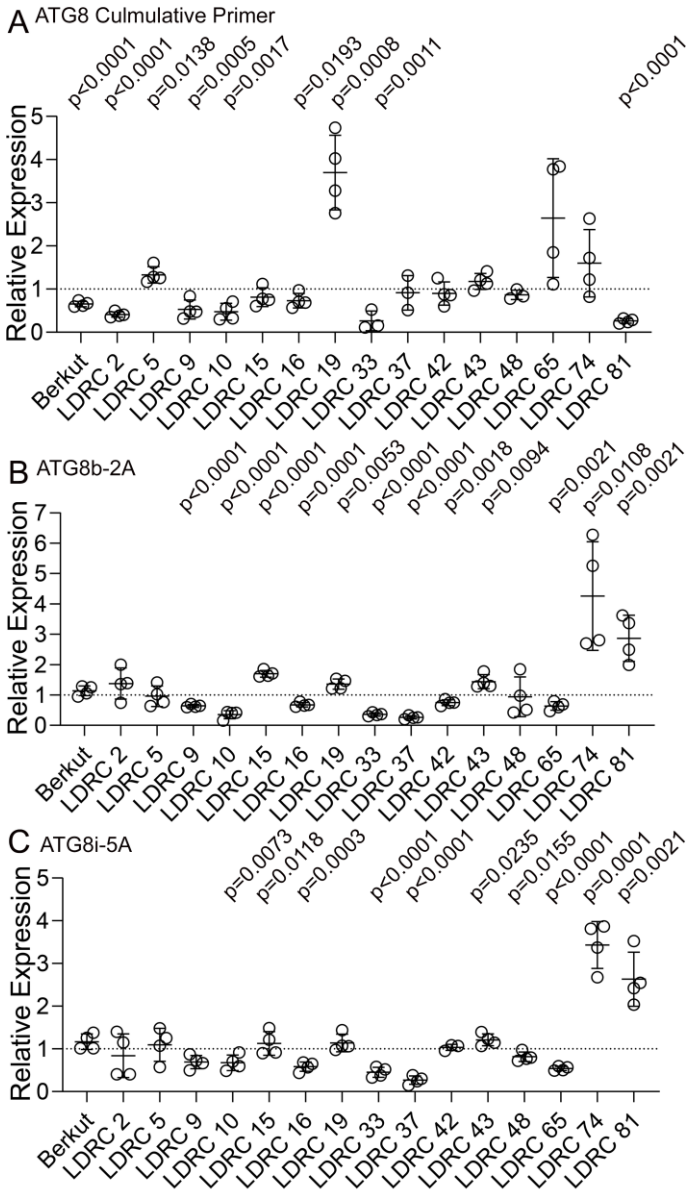

Figure 6.9: Impact of heat and drought stress on ATG8 transcription. **A,** Fold change of cumulative transcription level of *ATG8c-2A, ATG8f-2D, ATG8d-2B,* and *ATG8l*-6B in response to heat and drought stress relative to control. Student's T-Test at 95% confidence. (n=4, two different plants in two independent experiments). **B,C,** Fold change of *ATG8b*-2A (**B**) or *ATG8i*-5A (**C**) transcription level in response to heat and drought stress relative to control. *ADP-ribosylation factor 2* was used as a housekeeping gene for normalization of the transcript level (Genebank: XM_044502292.1; Paolacci et al. 2009). (n=4, two different plants in two independent experiments). Student's T-Test at 95% confidence. (n=4, two different plants in two independent experiments).

ATG8b-2A and ATG8i-5A. At least one of the *ATG8* transcripts was up regulated in response to heat and drought stress relative to the control in genotypes LDRC5, LDRC15, LDRC19, LDRC65, LDRC74, and LDRC81. The rest of the genotypes maintained steady transcription level for all *ATG8* primer pairs (**Figure 6.9**).

Section 5: Impact of drought stress on transcription of all autophagy genes

To evaluate conservation of autophagic responses to stress, Dr. Yunus Sahin in collaboration with our laboratory performed transcriptomic analyses using published RNA-seq datasets from other plant species (**Figure 6.10**). We analyzed drought stress because it was the most represented stress in the Gene Expression Omnibus (GEO) repository for a broad range of species. Eleven GEO datasets were selected for *Arabidopsis thaliana*, *Oryza sativa*, *Zea mays*, *Sorghum bicolor*, *Solanum tuberosum*, and *Solanum lycopersicum*. Drought caused up-regulation of *ATG8* family members in both dicot and monocot species, *ATG3* and *ATG7* were upregulated mostly in monocots, and *ATG4* and *ATG18* were upregulated mostly in dicots. Hence, *ATG3* and *ATG7* could be markers of autophagic activity in wheat.

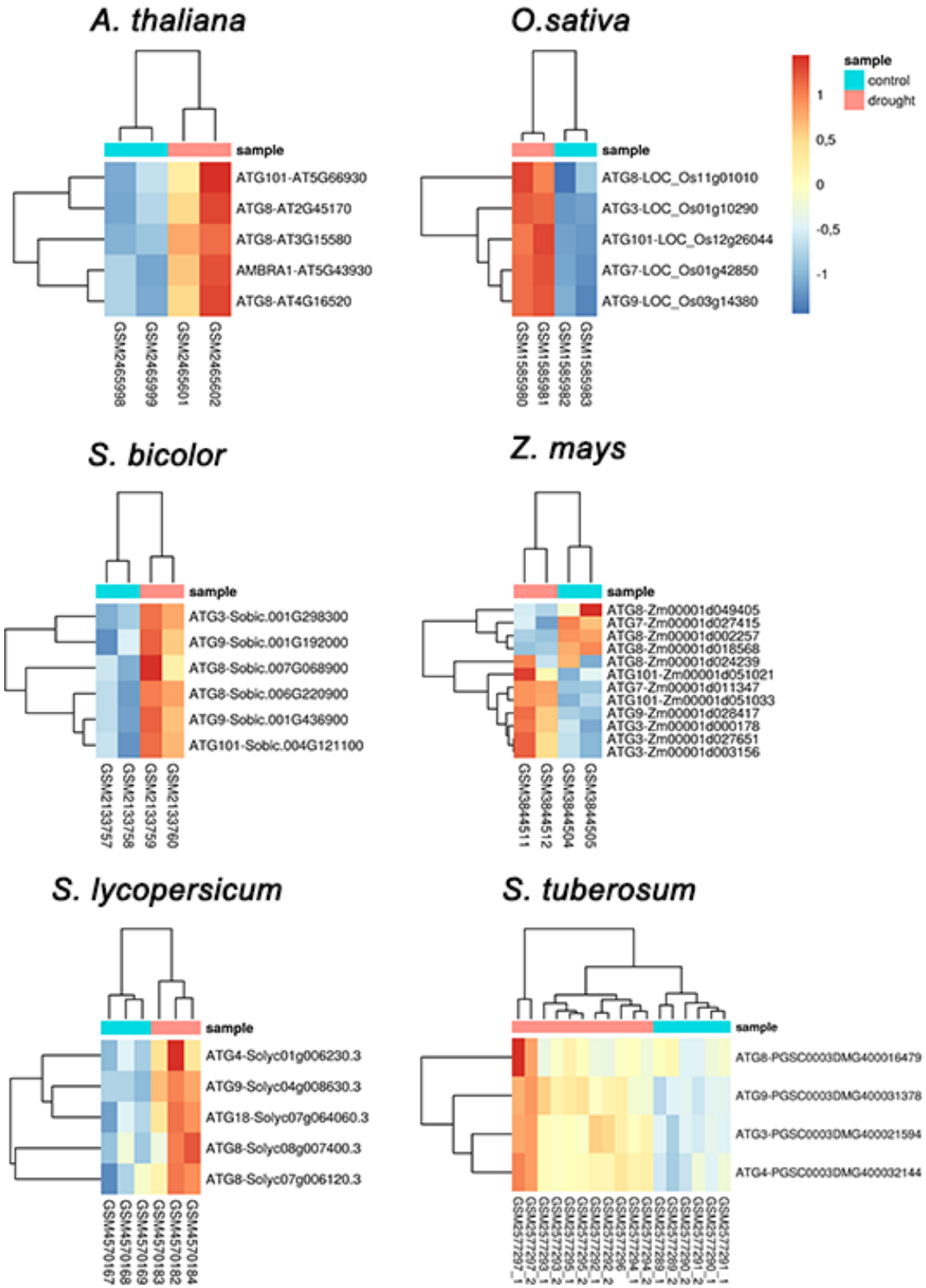

Figure 6.10: Heatmaps of autophagy-related genes that are differentially expressed in response to drought stress in *Z. mays, O. sativa, S. Bicolor, S. tuberosum, S. lycopersicum* and *A. thaliana.* Loci name of orthologs that were mapped to autophagy-related genes indicated beside gene names. This figure was produced by Dr. Yunus Sahin.

As both ATG3 and ATG7 function together in the pathway responsible for lipidation of ATG8, we only examined response of ATG7 to heat and drought stress. A polyclonal antibody against wheat ATG7 was produced in mice. An immuno-depletion assay with ATG7 antigen confirmed that antibody specifically recognizes ATG7 band corresponding to ca. 90 kD (**Figure 6.11A**). The impact of heat and drought stress on ATG7 protein abundance was measured in 16 genotypes (**Figure 6.11B-D**). In all genotypes anti-ATG7 cross-reacted with a single band. Overall, heat and drought stress caused higher ATG7 abundance in all genotypes with the exception of Berkut, where the abundance of ATG7 was reduced (**Figure 6.11E**). A significant increase of ATG7 abundance was found in LDRC5, LDRC16, and LDRC43.

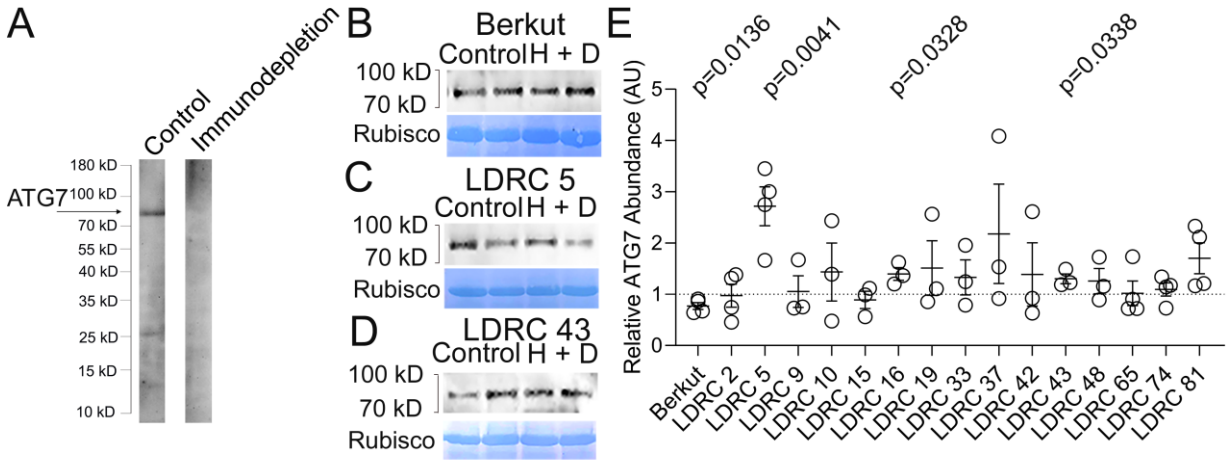

Figure 6.11: Impact of heat and drought on ATG7. **A,** Western blotting images of the total leaf extract from Berkut probed with anti-ATG7 or immunodepleted anti-ATG7. Pre-incubation of the serum with ATG7 protein abrogates the signal. **B-D**, Western blotting with anti-ATG7 of total protein extracts from leaves of control and heat + drought stressed (H+D) Berkut (**B**), LDRC5 (**C**), LDRC43 (**D**). Bars and number indicate position and corresponding size of molecular weight markers. Corresponding membrane stained with amidoblack shows Rubisco protein in each lane. Intensity of Rubisco band was used for normalization of the signal on the western blotting. **E**, Fold change of ATG7 protein abundance in response to heat and drought stress relative to the control. P-values represent statistical differences between control and stress treatments for Student's T-Test at 95% confidence (n=4, two different plants in two independent experiments).

Section 6: Impact of heat and drought on NBR1 activity

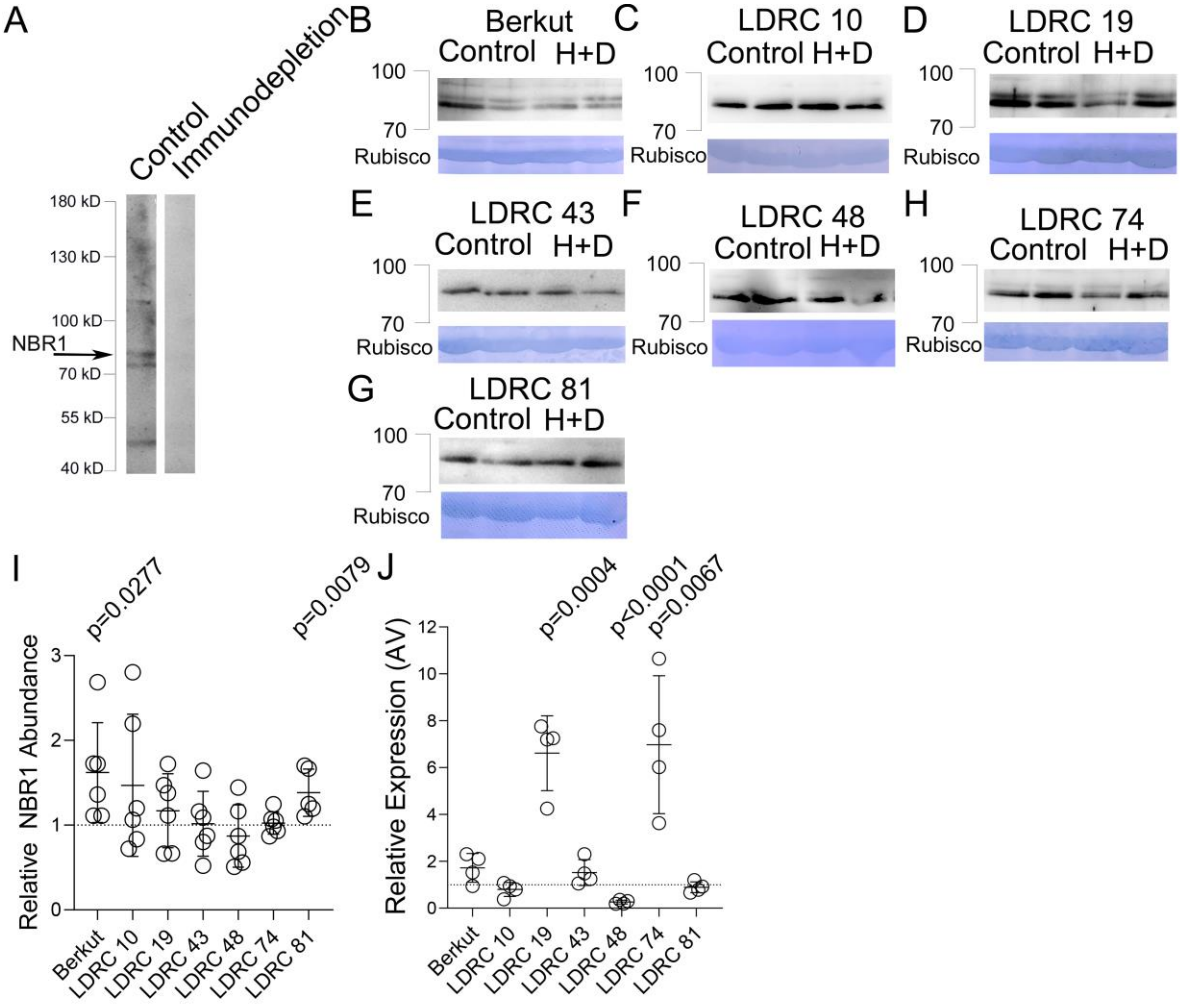

Figure 6.12: Impact of heat and drought stress on NBR1. **A,** Western blotting images of the total leaf extract from Berkut probed with anti-NBR1 or immunodepleted anti-NBR1. Pre-incubation of the serum with NBR1 protein abrogates the signal. **B-G**, Western blotting with anti-NBR1 of total protein extracts from leaves of well-watered (control) and heat + drought stressed (H+D) from Berkut (**B**), LDRC10 (**C**), LDRC19 (**D**), LDRC43 (**E**), LDRC48 (**F**), LDRC74 (**H**), LDRC81 (**G**). Bars and number indicate position and corresponding size of molecular weight markers. Amidoblack staining of the corresponding western blotting membrane shows Rubisco protein. **H**, Fold change of NBR1 protein abundance in response to heat and drought stress relative to the control. P-values represent statistical differences between control and stress treatments for Student's T-Test at 95% confidence (n=4, two different plants in two independent experiments). **I,** Fold change of *NBR1* transcript abundance in response to heat and drought stress relative to the control. *ADP-ribosylation factor 2* (Genebank: XM_044502292.1; Paolacci et al. 2009) was used as a housekeeping gene for normalization of RT-qPCR values. P-values represent statistical differences between control and stress treatments for Student's T-Test at 95% confidence (n=4, two different plants in two independent experiments).

Heat stress causes misfolding and damaging of proteins, which could cause cytotoxicity. The selective autophagy receptor NBR1 plays a role in specific targeting of protein aggregates for autophagy (Zhou et al. 2013; Zhou et al. 2014). NBR1 interacts

with ATG8 and degrades together with the autophagosome in the vacuole. Therefore, activation of autophagy is expected to increase NBR1 turnover. We examine NBR1 protein level in seven varieties that showed different response of ATG8 to the stress. Polyclonal anti-NBR1 was generated in mice (**Figure 6.12A**). In some genotypes the antibody cross-reacted with one band and in others with a doublet (**Figure 6.12B-H**). Heat and drought stress did not affect the band pattern and caused an increase of NBR1 abundance only in Berkut and LDRC81 (**Figure 6.12I**). The wheat genome has three homeologs of *NBR1*. We designed a pair of primers that targets all three of them and measured impact of heat and drought stress on transcription of *NBR1* by RT-qPCR. Transcription of NBR1 was up regulated in Berkut, LDRC19, LDRC43, and LDRC74 and downregulated in LDRC48 (**Figure 6.12J**).

Section 7: Relationship of autophagy markers and yield

We examined correlation between changes of autophagy markers and yield in both field trials individually and the average yield values. None of four measurements of ATG8-relatd bands (15 kD, 30 kD, 50 kD from one membrane and 15 kD measured individually) and ATG7 correlated with yield parameters in the population of 16 genotypes (**Figure 6.13A-B**). However, the ratios of 15kd/30kD and 30kD/50kD bands of ATG8 correlated negatively with yield (R^2=-0.5395 and -0.4423 respectively). Interestingly, all values derived from quantification of ATG8 bands showed a strong positive correlation (**Figure 6.13B**).

Correlations	R^2
Lind Yield vs. Othello Yield	0.7218
Lind Yield vs. Total Yield	0.8754
Othello Yield vs. Total Yield	0.9648
Othello Yield vs. 15kD/30kD Ratio	-0.5395
Othello Yield vs. 50kD/15kD Ratio	0.6761
Othello Yield vs. 30kD/50kD Ratio	-0.4423
Lind Yield vs. 15kD/30kD Ratio	-0.6539
Lind Yield vs. 50kD/15kD Ratio	0.6725
Lind Yield vs. 30kD/50kD Ratio	-0.5516
Total Yield Yield vs. 15kD/30kD Ratio	-0.6024
Total Yield Yield vs. 50kD/15kD Ratio	0.7022
Total Yield Yield vs. 30kD/50kD Ratio	-0.4907
ATG8 Abundance vs. 15kD Abundance	0.8274
ATG8 Abundance vs. 30kD Abundance	0.7466
ATG8 Abundance vs. 50kD Abundance	0.8597
ATG8 Abundance vs. Total Intensity	0.8224
15kD Abundance vs. 30kD Abundance	0.7264
15kD Abundance vs. Total Intensity	0.8448
15kD Abundance vs. 50kD Abundance	0.8448
30kD Abundance vs. 50kD Abundance	0.678
50kD Abundance vs. Total Intensity	0.8792
15kD/30kD Ratio vs 50/30kD Ratio	0.6427
15kD/50kD Ratio vs 30/50kD Ratio	0.8426

Correlations	R^2
Lind Yield vs. Othello Yield	0.7608
Lind Yield vs. Total Yield	0.8719
Othello Yield vs. Total Yield	0.9603
Othello Yield vs. 15kD/50kD Ratio	-0.8914
Othello Yield vs. 30kD/50kD Ratio	-0.8343
Lind Yield vs. 15kD/50kD Ratio	-0.8692
Lind Yield vs. 30kD/50kD Ratio	-0.8889
Total Yield vs. 15kD/50kD Ratio	-0.9278
Total Yield vs. 30kD/50kD Ratio	-0.8995
Lind Yield vs. *ATG8i*	0.5898
Lind Yield vs. *ATG8b*	0.6598
ATG8 Abundance vs. 15kD Abundance	0.9443
ATG8 Abundance vs. 30kD Abundance	0.8278
ATG8 Abundance vs. 50kD Abundance	0.8276
ATG8 Abundance vs. Total Intensity	0.9492
15kD Abundance vs. 30kD Abundance	0.9399
15kD Abundance vs. Total Intensity	0.8603
15kD Abundance vs. 50kD Abundance	0.97
30kD Abundance vs. 50kD Abundance	0.7356

Correlations	R^2
30kD Abundance vs. Total Intensity	0.9371
50kD Abundance vs. Total Intensity	0.8685
NBR1 Abundance vs. Lind Yield	-0.5677
NBR1 Abundance vs. Othello Yield	-0.7282
NBR1 Abundance vs. Total Yield	-0.7354
NBR1 Abundance vs. 50kD Abundance	-0.7089
NBR1 Abundance vs. 15kD/50kD Ratio	0.7121
NBR1 Abundance vs. 30kD/50kD Ratio	0.7981
NBR1 Abundance vs. 50kD/15kD Ratio	-0.5668
NBR1 Abundance vs. 50kD/30kD Ratio	-0.6486
NBR1 vs. *ATG8i* Universal	0.7966
NBR1 vs. *ATG8i*	0.4916
NBR1 vs. *ATG8b*	0.5571
NBR1 vs. 30kD Abundance	-0.568
ATG8i vs. *ATG8b*	0.9898
ATG8i vs. 15kD/50kD Ratio	0.7601
ATG8b vs. 15kD/50kD Ratio	0.7841
ATG8i vs. 30kD/50kD Ratio	-0.5428
ATG8b vs. 30kD/50kD Ratio	-0.6389

Figure 6.13: Relationship between yield and autophagy**. A,** Principal component analysis of yield, ATG8 parameters, and ATG7 for all genotypes. **B,** R^2 for PCA **(A). C,** Principal component analysis of yield ATG8 parameters, ATG7, and NBR1 parameters for 7 genotypes. **D,** R^2 for PCA **(C).**

Amongst seven genotypes selected for analysis of *NBR1* transcript and NBR1 protein abundance, both *ATG8i* and *ATG8b* correlated positively with yield in Lind trial (R^2=0.5898 and 0.6598 respectively; **Figure 6.13C-D**). NBR1 abundance correlated negatively with yield in both Lind and Othello trials (R^2=-0.5677 and -0.7354 respectively) whereas *NBR1* correlated positively with abundance of all *ATG8* transcriptions (R^2=0.7966, 0.4916, and 0.5571 respectively). *ATG8b* and *ATG8i* abundance correlated positively with each other (R^2=0.9898). As in case of the whole set of genotypes, the ratios of 15kD/50kD and 30kD/50kD ATG8 bands correlated negatively with yield. Thus, the ratios between ATG8 bands and abundance of NBR1 can be used for identification of autophagy markers associated with higher yield.

Section 8: Discussion and conclusions

Recycling of dysfunctional cellular components plays a key role in both development and stress (Marshall and Viestra, 2018; Tang and Bassham, 2018; Wang et al. 2021). Therefore, cellular mechanisms of adaptation to harsh environmental conditions rely on autophagy. We have previously shown that reduction of ATG8 abundance in two tolerant spring wheat genotypes under drought stress was accompanied by up-regulation of *ATG8* genes (Hickey et al. 2022). Here we analyzed heat and drought responses of autophagic markers ATG8, ATG7, and NBR1 in a diverse panel of tolerant and susceptible wheat genotypes.

It has been shown that lipidation of ATG8 generates an additional isoform that on the SDS-PAGE gels runs at ~15kD (Yoshimoto et al. 2004; Fujioka et al. 2008). However,

in addition to nascent ATG8 and ATG8-PE isoforms, antibodies against ATG8 cross react with multiple bands running below ~15kD in *Arabidopsis* (Yoshimoto et al. 2004; Thompson et al. 2005; Philips et al. 2008; Chung et al. 2009; Chung et al. 2010). Our immunoaffinity purified antibody against wheat ATG8 cross-reacts with multiple bands ranging between 12 and 90 kD. A similar range of ATG8 bands was detected with anti-ATG8 in rice and Brachypodium. The fact that proteomics analysis identified ATG8 in all but ~90 kD band suggests that higher molecular weight isoforms represent ATG8 species or ATG8-conjugates. The reason for the absence of ATG8 in the ~90 kD band could be explained by low abundance of ATG8 in this material. A wider size range of bands was detected in total protein extracts from Arabidopsis using commercially available ATG8 antibodies (Jasieniecka-Gazarkiewicz et al. 2021) and also with our immuno-affinity purified antibodies. Thus, ATG8 protein comprises heterogeneous isoforms in both monocot and dicot species.

Size heterogeneity of ATG8 bands could have multiple origins. As mentioned above, one reason is lipidation. Consistent with this hypothesis, some heterogeneity of ATG8 was lost following treatment with lipase. However, even after delipidation reaction the pattern of ATG8 bands remained complex. Other posttranslational modifications could also contribute to changing size of nascent ATG8, e.g. ATG8 undergoes phosphorylation, ubiquitination, and acetylation in mammalian cells (Reid et al. 2022; Nieto-Torres et al. 2023).

Second, sequence diversity of ATG8 paralogs. Hexaploid wheat genome contains 12 ATG8 paralogs of which nine are evolutionarily conserved. Three ATG8 homoeologs

on chromosome 6 contain unique intrinsically disordered regions. Based on the phylogenetic tree analysis, these homoeologs are wheat-specific with predicted molecular weight of 28 kD. Hence, the ~30 kD bands on the western blotting in **Figure 6.3A** could correspond to these paralogs.

Third, interaction with other proteins or oligomerization. For example, it has been shown that ATG8 can dimerize in yeast cells (Nakatogawa et al. 2007). ATG8-ATG3 conjugates in Arabidopsis run on a SDS-PAGE gel between ~75 and ~50kD (Yoshimoto et al. 2004; Fujioka et al. 2008). Recently, ATG8 was shown to interact with CLATHRIN LIGHT CHAIN 2 (CLC2) during Golgi remodeling after heat stress in *Arabidopsis* (Zhou et al. 2023). Two *Arabidopsis* paralogs ATG8a and ATG8i interact with the ESCRT component FREE1 to regulate autophagosome closure (Zeng et al. 2023). Some of these interactions could be covalent or withstand conditions of SDS-PAGE. As ATG8 plays a role of an autophagy receptor, ATG8-ation of ligands could contribute to a greater specificity of the autophagy process.

Interestingly, the pattern of ATG8 bands changes in response to stress. This fact suggests that each of the above mechanisms responsible for ATG8 heterogeneity would not only alter the size but also generate ATG8 forms with specialized functions. Functional diversity and different localization were shown for two ATG8 subfamilies in mammalian cells: MAP1LC3 (microtubule-associated protein 1 light chain 3–hereafter referred as to LC3) and GABARAP (γ-aminobutyric acid receptor-associated protein). The LC3 subfamily primary functions in autophagore elongation, whereas GABARAP functions in autophagsome-lysosome fusion (Varga et al. 2022). Additionally, some

mammalian ATG8 paralogs participate in other processes besides autophagy. For example, LC3C is involved in COPII-dependent ER export (Stadel et al. 2015) and GATE-16 (GABARAPL2/ATG8) functions in intra-Golgi trafficking (Sagiv et al. 2000).

Plant ATG8 paralogs show different capacity of post-translational modifications. For example, all *Arabidopsis* ATG8 with exception of ATG8h and ATG8i are cleaved by ATG4 (Yoshimoto et al. 2004). Analysis of ATG8 transcription patterns provides further support to the hypothesis of functional specialization. *Zhou et al. 2023*, reported that all ATG8 isoforms (ATg8a-ATG8i) are expressed in *Arabidopsis* roots/leaves. GUS-reporter assays demonstrated that out of 5 *ATG8* family members (*ATG8a*, *ATG8c, ATG8f, ATG8e*, and *ATG8h*) only *ATG8a* and *ATG8h* were up-regulated in response to sugar starvation (Sláviková et al. 2005). The five maize *ATG8* are expressed in multiple tissues including shoot apex, seedling leaves (L4, L3, and L2 order of appearance), nonpollinated ears, and tassels (Chung et al. 2009). However, the expression level was different, for example, *ZmATG8c* had higher expression in shoot apex, while *ZmATG8d* was expressed in older leaves (Chung et al. 2009).

Analysis of other proteins revealed lack of heterogeneity in case of ATG7 and genotype-specific heterogeneity in case of NBR1. Of seven genotypes analyzed, two showed distinguishable NBR1 double bands in all biological replicates under both heat and drought stress conditions (**Figure 6.12**). The upper band may represent a ubiquitylation post-translationally modified form of NBR1, as suggested by two studies in Arabidopsis (Kim et al. 2013; Jung et al. 2020). While heterogeneity of ATG8 was affected by the heat and drought stress, the pattern of NBR1 bands remained similar under all

growth conditions. Determining functional significance of NBR1 heterogeneity needs further analysis.

As autophagy encompasses turnover of proteins that associate with the autophagosomes, higher autophagic activity should be accompanied by reduced or constant ATG8 protein abundance. Sustaining ATG8 production under higher autophagic activity would require higher transcription of *ATG8*. Many publications show transcriptional up-regulation of *ATG8* and other autophagic proteins in response to stress. *ATG1*, *ATG4*, *ATG5*, *ATG8a*, and *ATG18b* were upregulated, while *ATG8g* was downregulated, during drought stress in *Medicago truncatula* (Yang et al. 2021). In tomato, eighteen autophagy genes including *ATG1*, *ATG3*, *ATG7*, *ATG8*, *ATG9*, were upregulated by drought stress (Wang et al. 2015) and *ATG5*, *ATG7*, and *NBR1* were upregulated by 45°C heat stress (Zhou et al. 2014). *ATG8* was upregulated in both roots and leaves during osmotic stress in *T. dicoccoides* (Kuzuoglu-Ozturk et al. 2012). It was shown that ethylene response factor, *ERF5*, induced by drought stress binds directly to *ATG8d* in tomato to increase both gene transcription and autophagic activity (Zhu et al. 2018).

Using publicly available RNA-seq datasets, we found that drought stress causes up-regulation of *ATG8* transcript in both dicots and monocots whereas *ATG3*, *ATG7*, *ATG9*, and *ATG101* were consistently upregulated in three monocots species, *O. sativa*, *Z. mays*, and *S bicolor*, but not in dicot species *A. thaliana*, *S. tuberosum*, and *S. lycopersicum* (**Figure 6.10**). Analysis of ATG8 transcription in the genetic diversity panel using three pairs of primers revealed that level of at least one *ATG8* transcript was up-

regulated in eight of sixteen genotypes (**Figure 6.7**). Only one genotype, LDRC74, showed upregulation of all tested *ATG8* in response to heat and drought stress. *ATG8* transcription was reduced or not affected in the remaining eight genotypes. ATG8 total protein level was reduced or remained constant in LDRC19, LDRC43, LDRC74, and LDRC81. This outcome is consistent with up-regulation of autophagy in four of sixteen genotypes. Providing that both *ATG8* transcripts and ATG8 protein level were measured accurately under our experimental conditions, and both parameters could be considered as a reliable marker of autophagic activity, our data demonstrates that activation of autophagy may not be the default response to heat and drought in wheat.

Heat and drought stress altered ATG8 heterogeneity in the genotype-specific manner. Reduction of total ATG8 protein abundance in LDRC19, LDRC43, LDRC74, and LDRC81 was accompanied by reduction of the 30 kD band (**Figure 6.5**). However, abundance of 15 kD bands in LDRC74 increased in response to heat and drought stress. Abundance of 30kD and 50kD bands increased in LDRC9 and LDRC37, while the abundance of 50kD band increased only in LDRC43 and LDRC65 and decreased in LDRC10. These data indicate that ATG8 isoforms play different roles in the stress response.

The patterning of 30kD and 50kD bands also showed genotype- and treatment-specific variability. However, the stress-induced changes in these bands were not consistent amongst biological replicates and treatments. For example, two bands at 30kD were detected in Berkut, LDRC10, LDRC19, LDRC65, and LDRC74 under both control and stress treatments. Furthermore, two 50kD bands were detected in LDRC10 under

both conditions, whereas in Berkut, LDRC16, LDRC33, LDRC65, and LDRC81, the 50kD doublet appeared only in control. Under heat and drought stress there were three or one 50kD bands in Berkut and three or two bands in LDRC9. Three 50kD bands in LDRC2 persisted under heat and drought stress but at lower abundance. It means that ATG8 isoforms perform different functions. This conclusion is supported by the fact that majority of ATG8 proteins remained unclustered in the high-stringency phylogenetic analysis (**Figure 6.2**). Functional conservation would lead to more clades. Furthermore, heterogeneity of the 30kD and 50kD reflects contribution of autophagy to the interactions between genotype and environment.

Multiple evidence highlights the contribution of autophagy to stress tolerance. For example, overexpression of ATG10 in apples enhances salt stress tolerance (Huo et al. 2020), overexpression of *ATG3b* in *Arabidopsis* leads to both salt and osmotic stress tolerance (Wang et al. 2017), and overexpression of *ATG5* or *ATG7* in *Arabidopsis* promotes ATG8 lipidation, autophagosome formation, and autophagic activity (Minina et al. 2018). The latter transgenic lines are more resistant to oxidative stress (treatment with methyl viologen) and necrotrophic pathogens. *ATG2* and *ATG7* also contribute to salt stress tolerance in wheat through suppression of salt-induced programmed cell death (Yue, 2021). ATG10 was shown to play a role in salt tolerance and resistance to methyl viologen in rice (Shin e al, 2009), whereas ATG6 contributes to heat, cold, and drought stress responses in rice (Rana et al. 2012).

Analysis of sixteen diverse genotypes in our work demonstrated poor correlation between relative abundance of total ATG7, ATG8, or the ~15kD ATG8 species and yield

under heat and drought stress ($-0.106<R^2<0.267$; **Figure 6.13**). However, parameters derived from the heterogeneity of ATG8 were more sensitive in the principal component analysis. In particular, the ratios between ~15kd and ~30kD, and ~30kD and ~50kD bands correlated negatively with yield. Thus, these ratios could be used to

Heat stress is known to cause protein misfolding and aggregation (Zhou et al. 2013), which are recycled through a specific type of autophagy known as aggrephagy (Zhou et al. 2014; Jung et al. 2020). NBR1 acts as a cargo receptor for protein aggregates and becomes recruited to the autophagosome through interaction with ATG8 (Zhou et al. 2013). The importance of NBR1 for stress tolerance is supported by several studies. First, Arabidopsis *nbr1* mutants are hypersensitive to heat stress and oxidative stress (methyl viologen; Zhou et al. 2013). Second, overexpression of *NBR1* results in greater UV-B and heat stress tolerance in *Arabidopsis* (Zhang and Ling, 2023), and in lower abundance of reactive oxygen species under salt stress, higher transcription of *ATG8,* greater autophagosome abundance, and reduced accumulation of insoluble proteins under salt stress in poplar (Su et al. 2021).

As an autophagosome cargo receptor, NBR1 degrades in the vacuole together with ATG8 and the autophagosome. Hence, higher autophagic activity should be accompanied by up-regulation of *NBR1* transcription and constant or lower NBR1 protein levels. Four out of seven genotypes show this type of response: up-regulation of *NBR1* transcription was accompanied by constant protein abundance in LDRC19, LDRC43, and LDRC74; constant transcription level of *NBR1* was accompanied by reduced protein abundance in LDRC48 (**Figure 6.12**). Changes of NBR1 protein abundance negatively

correlated with yield under heat and drought stress in both locations (**Figure 6.13**). These data demonstrate that NBR1 could be used as a marker of heat and drought stress resilience.

Many published data points out an enormous potential of autophagy trait for improving resilience of crops to abiotic and biotic stress factors. Exploiting autophagy in breeding programs is hindered by the lack of corresponding phenotyping tools. Robust phenotyping would enable identification of genetic markers for autophagy that could be used in genomic selection. Application of three common markers for assessing autophagic activity, ATG7, ATG8, and NBR1, under heat and drought stress in genetically diverse wheat genotypes led to the following conclusions.

1. Changes of ATG8 and NBR1 protein and transcript abundance in response to heat and drought stress in LDRC19, LDRC43, and LDRC74 is consistent with up-regulation of autophagy. These genotypes belong to distant phylogenetic clades and originate from different regions: LDRC19 from Uruguay, LDRC43 from Mozambique, and LDRC74 from Afghanistan (**Figure 6.4**). All three genotypes were in the high-yielding group. This outcome means that autophagy trait was selected independently by several breeding programs in different geographical locations most likely due to better performance. These genotypes are suitable for identification of genetic markers for autophagic activity.

2. Relative changes of ATG8 isoforms and NBR1 abundance negatively correlate with yield. These parameters show a strong positive correlation with each other. Thus, abundance of ATG8 isoforms and NBR1 could be used as markers of autophagic

response to stress. Simultaneous measuring NBR1 and ATG8 increases accuracy of the phenotyping. Abundance of ATG7 shows limited variability and poor correlation with yield. This parameter needs further development before using in phenotyping autophagy.

3. Changes of ATG8 parameters under heat and drought stress in several genotypes suggested no up-regulation or even failure of autophagy. For example, accumulation of ATG8 protein in LDRC9 and LDRC48 was accompanied by no changes of ATG8 gene transcription. Increase of ATG8 abundance accompanied by similar or lower level of *ATG8* transcription indicates slower ATG8 degradation and relatively low autophagic activity. In LDRC10, ATG8 protein abundance remained constant after the stress and *ATG8* transcripts as detected by all 3 pairs of primers were downregulated. Genotypes LDRC2, LDRC33, and LDRC37 lack changes of both ATG8 protein and *ATG8* transcript abundance in response to stress. Constant abundance of ATG8 was accompanied by down-regulation of at least one *ATG8* transcript in Berkut, LDRC9, LDRC16, LDRC42, LDRC48, and LDRC65. Yet LDRC48 and LDRC9 were among the high-yielding genotypes. It means that lower autophagic activity could be dispensable for the stress tolerance.

It could be that suppression of autophagy and accumulation of autophagy markers under stress is a common outcome. For example, accumulation of autophagosomes and downregulation of *ATG8c* under heat stress was reported in pepper (Zhai et al. 2016), and accumulation of autophagosomes correlated with accumulation of LC3-II (ATG8) response to aggregation-prone proteins mHTT and alpha-synuclein in mammalian cells (Button et al. 2017). One explanation for the low frequency of autophagy trait in the

population is negatively selected during in some geographical locations due to the pressure from another environmental factor e.g. pathogens. This possibility also seems unlikely considering importance of autophagy for all processes related to plant health including immunity. Another possibility could be sensitivity of autophagy pathway to heat stress. In this case other mechanisms compensate for the lack of autophagy in sustaining the yield. As the selection of landraces was likely based on yield and end-user qualities, the tolerance traits were selected randomly. Testing this prediction would require developing varieties with efficient autophagy using phenotyping tools developed in our work and examining their genotype by environment interactions.

CHAPTER 7: CONCLUSIONS AND FUTURE DIRECTIONS

This dissertation is dedicated to understanding cellular protection mechanisms of heat and drought stress resiliency in wheat. Cellular protection mechanisms include maintaining ROS homeostasis through scavenging ROS and using autophagy to degrade damaged cellular components. The main goal of this dissertation was to understand ROS homeostasis contributed to heat and drought tolerance in the context of well characterized mechanisms including root architecture and chlorophyll fluorescence. During this research, molecular markers for ROS homeostasis and autophagy were identified. In this dissertation: (1) Chapter 3 compared the growth and development of genetically different wheat varieties through flowering time and root architecture; (2) Chapter 4 analysed photosynthetic and ROS activity under drought; (3) Chapter 5 identified molecular markers for ROS homeostasis and regulators of peroxisome proliferation; and (4) Chapter 6 analysed autophagy under heat and drought identifying molecular markers of autophagy. We found that resilient genotypes exploit multiple strategies to overcome the stress. Furthermore, each genotype did not possess all strategies analysed. It means there is potential to increase crop resiliency by combining more resiliency mechanisms in one genotype.

During this dissertation *PEX11C*, *CAT2*, ATG8, ATG7, and NBR1 were identified as molecular markers for ROS homeostasis and autophagy. Four polyclonal antibodies were developed for wheat proteins: catalase, ATG8, ATG7, and NBR1. All polyclonal antibodies were first produced in mice and catalase, ATG8, and NBR1 were subsequently produced in rabbits. Anti-ATG7 could be produced in rabbits in the future. Anti-ATG8 was

affinity purified. Anti-catalase and anti-NBR1 will need to be affinity purified in the future using the same method. Additionally, these antibodies can be used to develope high-throughput phenotyping techniques to screen large wheat breeding populations for responses of ROS homeostasis and autophagy. Development phenotyping techniques like ELISA would facilitate integrating underutilized heat and drought resilient mechanisms in the future.

Affinity purified anti-ATG8 captured multiple isoforms of ATG8 during western blotting. Discovering the origin of ATG8 heterogeneity is another direction for work in the future. This heterogeneity could be due to sequence diversity of ATG8 paralogs, interaction with other proteins or oligomerization, or post-translational modifications. To determine origins of the heterogeneity methods including size-exclusion chromatography and developing transgenic wheat plants to visualize *in planta* could be used. The ATG8 heterogeneity is an exciting discovery that presents numerous opportunities to characterize autophagy and ATG8 behavior in wheat and other species.

Additionally, NBR1 protein bands present genotype-specific heterogeneity. This heterogeneity may be to NBR1 paralogs or post-translational modifications. Determining the origin of genotype specific NBR1 heterogeneity through techniques including immunoprecipitation-mass spectroscopy or developing transgenic wheat plants to visualize *in planta* and use antibodies for the post-translational modifications could facilitate the discovery of genotype specific differences and unraveling functional significance of these differences. Determining the functional significance of NBR1

heterogeneity would advance our understanding of autophagy under normal and stress conditions.

Identification of genetic regulators of *CAT* and *PEX11* gene would provide targets for increasing cellular protection under stress. To identify the genetic regulation of stress induced peroxisome proliferation, we developed materials to perform a Streptavidin Affinity Chromatography. The methods and experimental setup were optimized in promoter cloning and amplification, nuclear protein extraction, and streptavidin resin column usage. Once the DNA-protein affinity chromatography is complete, identification and characterization of protein interactors would take place. Protein interactors would have to be confirmed through techniques like bimolecular fluorescence. Once protein interactors are confirmed, the fundamental understanding regulation of peroxisome proliferation under stress would increase and these proteins could provide targets to increase ROS homeostasis during breeding.

Overall, this dissertation demonstrates the importance of cellular protection mechanisms to sustain yield under stress. Stress resiliency strategies combine developmental, physiological, cellular, and molecular mechanisms. During this dissertation, it was found that stress resilient wheat genotypes combined numerous strategies to combat heat and drought stress. Genotype-specific responses included morphology of root architecture, development timeline (e.g. flowering timing), responses and regulation in the photosystems, and cellular responses of ROS scavengers, peroxisomes, and autophagy. Further development of techniques to analyze ROS homeostasis, peroxisome dynamics, and autophagy are essential to breeding resilient

wheat. *PEX11C*, *CAT2*, ATG8, ATG7, and NBR1 were identified as molecular markers for ROS homeostasis and autophagy and these markers can be exploited in the future. Additionally, mechanisms for resiliency including root architecture and photosynthetic traits establish that combining multiple protection mechanisms is a promising strategy to advance crop resiliency through introgression of several methods. Future identification and characterization of genetic markers for cellular protection mechanisms such as ROS homeostasis, peroxisome proliferation and autophagy is crucial for breeding wheat with greater stress resiliency.

REFERENCES

1. **Agati, G., Azzarello, E., Pollastri, S., & Tattini, M**. (2012). Flavonoids as antioxidants in plants: Location and functional significance. Plant Science, 196, 67–76. https://doi.org/10.1016/j.plantsci.2012.07.014

2. **Akter, N., & Rafiqul Islam, M**. (2017). Heat stress effects and management in wheat. A review. Agronomy for Sustainable Development, 37(5), 37. https://doi.org/10.1007/s13593-017-0443-9

3. **Al-Naggar, A. M. M., Shafik, M. M., & Elsheikh, M. O. A**. (2019). Putative Mechanisms of Drought Tolerance in Maize (Zea mays L.) via Root System Architecture Traits. Annual Research & Review in Biology, 32(2), 1–19. https://doi.org/10.9734/arrb/2019/v32i230079

4. **Anderson, C. M., Mattoon, E. M., Zhang, N., Becker, E., McHargue, W., Yang, J., Patel, D., Dautermann, O., McAdam, S. A. M., Tarin, T., Pathak, S., Avenson, T. J., Berry, J., Braud, M., Niyogi, K. K., Wilson, M., Nusinow, D. A., Vargas, R., Czymmek, K. J., … Zhang, R.** (2021). High light and temperature reduce photosynthetic efficiency through different mechanisms in the C4 model Setaria viridis. Communications Biology, 4(1), 1092. https://doi.org/10.1038/s42003-021-02576-2

5. **Anjum, S. A., Ashraf, U., Tanveer, M., Khan, I., Hussain, S., Shahzad, B., Zohaib, A., Abbas, F., Saleem, M. F., Ali, I., & Wang, L. C.** (2017). Drought induced changes in growth, osmolyte accumulation and antioxidant metabolism of three maize hybrids. Frontiers in Plant Science, 8(FEBRUARY). https://doi.org/10.3389/fpls.2017.00069

6. **Araus, J., Ferrio, J., Buxo, R., & Voltas, J.** (2006). The historical perspective of dryland agriculture: lessons learned from 10 000 years of wheat cultivation. Journal of Experimental Botany, 58(2), 131–145. https://doi.org/10.1093/jxb/erl133

7. **Asseng, S., Kassie, B. T., Labra, M. H., Amador, C., & Calderini, D. F**. (2017). Simulating the impact of source-sink manipulations in wheat. Field Crops Research, 202, 47–56. https://doi.org/10.1016/j.fcr.2016.04.031

8. **Baniulis, D., Hasan, S. S., Stofleth, J. T., & Cramer, W. A**. (2013). Mechanism of Enhanced Superoxide Production in the Cytochrome b 6 f Complex of Oxygenic Photosynthesis. Biochemistry, 52(50), 8975–8983. https://doi.org/10.1021/bi4013534

9. **Bao, Y., Song, W.-M., Wang, P., Yu, X., Li, B., Jiang, C., Shiu, S.-H., Zhang, H., & Bassham, D. C.** (2020). COST1 regulates autophagy to control plant drought tolerance. Proceedings of the National Academy of Sciences, 117(13), 7482–7493. https://doi.org/10.1073/pnas.1918539117

10. **Bassham, D. C**. (2015). Methods for analysis of autophagy in plants. Methods, 75, 181–188. https://doi.org/10.1016/j.ymeth.2014.09.003

11. **Basu, S., Ramegowda, V., Kumar, A., & Pereira, A**. (2016). Plant adaptation to drought stress. F1000Research, 5. https://doi.org/10.12688/f1000research.7678.1

12. **Bilgrami, S. S., Ramandi, H. D., Shariati, V., Razavi, K., Tavakol, E., Fakheri, B. A., Mahdi Nezhad, N., & Ghaderian, M.** (2020). Detection of genomic regions associated with tiller number in Iranian bread wheat under different water regimes using genome-wide association study. Scientific Reports, 10(1). https://doi.org/10.1038/s41598-020-69442-9

13. **Blake, N. K., Pumphrey, M., Glover, K., Chao, S., Jordan, K., Jannick, J.-L., Akhunov, E. A., Dubcovsky, J., Bockelman, H., & Talbert, L. E**. (2019). Registration of the Triticeae-CAP Spring Wheat Nested Association Mapping Population. Journal of Plant Registrations, 13(2), 294–297. https://doi.org/10.3198/jpr2018.07.0052crmp

14. **Bolger, A. M., Lohse, M., & Usadel, B.** (2014). Trimmomatic: A flexible trimmer for Illumina sequence data. Bioinformatics, 30(15), 2114–2120. https://doi.org/10.1093/bioinformatics/btu170

15. **Bowne, J. B., Erwin, T. A., Juttner, J., Schnurbusch, T., Langridge, P., Bacic, A., & Roessner, U.** (2012). Drought Responses of Leaf Tissues from Wheat Cultivars of Differing Drought Tolerance at the Metabolite Level. Molecular Plant, 5(2), 418–429. https://doi.org/10.1093/mp/ssr114

16. **Burton, A. L., Johnson, J. M., Foerster, J. M., Hirsch, C. N., Buell, C. R., Hanlon, M. T., Kaeppler, S. M., Brown, K. M., & Lynch, J. P**. (2014). QTL mapping and phenotypic variation for root architectural traits in maize (Zea mays L.). Theoretical and Applied Genetics, 127(11), 2293–2311. https://doi.org/10.1007/s00122-014-2353-4

17. **Bussell, J. D., Behrens, C., Ecke, W., & Eubel, H.** (2013). Arabidopsis peroxisome proteomics. Frontiers in Plant Science, 4(APR), 101. https://doi.org/10.3389/fpls.2013.00101

18. **Button, R. W., Roberts, S. L., Willis, T. L., Hanemann, C. O., & Luo, S**. (2017). Accumulation of autophagosomes confers cytotoxicity. Journal of Biological Chemistry, 292(33), 13599–13614. https://doi.org/10.1074/jbc.M117.782276

19. **Calero-Muñoz, N., Exposito-Rodriguez, M., Collado-Arenal, A. M., Rodríguez-Serrano, M., Laureano-Marín, A. M., Santamaría, M. E., Gotor, C., Díaz, I., Mullineaux, P. M., Romero-Puertas, M. C., Olmedilla, A., & Sandalio, L. M**. (2019). Cadmium induces reactive oxygen species-dependent pexophagy in Arabidopsis leaves. Plant Cell and Environment, 42(9), 2696–2714. https://doi.org/10.1111/pce.13597

20. **Castillo, M. C., Sandalio, L. M., Del Río, L. A., & León, J.** (2008). Peroxisome proliferation, wound-activated responses and expression of peroxisome-associated genes are cross-regulated but uncoupled in Arabidopsis thaliana. Plant, Cell & Environment, 31(4), 492–505. https://doi.org/10.1111/j.1365-3040.2008.01780.x

21. **Caverzan, A., Casassola, A., & Brammer, S. P.** (2016). Antioxidant responses of wheat plants under stress. Genetics and Molecular Biology, 39(1), 1–6. https://doi.org/10.1590/1678-4685-GMB-2015-0109

22. **Chen, L., Lv, Q., Yang, W., Yang, H., Chen, Q., Wang, B., Lei, Y., & Xie, Y.** (2022). TaNBR1, a Novel Wheat NBR1-like Domain Gene Negatively Regulates Drought Stress Tolerance in Transgenic Arabidopsis. International Journal of Molecular Sciences, 23(9), 4519. https://doi.org/10.3390/ijms23094519

23. **Chen, L., Wu, R., Feng, J., Feng, T., Wang, C., Hu, J., Zhan, N., Li, Y., Ma, X., Ren, B., Zhang, J., Song, C. P., Li, J., Zhou, J. M., & Zuo, J.** (2020). Transnitrosylation Mediated by the Non-canonical Catalase ROG1 Regulates Nitric Oxide Signaling in Plants. Developmental Cell, 53(4), 444-457.e5. https://doi.org/10.1016/j.devcel.2020.03.020

24. **Chen, Q., Soulay, F., Saudemont, B., Elmayan, T., Marmagne, A., & Masclaux-Daubresse, C.** (2019). Overexpression of ATG8 in Arabidopsis Stimulates Autophagic Activity and Increases Nitrogen Remobilization Efficiency and Grain Filling. Plant and Cell Physiology, 60(2), 343–352. https://doi.org/10.1093/pcp/pcy214

25. **Choudhury, F. K., Rivero, R. M., Blumwald, E., & Mittler, R.** (2017). Reactive oxygen species, abiotic stress and stress combination. The Plant Journal, 90(5), 856–867. https://doi.org/10.1111/tpj.13299

26. **Chugh, V., Kaur, N., & Gupta, A. K.** (2011). Evaluation of oxidative stress tolerance in maize (Zea mays L.) seedlings in response to drought. Indian Journal of Biochemistry & Biophysics, 48(1), 47–53.

27. **Chung, T., Suttangkakul, A., & Vierstra, R. D**. (2009). The ATG Autophagic Conjugation System in Maize: ATG Transcripts and Abundance of the ATG8-Lipid Adduct Are Regulated by Development and Nutrient Availability. *Plant Physiology*, 149(1), 220–234. https://doi.org/10.1104/pp.108.126714

28. **Condon, A. G., Richards, R. A., Rebetzke, G. J., & Farquhar, G. D**. (2004). Breeding for high water-use efficiency. Journal of Experimental Botany, 55(407), 2447–2460. https://doi.org/10.1093/jxb/erh277

29. **Condon AG, Farquhar GD, Rebetzke GJ, R. R**. (2006). The application of carbon isotope discrimination in cereal improvement for water-limited environments. In Ribaut JM (Ed.), Drought adaptation in cereals (pp. 171–222). Food Products Press.

30. **Cui, P., Liu, H., Islam, F., Li, L., Farooq, M. A., Ruan, S., & Zhou, W**. (2016). OsPEX11, a Peroxisomal Biogenesis Factor 11, Contributes to Salt Stress Tolerance in Oryza sativa. Frontiers in Plant Science, 7. https://doi.org/10.3389/fpls.2016.01357

31. **Dalal, M., Sahu, S., Tiwari, S., Rao, A. R., & Gaikwad, K.** (2018). Transcriptome analysis reveals interplay between hormones, ROS metabolism and cell wall biosynthesis for drought-induced root growth in wheat. Plant Physiology and Biochemistry, 130, 482–492. https://doi.org/10.1016/j.plaphy.2018.07.035

32. **Das, K., & Roychoudhury, A.** (2014). Reactive oxygen species (ROS) and response of antioxidants as ROS-scavengers during environmental stress in plants. Frontiers in Environmental Science, 2. https://doi.org/10.3389/fenvs.2014.00053

33. **del Río, L. A., & López-Huertas, E.** (2016). ROS Generation in Peroxisomes and its Role in Cell Signaling. Plant and Cell Physiology, 57(7), pcw076. https://doi.org/10.1093/pcp/pcw076

34. **Demidchik, V.** (2015). Mechanisms of oxidative stress in plants: From classical chemistry to cell biology. Environmental and Experimental Botany, 109, 212–228. https://doi.org/10.1016/J.ENVEXPBOT.2014.06.021

35. **Dempewolf, H., Baute, G., Anderson, J., Kilian, B., Smith, C., & Guarino, L.** (2017). Past and Future Use of Wild Relatives in Crop Breeding. Crop Science, 57(3), 1070–1082. https://doi.org/10.2135/cropsci2016.10.0885

36. **Desai, M., & Hu, J.** (2008). Light Induces Peroxisome Proliferation in Arabidopsis Seedlings through the Photoreceptor Phytochrome A, the Transcription Factor HY5 HOMOLOG, and the Peroxisomal Protein PEROXIN11b. Plant Physiology, 146(3), 1117–1127. https://doi.org/10.1104/pp.107.113555

37. **Duan, J., Zhang, M., Zhang, H., Xiong, H., Liu, P., Ali, J., Li, J., & Li, Z.** (2012). OsMIOX, a myo-inositol oxygenase gene, improves drought tolerance through scavenging of reactive oxygen species in rice (Oryza sativa L.). Plant Science, 196, 143–151. https://doi.org/10.1016/j.plantsci.2012.08.003

38. **Ebeed, H. T., Stevenson, S. R., Cuming, A. C., & Baker, A**. (2018). Conserved and differential transcriptional responses of peroxisome associated pathways to drought, dehydration and ABA. Journal of Experimental Botany, 69(20), 4971–4985. https://doi.org/10.1093/jxb/ery266

39. **Efeoğlu, B., Ekmekçi, Y., & Çiçek, N**. (2009). Physiological responses of three maize cultivars to drought stress and recovery. South African Journal of Botany, 75(1), 34–42. https://doi.org/10.1016/j.sajb.2008.06.005

40. **Eisenhut, M., Br, A., Autigam, €, Timm, S., Florian, A., Tohge, T., Fernie, A. R., Bauwe, H., & Weber, A. P. M**. (2017). Photorespiration Is Crucial for Dynamic Response of Photosynthetic Metabolism and Stomatal Movement to Altered CO 2 Availability. https://doi.org/10.1016/j.molp.2016.09.011

41. **Erenstein, O., Jaleta, M., Mottaleb, K.A., Sonder, K., Donovan, J., Braun, HJ.** (2022). Global Trends in Wheat Production, Consumption and Trade. In: Reynolds, M.P., Braun, HJ. (eds) Wheat Improvement. Springer, Cham. https://doi.org/10.1007/978-3-030-90673-3_4

42. **Exposito-Rodriguez, M., Laissue, P. P., Yvon-Durocher, G., Smirnoff, N., & Mullineaux, P. M.** (2017). Photosynthesis-dependent H2O2 transfer from chloroplasts to nuclei provides a high-light signalling mechanism. Nature Communications, 8(1), 49. https://doi.org/10.1038/s41467-017-00074-w

43. **Fahad, S., Bajwa, A. A., Nazir, U., Anjum, S. A., Farooq, A., Zohaib, A., Sadia, S., Nasim, W., Adkins, S., Saud, S., Ihsan, M. Z., Alharby, H., Wu, C., Wang, D., & Huang, J.** (2017). Crop production under drought and heat stress: Plant responses and management options. In Frontiers in Plant Science (Vol. 8). Frontiers Media S.A. https://doi.org/10.3389/fpls.2017.01147

44. **Fahad, S., Bajwa, A. A., Nazir, U., Anjum, S. A., Farooq, A., Zohaib, A., Sadia, S., Nasim, W., Adkins, S., Saud, S., Ihsan, M. Z., Alharby, H., Wu, C., Wang, D., & Huang, J.** (2017). Crop Production under Drought and Heat Stress: Plant Responses and Management Options. Frontiers in Plant Science, 8, 1147. https://doi.org/10.3389/fpls.2017.01147

45. **Fahy, D., Sanad, M. N. M. E., Duscha, K., Lyons, M., Liu, F., Bozhkov, P., Kunz, H.-H., Hu, J., Neuhaus, H. E., Steel, P. G., & Smertenko, A**. (2017). Impact of salt stress, cell death, and autophagy on peroxisomes: quantitative and morphological analyses using small fluorescent probe N-BODIPY. Scientific Reports, 7(1), 39069. https://doi.org/10.1038/srep39069

46. **Fang, Y., & Xiong, L.** (2015). General mechanisms of drought response and their application in drought resistance improvement in plants. In Cellular and Molecular Life Sciences (Vol. 72, Issue 4, pp. 673–689). Birkhauser Verlag AG. https://doi.org/10.1007/s00018-014-1767-0

47. **Farmer, L. M., Rinaldi, M. A., Young, P. G., Danan, C. H., Burkhart, S. E., & Bartel, B**. (2013). Disrupting autophagy restores peroxisome function to an arabidopsis lon2 mutant and reveals a role for the LON2 protease in peroxisomal matrix protein degradation. Plant Cell, 25(10), 4085–4100. https://doi.org/10.1105/tpc.113.113407

48. **Farooq, M. A., Niazi, A. K., Akhtar, J., Saifullah, Farooq, M., Souri, Z., Karimi, N., & Rengel, Z.** (2019). Acquiring control: The evolution of ROS-Induced oxidative stress and redox signaling pathways in plant stress responses. In Plant Physiology and Biochemistry (Vol. 141, pp. 353–369). Elsevier Masson SAS. https://doi.org/10.1016/j.plaphy.2019.04.039

49. **Faseela, P., Sinisha, A. K., Brestič, M., & Puthur, J. T**. (2020). Chlorophyll a fluorescence parameters as indicators of a particular abiotistress in rice. Photosynthetica, 58(Special Issue), 293–300. https://doi.org/10.32615/ps.2019.147

50. Food security. (2022). In Climate Change and Land (pp. 437–550). Cambridge University Press. https://doi.org/10.1017/9781009157988.007

51. **Ford, K. L., Cassin, A., & Bacic, A**. (2011). Quantitative proteomic analysis of wheat cultivars with differing drought stress tolerance. Frontiers in Plant Science, 2, 44. https://doi.org/10.3389/fpls.2011.00044

52. **Foyer, C. H., & Noctor, G**. (2000). Oxygen processing in photosynthesis: Regulation and signalling. In New Phytologist (Vol. 146, Issue 3, pp. 359–388). https://doi.org/10.1046/j.1469-8137.2000.00667.x

53. **Foyer, C. H., & Noctor, G**. (2003). Redox sensing and signalling associated with reactive oxygen in chloroplasts, peroxisomes and mitochondria. Physiologia Plantarum, 119(3), 355–364. https://doi.org/10.1034/j.1399-3054.2003.00223.x

54. **Foyer, C. H., & Noctor, G.** (2016). Stress-triggered redox signalling: what's in pROSpect? Plant, Cell & Environment, 39(5), 951–964. https://doi.org/10.1111/pce.12621

55. **Foyer, C. H., & Shigeoka, S**. (2011). Understanding oxidative stress and antioxidant functions to enhance photosynthesis. Plant Physiology, 155(1), 93–100. https://doi.org/10.1104/pp.110.166181

56. **Fujioka, Y., Noda, N. N., Fujii, K., Yoshimoto, K., Ohsumi, Y., & Inagaki, F.** (2008). In vitro reconstitution of plant Atg8 and Atg12 conjugation systems essential for autophagy. Journal of Biological Chemistry, 283(4), 1921–1928. https://doi.org/10.1074/jbc.M706214200

57. **Ghimire, B., Hulbert, S. H., Steber, C. M., Garland-Campbell, K., & Sanguinet, K. A.** (2020). Characterization of root traits for improvement of spring wheat in the Pacific Northwest. Agronomy Journal, 112(1), 228–240. https://doi.org/10.1002/agj2.20040

58. **Giménez, M. J., Pistón, F., & Atienza, S. G.** (2011). Identification of suitable reference genes for normalization of qPCR data in comparative transcriptomics analyses in the Triticeae. Planta, 233(1), 163–173. https://doi.org/10.1007/s00425-010-1290-y

59. **Goto-Yamada, S., Mano, S., Yamada, K., Oikawa, K., Hosokawa, Y., Hara-Nishimura, I., & Nishimura, M.** (2015). Dynamics of the Light-Dependent Transition of Plant Peroxisomes: Fig. 1. Plant and Cell Physiology, 56(7), 1264–1271. https://doi.org/10.1093/pcp/pcv081

60. **Guiboileau, A., Yoshimoto, K., Soulay, F., Bataillé, M., Avice, J., & Masclaux-Daubresse, C.** (2012). Autophagy machinery controls nitrogen remobilization at the whole-plant level under both limiting and ample nitrate conditions in Arabidopsis. New Phytologist, 194(3), 732–740. https://doi.org/10.1111/j.1469-8137.2012.04084.x

61. **Guo, P., Baum, M., Varshney, R. K., Graner, A., Grando, S., & Ceccarelli, S.** (2008). QTLs for chlorophyll and chlorophyll fluorescence parameters in barley under post-flowering drought. Euphytica, 163(2), 203–214. https://doi.org/10.1007/s10681-007-9629-6

62. **Guo, Y. Y., Tian, S. S., Liu, S. S., Wang, W. Q., & Sui, N**. (2018). Energy dissipation and antioxidant enzyme system protect photosystem II of sweet sorghum under drought stress. Photosynthetica, 56(3), 861–872. https://doi.org/10.1007/s11099-017-0741-0

63. **Hackenberg, T., Juul, T., Auzina, A., Gwiżdż, S., Małolepszy, A., Van Der Kelen, K., Dam, S., Bressendorff, S., Lorentzen, A., Roepstorff, P., Lehmann Nielsen, K., Jørgensen, J.-E., Hofius, D., Breusegem, F. Van, Petersen, M., & Andersen, S. U.** (2013). Catalase and NO CATALASE ACTIVITY1 Promote Autophagy-Dependent Cell Death in Arabidopsis. The Plant Cell, 25(11), 4616–4626. https://doi.org/10.1105/tpc.113.117192

64. **Hasanuzzaman, M., Bhuyan, M. H. M. B., Anee, T. I., Parvin, K., Nahar, K., Mahmud, J. Al, & Fujita, M**. (2019). Regulation of Ascorbate-Glutathione Pathway in Mitigating Oxidative Damage in Plants under Abiotic Stress. Antioxidants, 8(9), 384. https://doi.org/10.3390/antiox8090384

65. **Hasanuzzaman, M., Nahar, K., Alam, Md., Roychowdhury, R., & Fujita, M**. (2013). Physiological, Biochemical, and Molecular Mechanisms of Heat Stress Tolerance in Plants. International Journal of Molecular Sciences, 14(5), 9643–9684. https://doi.org/10.3390/ijms14059643

66. **He, X., Qu, B., Li, W., Zhao, X., Teng, W., Ma, W., Ren, Y., Li, B., Li, Z., & Tong, Y.** (2015). The nitrate inducible NAC transcription factor TaNAC2-5A controls nitrate response and increases wheat yield. Plant Physiology, pp.00568.2015. https://doi.org/10.1104/pp.15.00568

67. **Held, P.** (2015). An Introduction to Reactive Oxygen Species Measurement of ROS in Cells.

68. **Henry, A., Gowda, V. R. P., Torres, R. O., McNally, K. L., & Serraj, R.** (2011). Variation in root system architecture and drought response in rice (Oryza sativa): Phenotyping of the OryzaSNP panel in rainfed lowland fields. Field Crops Research, 120(2), 205–214. https://doi.org/10.1016/j.fcr.2010.10.003

69. **Hickey, K., Wood, M., Sexton, T., Sahin, Y., Nazarov, T., Fisher, J., Sanguinet, K. A., Cousins, A., Kirchhoff, H., & Smertenko, A.** (2022). Drought Tolerance Strategies and Autophagy in Resilient Wheat Genotypes. Cells, 11(11), 1765. https://doi.org/10.3390/cells11111765

70. **Higashi, Y., Okazaki, Y., Myouga, F., Shinozaki, K., & Saito, K.** (2015). Landscape of the lipidome and transcriptome under heat stress in Arabidopsis thaliana. Scientific Reports, 5(1), 10533. https://doi.org/10.1038/srep10533

71. **Hinojosa, L., Sanad, M. N. M. E., Jarvis, D. E., Steel, P., Murphy, K., & Smertenko, A.** (2019). Impact of heat and drought stress on peroxisome proliferation in quinoa. The Plant Journal, 99(6), 1144–1158. https://doi.org/10.1111/tpj.14411

72. **Hu, J.** (2010). Molecular Basis of Peroxisome Division and Proliferation in Plants. Elsevier Inc. https://doi.org/10.1016/S1937-6448(10)79003-1

73. **Hu, J., Baker, A., Bartel, B., Linka, N., Mullen, R. T., Reumann, S., & Zolman, B. K.** (2012). Plant Peroxisomes: Biogenesis and Function. The Plant Cell, 24(6), 2279–2303. https://doi.org/10.1105/tpc.112.096586

74. **Hu, S., Ding, Y., & Zhu, C.** (2020). Sensitivity and Responses of Chloroplasts to Heat Stress in Plants. Frontiers in Plant Science, 11. https://doi.org/10.3389/fpls.2020.00375

75. **Huang, H., Ullah, F., Zhou, D. X., Yi, M., & Zhao, Y.** (2019). Mechanisms of ROS regulation of plant development and stress responses. In Frontiers in Plant Science (Vol. 10, p. 800). Frontiers Media S.A. https://doi.org/10.3389/fpls.2019.00800

76. **Huo, L., Guo, Z., Jia, X., Sun, X., Wang, P., Gong, X., & Ma, F.** (2020). Increased autophagic activity in roots caused by overexpression of the autophagy-related gene MdATG10 in apple enhances salt tolerance. Plant Science, 294, 110444. https://doi.org/10.1016/j.plantsci.2020.110444

77. **Hura, T., Hura, K., Ostrowska, A., Gadzinowska, J., Grzesiak, M. T., Dziurka, K., & Dubas, E.** (2018). Rieske iron-sulfur protein of cytochrome-b6f is involved in plant recovery after drought stress. Environmental and Experimental Botany, 156, 228–239. https://doi.org/10.1016/j.envexpbot.2018.09.003

78. **International Wheat Genome Sequencing Consortium (IWGSC), T. I. W. G. S. C.** (2014). A chromosome-based draft sequence of the hexaploid bread wheat (Triticum aestivum) genome. Science (New York, N.Y.), 345(6194), 1251788. https://doi.org/10.1126/science.1251788

79. **International Wheat Genome Sequencing Consortium (IWGSC), T. I. W. G. S. C., IWGSC** RefSeq principal investigators:, I. R. principal, Appels, R., Eversole, K., Feuillet, C., Keller, B., Rogers, J., Stein, N., IWGSC whole-genome assembly principal investigators:, I. whole-genome assembly principal, Pozniak, C. J., Stein, N., Choulet, F., Distelfeld, A., Eversole, K., Poland, J., Rogers, J., Ronen, G., Sharpe, A. G., Whole-genome sequencing and assembly:, W. sequencing and, … Uauy, C. (2018). Shifting the limits in wheat research and breeding using a fully annotated reference genome. Science (New York, N.Y.), 361(6403), eaar7191. https://doi.org/10.1126/science.aar7191

80. **Ishida, H., Yoshimoto, K., Izumi, M., Reisen, D., Yano, Y., Makino, A., Ohsumi, Y., Hanson, M. R., & Mae, T.** (2008). Mobilization of Rubisco and Stroma-Localized Fluorescent Proteins of Chloroplasts to the Vacuole by an ATG Gene-Dependent Autophagic Process . Plant Physiology, 148(1), 142–155. https://doi.org/10.1104/pp.108.122770

81. **IPCC**. (2022). Summary for Policymakers Climate Change and Land (pp. 1–36). Cambridge University Press. https://doi.org/10.1017/9781009157988.001

82. **Jacott, C. N., & Boden, S. A**. (2020). Feeling the heat: developmental and molecular responses of wheat and barley to high ambient temperatures. Journal of Experimental Botany, 71(19), 5740–5751. https://doi.org/10.1093/jxb/eraa326

83. **Jasieniecka-Gazarkiewicz, K., Demski, K., Gidda, S. K., Klińska, S., Niedojadło, J., Lager, I., Carlsson, A. S., Minina, E. A., Mullen, R. T., Bozhkov, P. V., Stymne, S., & Banaś, A.** (2021). Subcellular localization of Acyl-CoA: Lysophosphatidylethanolamine acyltransferases (LPEATs) and the effects of knocking-out and overexpression of their genes on autophagy markers level and life span of A. thaliana. International Journal of Molecular Sciences, 22(6), 1–22. https://doi.org/10.3390/ijms22063006

84. **Ji, X., Shiran, B., Wan, J., Lewis, D. C., Jenkins, C. L. D., Condon, A. G., Richards, R. A., & Dolferus, R.** (2010). Importance of pre-anthesis anther sink strength for maintenance of grain number during reproductive stage water stress in wheat. Plant, Cell and Environment, 33(6), 926–942. https://doi.org/10.1111/j.1365-3040.2010.02130.x

85. **Juliana, P., Singh, R. P., Poland, J., Shrestha, S., Huerta-Espino, J., Govindan, V., Mondal, S., Crespo-Herrera, L. A., Kumar, U., Joshi, A. K., Payne, T., Bhati, P. K., Tomar, V., Consolacion, F., & Campos Serna, J. A**. (2021). Elucidating the genetics of grain yield and stress-resilience in bread wheat using a large-scale genome-wide association mapping study with 55,568 lines. Scientific Reports, 11(1). https://doi.org/10.1038/s41598-021-84308-4

86. **Jumper, J., Evans, R., Pritzel, A., Green, T., Figurnov, M., Ronneberger, O., Tunyasuvunakool, K., Bates, R., Žídek, A., Potapenko, A., Bridgland, A., Meyer, C., Kohl, S. A. A., Ballard, A. J., Cowie, A., Romera-Paredes, B., Nikolov, S., Jain, R., Adler, J., … Hassabis, D.** (2021). Highly accurate protein structure prediction with AlphaFold. Nature, 596(7873), 583–589. https://doi.org/10.1038/s41586-021-03819-2

87. **Jung, H., Lee, H. N., Marshall, R. S., Lomax, A. W., Yoon, M. J., Kim, J., Kim, J. H., Vierstra, R. D., & Chung, T**. (2020). Arabidopsis cargo receptor NBR1 mediates selective autophagy of defective proteins. Journal of Experimental Botany, 71(1), 73–89. https://doi.org/10.1093/jxb/erz404

88. **Kao, Y.-T., Gonzalez, K. L., & Bartel, B.** (2018). Peroxisome Function, Biogenesis, and Dynamics in Plants. Plant Physiology, 176(1), 162–177. https://doi.org/10.1104/pp.17.01050

89. **Kidwell, K. K., Shelton, G. B., DeMacon, V. L., Burns, J. W., Carter, B. P., Morris, C. F., Chen, X. M., & Bosque-Perez, N. A.** (2004). Registration of 'Hollis' wheat. In Crop Science (Vol. 44, Issue 5, pp. 1871–1872). Crop Science Society of America. https://doi.org/10.2135/cropsci2004.1871

90. **Kitony, J. K.** (2023). Nested association mapping population in crops: current status and future prospects. Journal of Crop Science and Biotechnology, 26(1), 1–12. https://doi.org/10.1007/s12892-022-00158-0

91. **Klionsky, D. J., Abdel-Aziz, A. K., Abdelfatah, S., Abdellatif, M., Abdoli, A., Abel, S., Abeliovich, H., Abildgaard, M. H., Abudu, Y. P., Acevedo-Arozena, A., Adamopoulos, I. E., Adeli, K., Adolph, T. E., Adornetto, A., Aflaki, E., Agam, G., Agarwal, A., Aggarwal, B. B., Agnello, M., … Tong, C. K.** (2021). Guidelines for the use and interpretation of assays for monitoring autophagy (4th edition)1. In Autophagy (Vol. 17, Issue 1, pp. 1–382). Taylor and Francis Ltd. https://doi.org/10.1080/15548627.2020.1797280

92. **Klughammer, C., & Schreiber, U.** (2016). Deconvolution of ferredoxin, plastocyanin, and P700 transmittance changes in intact leaves with a new type of kinetic LED array spectrophotometer. Photosynthesis Research, 128(2), 195–214. https://doi.org/10.1007/s11120-016-0219-0

93. **Kneeshaw, S., Keyani, R., Delorme-Hinoux, V., Imrie, L., Loake, G. J., Le Bihan, T., Reichheld, J.-P., & Spoel, S. H.** (2017). Nucleoredoxin guards against oxidative stress by protecting antioxidant enzymes. Proceedings of the National Academy of Sciences of the United States of America, 114(31), 8414–8419. https://doi.org/10.1073/pnas.1703344114

94. **Koch, A., Schneider, G., Lüers, G. H., & Schrader, M.** (2004). Peroxisome elongation and constriction but not fission can occur independently of dynamin-like protein 1. Journal of Cell Science, 117(Pt 17), 3995–4006. https://doi.org/10.1242/jcs.01268

95. **Koch, J., Pranjic, K., Huber, A., Ellinger, A., Hartig, A., Kragler, F., & Brocard, C.** (2010). PEX11 family members are membrane elongation factors that coordinate peroxisome proliferation and maintenance. Journal of Cell Science, 123(19), 3389–3400. https://doi.org/10.1242/jcs.064907

96. **Kohzuma, K., Cruz, J. A., Akashi, K., Hoshiyasu, S., Munekage, Y. N., Yokota, A., & Kramer, D. M.** (2009). The long-term responses of the photosynthetic proton circuit to drought. Plant, Cell and Environment, 32(3), 209–219. https://doi.org/10.1111/j.1365-3040.2008.01912.x

97. **Kuzuoglu-Ozturk, D., Yalcinkaya, O. C., Akpinar, B. A., Mitou, G., Korkmaz, G., Gozuacik, D., & Budak, H**. (2012). Autophagy-related gene, TdAtg8, in wild emmer wheat plays a role in drought and osmotic stress response. Planta, 236(4), 1081–1092. https://doi.org/10.1007/s00425-012-1657-3

98. **Landrum, M., Smertenko, A., Edwards, R., Hussey, P. J., & Steel, P. G.** (2010). BODIPY probes to study peroxisome dynamics in vivo. The Plant Journal, 62(3), 529–538. https://doi.org/10.1111/j.1365-313X.2010.04153.x

99. **Lee, H. N., Chacko, J. V., Gonzalez Solís, A., Chen, K.-E., Barros, J. A., Signorelli, S., Millar, H., David Vierstra, R., Eliceiri, K. W., & Otegui, M. S.** (2023). The autophagy receptor NBR1 directs the clearance of photodamaged chloroplasts. https://doi.org/10.7554/eLife

100. **Leng, G., & Hall, J.** (2019). Crop yield sensitivity of global major agricultural countries to droughts and the projected changes in the future. Science of The Total Environment, 654, 811–821. https://doi.org/10.1016/J.SCITOTENV.2018.10.434

101. **Li, B., Fan, R., Sun, G., Sun, T., Fan, Y., Bai, S., Guo, S., Huang, S., Liu, J., Zhang, H., Wang, P., Zhu, X., & Song, C.** (2021). Flavonoids improve drought tolerance of maize seedlings by regulating the homeostasis of reactive oxygen species. Plant and Soil. https://doi.org/10.1007/s11104-020-04814-8

102. **Li, J., & Hu, J**. (2015). Using Co-Expression Analysis and Stress-Based Screens to Uncover Arabidopsis Peroxisomal Proteins Involved in Drought Response. PLOS ONE, 10(9), e0137762. https://doi.org/10.1371/journal.pone.0137762

103. **Li, R., Guo, P., Michael, B., Stefania, G., & Salvatore, C.** (2006). Evaluation of Chlorophyll Content and Fluorescence Parameters as Indicators of Drought Tolerance in Barley. Agricultural Sciences in China, 5(10), 751–757. https://doi.org/10.1016/S1671-2927(06)60120-X

104. **Liao, Y., Smyth, G. K., & Shi, W.** (2014). featureCounts: an efficient general purpose program for assigning sequence reads to genomic features. Bioinformatics, 30(7), 923–930. https://doi.org/10.1093/bioinformatics/btt656

105. **Lin, Z., Wang, Y.-L., Cheng, L.-S., Zhou, L.-L., Xu, Q.-T., Liu, D.-C., Deng, X.-Y., Mei, F.-Z., & Zhou, Z.-Q.** (2021). Mutual regulation of ROS accumulation and cell autophagy in wheat roots under hypoxia stress. Plant Physiology and Biochemistry, 158, 91–102. https://doi.org/10.1016/j.plaphy.2020.11.049

106. **Lingard, M. J. Trelease, R. N.** (2006). Five Arabidopsis peroxin 11 homologs individually promote peroxisome elongation, duplication or aggregation. Journal of Cell Science, 119(9), 1961–1972. https://doi.org/10.1242/jcs.02904

107. **Liu, H., Li, T., Wang, Y., Zheng, J., Li, H., Hao, C., & Zhang, X**. (2019). TaZIM-A1 negatively regulates flowering time in common wheat (Triticum aestivum L.). Journal of Integrative Plant Biology, 61(3), 359–376. https://doi.org/10.1111/jipb.12720

108. **Liu, Y., Burgos, J. S., Deng, Y., Srivastava, R., Howell, S. H., & Bassham, D. C.** (2012). Degradation of the Endoplasmic Reticulum by Autophagy during Endoplasmic Reticulum Stress in Arabidopsis. The Plant Cell, 24(11), 4635–4651. https://doi.org/10.1105/tpc.112.101535

109. **Liu, Y., Xiong, Y., & Bassham, D. C.** (2009). Autophagy is required for tolerance of drought and salt stress in plants. Autophagy, 5(7). https://doi.org/10.4161/auto.5.7.9290

110. **Long, S. P., Humphries, S., & Falkowski, P. G.** (1994). Photoinhibition of Photosynthesis in Nature. Annual Review of Plant Physiology and Plant Molecular Biology, 45(1). https://doi.org/10.1146/annurev.pp.45.060194.003221

111. **Lopez-Huertas, E., Charlton, W. L., Johnson, B., Graham, I. A., & Baker, A.** (2000). Stress induces peroxisome biogenesis genes. EMBO Journal, 19(24), 6770–6777. https://doi.org/10.1093/emboj/19.24.6770

112. **Lou, L., Li, X., Chen, J., Li, Y., Tang, Y., & Lv, J.** (2018). Photosynthetic and ascorbate-glutathione metabolism in the flag leaves as compared to spikes under drought stress of winter wheat (Triticum aestivum L.). PLOS ONE, 13(3), e0194625. https://doi.org/10.1371/journal.pone.0194625

113. **Love, M. I., Huber, W., & Anders, S**. (2014). Moderated estimation of fold change and dispersion for RNA-seq data with DESeq2. Genome Biology, 15(12), 1–21. https://doi.org/10.1186/s13059-014-0550-8

114. **Luna, C. M., Pastori, G. M., Driscoll, S., Groten, K., Bernard, S., & Foyer, C. H.** (2005). Drought controls on H2O2 accumulation, catalase (CAT) activity and CAT gene expression in wheat. Journal of experimental botany, 56(411), 417–423. https://doi.org/10.1093/jxb/eri039

115. **Lynch, J. P.** (2013). Steep, cheap and deep: an ideotype to optimize water and N acquisition by maize root systems. Annals of Botany, 112(2), 347–357. https://doi.org/10.1093/aob/mcs293

116. **Ma, C., Hagstrom, D., Polley, S. G., & Subramani, S**. (2013). Redox-regulated cargo binding and release by the peroxisomal targeting signal receptor, Pex5. Journal of Biological Chemistry, 288(38), 27220–27231. https://doi.org/10.1074/jbc.M113.492694

117. **Ma, J., Stiller, J., Wei, Y., Zheng, Y.-L., Devos, K. M., Doležel, J., & Liu, C.** (2014). Extensive Pericentric Rearrangements in the Bread Wheat (Triticum aestivum L.) Genotype “Chinese Spring” Revealed from Chromosome Shotgun Sequence Data. Genome Biology and Evolution, 6(11), 3039–3048. https://doi.org/10.1093/gbe/evu237

118. **Manschadi, A. M., Christopher, J., deVoil, P., & Hammer, G. L.** (2006). The role of root architectural traits in adaptation of wheat to water-limited environments. Functional Plant Biology, 33(9), 823. https://doi.org/10.1071/FP06055

119. **Manschadi, A. M., Hammer, G. L., Christopher, J. T., & DeVoil, P.** (2008). Genotypic variation in seedling root architectural traits and implications for drought adaptation in wheat (Triticum aestivum L.). Plant and Soil, 303(1–2), 115–129. https://doi.org/10.1007/s11104-007-9492-1

120. **Marshall, R. S., Li, F., Gemperline, D. C., Book, A. J., & Vierstra, R. D.** (2015). Autophagic Degradation of the 26S Proteasome Is Mediated by the Dual ATG8/Ubiquitin Receptor RPN10 in Arabidopsis. Molecular Cell, 58(6), 1053–1066. https://doi.org/10.1016/j.molcel.2015.04.023

121. **Marshall, R. S., & Vierstra, R. D**. (2018). Autophagy: The Master of Bulk and Selective Recycling. Annual Review of Plant Biology, 69(1), 173–208. https://doi.org/10.1146/annurev-arplant-042817-040606

122. **Maruta, T., Noshi, M., Tanouchi, A., Tamoi, M., Yabuta, Y., Yoshimura, K., Ishikawa, T., & Shigeoka, S.** (2012). H2O2-triggered Retrograde Signaling from Chloroplasts to Nucleus Plays Specific Role in Response to Stress. Journal of Biological Chemistry, 287(15), 11717–11729. https://doi.org/10.1074/jbc.M111.292847

123. **Matsuura, A., Tsukada, M., Wada, Y., & Ohsumi, Y.** (1997). Apg1p, a novel protein kinase required for the autophagic process in Saccharomyces cerevisiae. Gene, 192(2), 245–250. https://doi.org/10.1016/S0378-1119(97)00084-X

124. **McCarthy, I., Romero-Puertas, M. C., Palma, J. M., Sandalio, L. M., Corpas, F. J., Gómez, M., & Del Río, L. A**. (2001). Cadmium induces senescence symptoms in leaf peroxisomes of pea plants. Plant, Cell & Environment, 24(10), 1065–1073. https://doi.org/10.1046/j.1365-3040.2001.00750.x

125. **Merkulova, E. A., Guiboileau, A., Naya, L., Masclaux-Daubresse, C., & Yoshimoto, K.** (2014). Assessment and Optimization of Autophagy Monitoring Methods in Arabidopsis Roots Indicate Direct Fusion of Autophagosomes with Vacuoles. Plant and Cell Physiology, 55(4), 715–726. https://doi.org/10.1093/pcp/pcu041

126. **Mhamdi, A., Noctor, G., & Baker, A.** (2012). Plant catalases: Peroxisomal redox guardians. Archives of Biochemistry and Biophysics, 525(2), 181–194. https://doi.org/10.1016/j.abb.2012.04.015

127. **Michaeli, S., Honig, A., Levanony, H., Peled-Zehavi, H., & Galili, G.** (2014). Arabidopsis ATG8-INTERACTING PROTEIN1 Is Involved in Autophagy-Dependent Vesicular Trafficking of Plastid Proteins to the Vacuole. The Plant Cell, 26(10), 4084–4101. https://doi.org/10.1105/tpc.114.129999

128. **Mignolet-Spruyt, L., Xu, E., Idänheimo, N., Hoeberichts, F. A., Mühlenbock, P., Brosché, M., Van Breusegem, F., & Kangasjärvi, J.** (2016). Spreading the news: subcellular and organellar reactive oxygen species production and signalling. Journal of Experimental Botany, 67(13), 3831–3844. https://doi.org/10.1093/jxb/erw080

129. **Miller, G., Suzuki, N., Ciftci-Yilmaz, S., & Mittler, R.** (2010). Reactive oxygen species homeostasis and signalling during drought and salinity stresses. Plant, Cell and Environment, 33(4), 453–467. https://doi.org/10.1111/j.1365-3040.2009.02041.x

130. **Minina, E. A., Moschou, P. N., Vetukuri, R. R., Sanchez-Vera, V., Cardoso, C., Liu, Q., Elander, P. H., Dalman, K., Beganovic, M., Lindberg Yilmaz, J., Marmon, S., Shabala, L., Suarez, M. F., Ljung, K., Novák, O., Shabala, S., Stymne, S., Hofius, D., & Bozhkov, P. V.** (2018). Transcriptional stimulation of rate-limiting components of the autophagic pathway improves plant fitness. Journal of Experimental Botany, 69(6), 1415–1432. https://doi.org/10.1093/jxb/ery010

131. **Mishra, K. B., Iannacone, R., Petrozza, A., Mishra, A., Armentano, N., La Vecchia, G., Trtílek, M., Cellini, F., & Nedbal, L.** (2012). Engineered drought tolerance in tomato plants is reflected in chlorophyll fluorescence emission. Plant Science, 182(1), 79–86. https://doi.org/10.1016/j.plantsci.2011.03.022

132. **Mitsuya, S., El-Shami, M., Sparkes, I. A., Charlton, W. L., De Marcos Lousa, C., Johnson, B., & Baker, A.** (2010). Salt Stress Causes Peroxisome Proliferation, but Inducing Peroxisome Proliferation Does Not Improve NaCl Tolerance in Arabidopsis thaliana. PLoS ONE, 5(2), e9408. https://doi.org/10.1371/journal.pone.0009408

133. **Mittler, R.** (2002). Oxidative stress, antioxidants and stress tolerance. In Trends in Plant Science (Vol. 7, Issue 9, pp. 405–410). Elsevier Current Trends. https://doi.org/10.1016/S1360-1385(02)02312-9

134. **Mittler, R.** (2017). ROS Are Good. Trends in Plant Science, 22(1), 11–19. https://doi.org/10.1016/J.TPLANTS.2016.08.002

135. **Mittler, R., Zandalinas, S. I., Fichman, Y., & Van Breusegem, F.** (2022). Reactive oxygen species signalling in plant stress responses. Nature Reviews Molecular Cell Biology, 23(10), 663–679. https://doi.org/10.1038/s41580-022-00499-2

136. **Møller, I. M., Jensen, P. E., & Hansson, A.** (2007). Oxidative Modifications to Cellular Components in Plants. Annual Review of Plant Biology, 58(1), 459–481. https://doi.org/10.1146/annurev.arplant.58.032806.103946

137. **Murata, N., Takahashi, S., Nishiyama, Y., & Allakhverdiev, S. I.** (2007). Photoinhibition of photosystem II under environmental stress. Biochimica et Biophysica Acta (BBA) - Bioenergetics, 1767(6). https://doi.org/10.1016/j.bbabio.2006.11.019

138. **Murchie, E. H., & Lawson, T.** (2013). Chlorophyll fluorescence analysis: a guide to good practice and understanding some new applications. Journal of Experimental Botany, 64(13), 3983–3998. https://doi.org/10.1093/jxb/ert208

139. **Nakatogawa, H., Ichimura, Y., & Ohsumi, Y.** (2007). Atg8, a Ubiquitin-like Protein Required for Autophagosome Formation, Mediates Membrane Tethering and Hemifusion. Cell, 130(1), 165–178. https://doi.org/10.1016/j.cell.2007.05.021

140. **NASA Global Climate Change**. (2019). Effects | Facts – Climate Change: Vital Signs of the Planet. 2019. Retrieved February 8, 2019, from https://climate.nasa.gov/effects/

141. **Nieto-Torres, J. L., Zaretski, S., Liu, T., Adams, P. D., & Hansen, M.** (2023). Post-translational modifications of ATG8 proteins – an emerging mechanism of autophagy control. Journal of Cell Science, 136(16). https://doi.org/10.1242/jcs.259725

142. **Nikolaeva, M. K., Maevskaya, S. N., Shugaev, A. G., & Bukhov, N. G.** (2010). Effect of drought on chlorophyll content and antioxidant enzyme activities in leaves of three wheat cultivars varying in productivity. Russian Journal of Plant Physiology, 57(1), 87–95. https://doi.org/10.1134/S1021443710010127

143. **Nilkens, M., Kress, E., Lambrev, P., Miloslavina, Y., Müller, M., Holzwarth, A. R., & Jahns, P.** (2010). Identification of a slowly inducible zeaxanthin-dependent component of non-photochemical quenching of chlorophyll fluorescence generated under steady-state conditions in Arabidopsis. Biochimica et Biophysica Acta (BBA) - Bioenergetics, 1797(4), 466–475. https://doi.org/10.1016/j.bbabio.2010.01.001

144. **Nuruzzaman, M., Sharoni, A. M., & Kikuchi, S.** (2013). Roles of NAC transcription factors in the regulation of biotic and abiotic stress responses in plants. Frontiers in Microbiology, 4. https://doi.org/10.3389/fmicb.2013.00248

145. **Nxele, X., Klein, A., & Ndimba, B. K.** (2017). Drought and salinity stress alters ROS accumulation, water retention, and osmolyte content in sorghum plants. South African Journal of Botany, 108, 261–266. https://doi.org/10.1016/j.sajb.2016.11.003

146. **Oikawa, K., Goto-Yamada, S., Hayashi, Y., Takahashi, D., Kimori, Y., Shibata, M., Yoshimoto, K., Takemiya, A., Kondo, M., Hikino, K., Kato, A., Shimoda, K., Ueda, H., Uemura, M., Numata, K., Ohsumi, Y., Hara-Nishimura, I., Mano, S., Yamada, K., & Nishimura, M.** (2022). Pexophagy suppresses ROS-induced damage in leaf cells under high-intensity light. Nature Communications, 13(1), 7493. https://doi.org/10.1038/s41467-022-35138-z

147. **Oksanen, E., Häikiö, E., Sober, J., & Karnosky, D. F.** (2004). Ozone-induced H2O2 accumulation in field-grown aspen and birch is linked to foliar ultrastructure and peroxisomal activity. New Phytologist, 161(3), 791–799. https://doi.org/10.1111/j.1469-8137.2003.00981.x

148. **op den Camp, R. G. L.** (2003). Rapid Induction of Distinct Stress Responses after the Release of Singlet Oxygen in Arabidopsis. THE PLANT CELL ONLINE, 15(10), 2320–2332. https://doi.org/10.1105/tpc.014662

149. **Orth, T., Reumann, S., Zhang, X., Fan, J., Wenzel, D., Quan, S., & Hu, J.** (2007). The PEROXIN11 Protein Family Controls Peroxisome Proliferation in Arabidopsis. The Plant Cell, 19(1), 333–350. https://doi.org/10.1105/tpc.106.045831

150. **Paolacci, A. R., Tanzarella, O. A., Porceddu, E., & Ciaffi, M.** (2009). Identification and validation of reference genes for quantitative RT-PCR normalization in wheat. BMC Molecular Biology, 10(1), 11. https://doi.org/10.1186/1471-2199-10-11

151. **Parent, B., Bonneau, J., Maphosa, L., Kovalchuk, A., Langridge, P., & Fleury, D.** (2017). Quantifying Wheat Sensitivities to Environmental Constraints to Dissect Genotype × Environment Interactions in the Field. Plant Physiology, 174(3), 1669–1682. https://doi.org/10.1104/pp.17.00372

152. **Pertea, M., Kim, D., Pertea, G. M., Leek, J. T., & Salzberg, S. L.** (2016). Transcript-level expression analysis of RNA-seq experiments with HISAT, StringTie and Ballgown. Nature Protocols, 11(9), 1650–1667. https://doi.org/10.1038/nprot.2016.095

153. **Petrov, V., Hille, J., Mueller-Roeber, B., & Gechev, T. S.** (2015). ROS-mediated abiotic stress-induced programmed cell death in plants. Frontiers in Plant Science, 6. https://doi.org/10.3389/fpls.2015.00069

154. **Pettersen, E. F., Goddard, T. D., Huang, C. C., Meng, E. C., Couch, G. S., Croll, T. I., Morris, J. H., & Ferrin, T. E.** (2021). UCSF ChimeraX: Structure visualization for researchers, educators, and developers. Protein Science, 30(1), 70–82. https://doi.org/10.1002/pro.3943

155. **Pieters, A. J., & El Souki, S.** (2005). Effects of drought during grain filling on PS II activity in rice. Journal of Plant Physiology, 162(8), 903–911. https://doi.org/10.1016/j.jplph.2004.11.001

156. **Pratap Singh, V., Singh, S., Kumar Tripathi, D., Mohan Prasad, S., & Kumar Chauhan, D.** (2018). Reactive Oxygen Species: Generation, Damage, and Quenching in Plants During Stress. https://onlinelibrary.wiley.com/doi/pdf/10.1002/9781119324928.ch5

157. **Queval, G., Issakidis-Bourguet, E., Hoeberichts, F. A., Vandorpe, M., Gakière, B., Vanacker, H., Miginiac-Maslow, M., Van Breusegem, F., & Noctor, G.** (2007). Conditional oxidative stress responses in the Arabidopsis photorespiratory mutant cat2 demonstrate that redox state is a key modulator of daylength-dependent gene expression, and define photoperiod as a crucial factor in the regulation of H2O2-induced cell death. The Plant Journal, 52(4), 640–657. https://doi.org/10.1111/j.1365-313X.2007.03263.x

158. **Rana, R. M., Dong, S., Ali, Z., Huang, J., & Zhang, H. S.** (2012). Regulation of ATG6/Beclin-1 homologs by abiotic stresses and hormones in rice (Oryza sativa L.). Genetics and Molecular Research, 11(4), 3676–3687. https://doi.org/10.4238/2012.August.17.3

159. **Reddy, A. R., Chaitanya, K. V., & Vivekanandan, M.** (2004). Drought-induced responses of photosynthesis and antioxidant metabolism in higher plants. Journal of Plant Physiology, 161(11), 1189–1202. https://doi.org/10.1016/j.jplph.2004.01.013

160. **Reid, S. E., Kolapalli, S. P., Nielsen, T. M., & Frankel, L. B.** (2022). Canonical and non-canonical roles for ATG8 proteins in autophagy and beyond. Frontiers in Molecular Biosciences, 9. https://doi.org/10.3389/fmolb.2022.1074701

161. **Reumann, S., Babujee, L., Changle, M., Wienkoop, S., Siemsen, T., Antonicelli, G. E., Rasche, N., Lüder, F., Weckwerth, W., & Jahnd, O.** (2007). Proteome analysis of Arabidopsis leaf peroxisomes reveals novel targeting peptides, metabolic pathways, and defense mechanisms. Plant Cell, 19(10), 3170–3193. https://doi.org/10.1105/tpc.107.050989

162. **Reynolds, M.P., Braun, HJ.** (2022). Wheat Improvement. Springer, Cham. https://doi.org/10.1007/978-3-030-90673-3_1

163. **Rivera-Amado, C., Molero, G., Trujillo-Negrellos, E., Reynolds, M., & Foulkes, J.** (2020). Estimating organ contribution to grain filling and potential for source upregulation in wheat cultivars with a contrasting source-sink balance. Agronomy, 10(10), 1–21. https://doi.org/10.3390/agronomy10101527

164. **Rodríguez-Serrano, M., Romero-Puertas, M. C., Sanz-Fernández, M., Hu, J., & Sandalio, L. M.** (2016). Peroxisomes Extend Peroxules in a Fast Response to Stress via a Reactive Oxygen Species-Mediated Induction of the Peroxin PEX11a 1[OPEN]. https://doi.org/10.1104/pp.16.00648

165. **Sagiv, Y.** (2000). GATE-16, a membrane transport modulator, interacts with NSF and the Golgi v-SNARE GOS-28. The EMBO Journal, 19(7), 1494–1504. https://doi.org/10.1093/emboj/19.7.1494

166. **Sairam, R. K., Rao, K. V., & Srivastava, G. C.** (2002). Differential response of wheat genotypes to long term salinity stress in relation to oxidative stress, antioxidant activity and osmolyte concentration. Plant Science, 163(5), 1037–1046. https://doi.org/10.1016/S0168-9452(02)00278-9

167. **Sallam, A., Alqudah, A. M., Dawood, M. F. A., Baenziger, P. S., & Börner, A.** (2019). Drought Stress Tolerance in Wheat and Barley: Advances in Physiology, Breeding and Genetics Research. International Journal of Molecular Sciences, 20(13). https://doi.org/10.3390/ijms20133137

168. **Sanad, M. N. M. E., Smertenko, A., & Garland-Campbell, K. A.** (2019). Differential dynamic changes of reduced trait model for analyzing the plastic response to drought phases: A case study in spring wheat. Frontiers in Plant Science, 10. https://doi.org/10.3389/fpls.2019.00504

169. **Sandalio, L. M., Gotor, C., Romero, L. C., & Romero-Puertas, M. C.** (2019). Multilevel regulation of peroxisomal proteome by post-translational modifications. In International Journal of Molecular Sciences (Vol. 20, Issue 19, p. 4881). MDPI AG. https://doi.org/10.3390/ijms20194881

170. **Sansaloni, C., Franco, J., Santos, B., Percival-Alwyn, L., Singh, S., Petroli, C., Campos, J., Dreher, K., Payne, T., Marshall, D., Kilian, B., Milne, I., Raubach, S., Shaw, P., Stephen, G., Carling, J., Pierre, C. Saint, Burgueño, J., Crosa, J., … Pixley, K.** (2020). Diversity analysis of 80,000 wheat accessions reveals consequences and opportunities of selection footprints. Nature Communications, 11(1), 4572. https://doi.org/10.1038/s41467-020-18404-w

171. **Saradadevi, R., Bramley, H., Palta, J. A., Edwards, E., & Siddique, K. H. M.** (2015). Root biomass in the upper layer of the soil profile is related to the stomatal response of wheat as the soil dries. https://doi.org/10.1071/FP15216

172. **Saxena, S. N., Kakani, R. K., Sharma, L. K., Agarwal, D., John, S., & Sharma, Y.** (2017). Genetic variation in seed quality and fatty acid composition of fenugreek (Trigonella foenum-graecum L.) genotypes grown under limited moisture conditions. Acta Physiologiae Plantarum, 39(10). https://doi.org/10.1007/s11738-017-2522-6

173. **Schapendonk, A. H. C. M., Xu, H. Y., Van Der Putten, P. E. L., & Spiertz, J. H. J.** (2007). Heat-shock effects on photosynthesis and sink-source dynamics in wheat (Triticum aestivum L.). NJAS - Wageningen Journal of Life Sciences, 55(1), 37–54. https://doi.org/10.1016/S1573-5214(07)80003-0

174. **Schindelin, J., Arganda-Carreras, I., Frise, E., Kaynig, V., Longair, M., Pietzsch, T., Preibisch, S., Rueden, C., Saalfeld, S., Schmid, B., Tinevez, J.-Y., White, D. J., Hartenstein, V., Eliceiri, K., Tomancak, P., & Cardona, A.** (2012). Fiji: an open-source platform for biological-image analysis. Nature Methods, 9(7), 676–682. https://doi.org/10.1038/nmeth.2019

175. **Schoppach, R., & Sadok, W.** (2012). Differential sensitivities of transpiration to evaporative demand and soil water deficit among wheat elite cultivars indicate different strategies for drought tolerance. Environmental and Experimental Botany, 84. https://doi.org/10.1016/j.envexpbot.2012.04.016

176. **Schrader, M., Bonekamp, N. A., & Islinger, M.** (2012). Fission and proliferation of peroxisomes. Biochimica et Biophysica Acta (BBA) - Molecular Basis of Disease, 1822(9), 1343–1357. https://doi.org/10.1016/J.BBADIS.2011.12.014

177. **Sebastian, J., Yee, M.-C., Goudinho Viana, W., Rellán-Álvarez, R., Feldman, M., Priest, H. D., Trontin, C., Lee, T., Jiang, H., Baxter, I., Mockler, T. C., Hochholdinger, F., Brutnell, T. P., & Dinneny, J. R.** (2016). Grasses suppress shoot-borne roots to conserve water during drought. Proceedings of the National Academy of Sciences of the United States of America, 113(31), 8861–8866. https://doi.org/10.1073/pnas.1604021113

178. **Sewelam, N., Jaspert, N., Van Der Kelen, K., Tognetti, V. B., Schmitz, J., Frerigmann, H., Stahl, E., Zeier, J., Van Breusegem, F., & Maurino, V. G.** (2014). Spatial H2O2 Signaling Specificity: H2O2 from Chloroplasts and Peroxisomes Modulates the Plant Transcriptome Differentially. Molecular Plant, 7(7), 1191–1210. https://doi.org/10.1093/mp/ssu070

179. **Sharma, P., Jha, A. B., Dubey, R. S., & Pessarakli, M.** (2012). Reactive Oxygen Species, Oxidative Damage, and Antioxidative Defense Mechanism in Plants under Stressful Conditions. Journal of Botany, 2012, 1–26. https://doi.org/10.1155/2012/217037

180. **Sharp, R. E., Silk, W. K., & Hsiao, T. C.** (1988). Growth of the Maize Primary Root at Low Water Potentials. Plant Physiology, 87(1), 50–57. https://doi.org/10.1104/pp.87.1.50

181. **Shavrukov, Y., Kurishbayev, A., Jatayev, S., Shvidchenko, V., Zotova, L., Koekemoer, F., de Groot, S., Soole, K., & Langridge, P.** (2017). Early Flowering as a Drought Escape Mechanism in Plants: How Can It Aid Wheat Production? Frontiers in Plant Science, 8, 1950. https://doi.org/10.3389/fpls.2017.01950

182. **Shibata, M., Oikawa, K., Yoshimoto, K., Kondo, M., Mano, S., Yamada, K., Hayashi, M., Sakamoto, W., Ohsumi, Y., & Nishimura, M.** (2013). Highly oxidized peroxisomes are selectively degraded via autophagy in Arabidopsis. Plant Cell, 25(12), 4967–4983. https://doi.org/10.1105/tpc.113.116947

183. **Shin, J. H., Yoshimoto, K., Ohsumi, Y., Jeon, J. S., & An, G.** (2009). OsATG10b, an autophagosome component, is needed for cell survival against oxidative stresses in rice. Molecules and Cells, 27(1), 67–74. https://doi.org/10.1007/s10059-009-0006-2

184. **Shiva, S., Samarakoon, T., Lowe, K. A., Roach, C., Vu, H. S., Colter, M., Porras, H., Hwang, C., Roth, M. R., Tamura, P., Li, M., Schrick, K., Shah, J., Wang, X., Wang, H., & Welti, R.** (2020). Leaf Lipid Alterations in Response to Heat Stress of Arabidopsis thaliana. Plants, 9(7), 845. https://doi.org/10.3390/plants9070845

185. **Sievers, F., Wilm, A., Dineen, D., Gibson, T. J., Karplus, K., Li, W., Lopez, R., McWilliam, H., Remmert, M., Söding, J., Thompson, J. D., & Higgins, D. G.** (2011). Fast, scalable generation of high-quality protein multiple sequence alignments using Clustal Omega. Molecular Systems Biology, 7(1). https://doi.org/10.1038/msb.2011.75

186. **Signorelli, S., Tarkowski, Ł. P., Van den Ende, W., & Bassham, D. C.** (2019). Linking Autophagy to Abiotic and Biotic Stress Responses. Trends in Plant Science, 24(5), 413–430. https://doi.org/10.1016/j.tplants.2019.02.001

187. **Sikorskaite, S., Rajamäki, M.-L., Baniulis, D., Stanys, V., & Valkonen, J. P.** (2013). Protocol: Optimised methodology for isolation of nuclei from leaves of species in the Solanaceae and Rosaceae families. Plant Methods, 9(1), 31. https://doi.org/10.1186/1746-4811-9-31

188. **Singh, S., Gupta, A. K., & Kaur, N.** (2012). Differential Responses of Antioxidative Defence System to Long-Term Field Drought in Wheat (Triticum aestivum L.) Genotypes Differing in Drought Tolerance. Journal of Agronomy and Crop Science, 198(3), 185–195. https://doi.org/10.1111/j.1439-037X.2011.00497.x

189. **Singh, S., Vikram, P., Sehgal, D., Burgueño, J., Sharma, A., Singh, S. K., Sansaloni, C. P., Joynson, R., Brabbs, T., Ortiz, C., Solis-Moya, E., Govindan, V., Gupta, N., Sidhu, H. S., Basandrai, A. K., Basandrai, D., Ledesma-Ramires, L., Suaste-Franco, M. P., Fuentes-Dávila, G., … Pixley, K. V.** (2018). Harnessing genetic potential of wheat germplasm banks through impact-oriented-prebreeding for future food and nutritional security. Scientific Reports, 8(1), 12527. https://doi.org/10.1038/s41598-018-30667-4

190. **Sláviková, S., Shy, G., Yao, Y., Glozman, R., Levanony, H., Pietrokovski, S., Elazar, Z., & Galili, G.** (2005). The autophagy-associated Atg8 gene family operates both under favourable growth conditions and under starvation stresses in Arabidopsis plants. Journal of Experimental Botany, 56(421), 2839–2849. https://doi.org/10.1093/jxb/eri276

191. **Ślesak, I., Libik, M., Karpinska, B., Karpinski, S., & Miszalski, Z.** (2007). The role of hydrogen peroxide in regulation of plant metabolism and cellular signalling in response to environmental stresses. Acta Biochimica Polonica, 54(1), 39–50. https://doi.org/10.18388/abp.2007_3267

192. **Smertenko, A.** (2017). Can Peroxisomes Inform Cellular Response to Drought? Trends in Plant Science, 22(12), 1005–1007. https://doi.org/10.1016/J.TPLANTS.2017.09.021

193. **Smirnoff, N., & Arnaud, D.** (2019). Hydrogen peroxide metabolism and functions in plants. New Phytologist, 221(3), 1197–1214. https://doi.org/10.1111/nph.15488

194. **Sofo, A., Scopa, A., Nuzzaci, M., & Vitti, A.** (2015). Ascorbate Peroxidase and Catalase Activities and Their Genetic Regulation in Plants Subjected to Drought and Salinity Stresses. International Journal of Molecular Sciences, 16(6), 13561–13578. https://doi.org/10.3390/ijms160613561

195. **Song, L., Prince, S., Valliyodan, B., Joshi, T., Maldonado dos Santos, J. V., Wang, J., Lin, L., Wan, J., Wang, Y., Xu, D., & Nguyen, H. T.** (2016). Genome-wide transcriptome analysis of soybean primary root under varying water-deficit conditions. BMC Genomics, 17(1), 57. https://doi.org/10.1186/s12864-016-2378-y

196. **Stadel, D., Millarte, V., Tillmann, K. D., Huber, J., Tamin-Yecheskel, B.-C., Akutsu, M., Demishtein, A., Ben-Zeev, B., Anikster, Y., Perez, F., Dötsch, V., Elazar, Z., Rogov, V., Farhan, H., & Behrends, C.** (2015). TECPR2 Cooperates with LC3C to Regulate COPII-Dependent ER Export. Molecular Cell, 60(1), 89–104. https://doi.org/10.1016/j.molcel.2015.09.010

197. **Stone, P. J., & Nicolas, M. E.** (1994). Wheat Cultivars Vary Widely in their Responses of Grain Yield and Quality to Short Periods of Post-anthesis Heat Stress. In Aust. J. Plant Physiol (Vol. 21).

198. **Su, T., Li, X., Yang, M., Shao, Q., Zhao, Y., Ma, C., & Wang, P.** (2020). Autophagy: An Intracellular Degradation Pathway Regulating Plant Survival and Stress Response. In Frontiers in Plant Science (Vol. 11, p. 164). Frontiers Media S.A. https://doi.org/10.3389/fpls.2020.00164

199. **Su, W., Bao, Y., Lu, Y., He, F., Wang, S., Wang, D., Yu, X., Yin, W., Xia, X., & Liu, C.** (2021). Poplar Autophagy Receptor NBR1 Enhances Salt Stress Tolerance by Regulating Selective Autophagy and Antioxidant System. Frontiers in Plant Science, 11. https://doi.org/10.3389/fpls.2020.568411

200. **Sukumaran, S., Reynolds, M. P., & Sansaloni, C.** (2018). Genome-wide association analyses identify QTL hotspots for yield and component traits in durum wheat grown under yield potential, drought, and heat stress environments. Frontiers in Plant Science, 9. https://doi.org/10.3389/fpls.2018.00081

201. **Sun, X., Wang, P., Jia, X., Huo, L., Che, R., & Ma, F.** (2018). Improvement of drought tolerance by overexpressing MdATG18a is mediated by modified antioxidant system and activated autophagy in transgenic apple. Plant Biotechnology Journal, 16(2), 545–557. https://doi.org/10.1111/pbi.12794

202. **Svenning, S., Lamark, T., Krause, K., & Johansen, T.** (2011). Plant NBR1 is a selective autophagy substrate and a functional hybrid of the mammalian autophagic adapters NBR1 and p62/SQSTM1. Autophagy, 7(9), 993–1010. https://doi.org/10.4161/auto.7.9.16389

203. **Tang, J., & Bassham, D. C.** (2018). Autophagy in crop plants: what's new beyond Arabidopsis? Open Biology, 8(12). https://doi.org/10.1098/rsob.180162

204. **Thirumalaikumar, V. P., Gorka, M., Schulz, K., Masclaux-Daubresse, C., Sampathkumar, A., Skirycz, A., Vierstra, R. D., & Balazadeh, S.** (2021). Selective autophagy regulates heat stress memory in Arabidopsis by NBR1-mediated targeting of HSP90.1 and ROF1. Autophagy, 17(9), 2184–2199. https://doi.org/10.1080/15548627.2020.1820778

205. **Thompson, J.** (1997). The CLUSTAL_X windows interface: flexible strategies for multiple sequence alignment aided by quality analysis tools. Nucleic Acids Research, 25(24), 4876–4882. https://doi.org/10.1093/nar/25.24.4876

206. **Tietz, S., Puthiyaveetil, S., Enlow, H. M., Yarbrough, R., Wood, M., Semchonok, D. A., Lowry, T., Li, Z., Jahns, P., Boekema, E. J., Lenhert, S., Niyogi, K. K., & Kirchhoff, H.** (2015). Functional Implications of Photosystem II Crystal Formation in Photosynthetic Membranes. Journal of Biological Chemistry, 290(22), 14091–14106. https://doi.org/10.1074/jbc.M114.619841

207. **Tricker, P. J., ElHabti, A., Schmidt, J., & Fleury, D.** (2018). The physiological and genetic basis of combined drought and heat tolerance in wheat. Journal of Experimental Botany, 69(13). https://doi.org/10.1093/jxb/ery081

208. **Tyagi, S., Shumayla, Madhu, Singh, K., & Upadhyay, S. K.** (2021). Molecular characterization revealed the role of catalases under abiotic and arsenic stress in bread wheat (Triticum aestivum L.). Journal of Hazardous Materials, 403(April 2020), 123585. https://doi.org/10.1016/j.jhazmat.2020.123585

209. **Uga, Y., Sugimoto, K., Ogawa, S., Rane, J., Ishitani, M., Hara, N., Kitomi, Y., Inukai, Y., Ono, K., Kanno, N., Inoue, H., Takehisa, H., Motoyama, R., Nagamura, Y., Wu, J., Matsumoto, T., Takai, T., Okuno, K., & Yano, M.** (2013). Control of root system architecture by DEEPER ROOTING 1 increases rice yield under drought conditions. Nature Genetics, 45(9), 1097–1102. https://doi.org/10.1038/ng.2725

210. **Ulloa, R. M., Raices, M., MacIntosh, G. C., Maldonado, S., & Tellez-Inon, M. T.** (2002). Jasmonic acid affects plant morphology and calcium-dependent protein kinase expression and activity in Solanum tuberosum. Physiologia Plantarum, 115(3), 417–427. https://doi.org/10.1034/j.1399-3054.2002.1150312.x

211. **USDA ERS** (2018). Irrigation & Water Use. https://www.ers.usda.gov/topics/farm-practices-management/irrigation-water-use/#crops

212. **van der Weele, C. M., Spollen, W. G., Sharp, R. E., & Baskin, T. I.** (2000). Growth of Arabidopsis thaliana seedlings under water deficit studied by control of water potential in nutrient-agar media. Journal of Experimental Botany, 51(350). https://doi.org/10.1093/jexbot/51.350.1555

213. **Varga, V. B., Keresztes, F., Sigmond, T., Vellai, T., & Kovács, T.** (2022). The evolutionary and functional divergence of the Atg8 autophagy protein superfamily. Biologia Futura, 73(4), 375–384. https://doi.org/10.1007/s42977-022-00123-6

214. **Varoquaux, N., Cole, B., Gao, C., Pierroz, G., Baker, C. R., Patel, D., Madera, M., Jeffers, T., Hollingsworth, J., Sievert, J., Yoshinaga, Y., Owiti, J. A., Singan, V. R., DeGraaf, S., Xu, L., Blow, M. J., Harrison, M. J., Visel, A., Jansson, C., … Purdom, E.** (2019). Transcriptomic analysis of field-droughted sorghum from seedling to maturity reveals biotic and metabolic responses. Proceedings of the National Academy of Sciences, 116(52), 27124–27132. https://doi.org/10.1073/pnas.1907500116

215. **Verma, A., Niranjana, M., Jha, S. K., Mallick, N., Agarwal, P., & Vinod.** (2020). QTL detection and putative candidate gene prediction for leaf rolling under moisture stress condition in wheat. Scientific Reports, 10(1). https://doi.org/10.1038/s41598-020-75703-4

216. **Voitsekhovskaja, O. V., Schiermeyer, A., & Reumann, S.** (2014). Plant peroxisomes are degraded by starvation-induced and constitutive autophagy in tobacco BY-2 suspension-cultured cells. Frontiers in Plant Science, 5(NOV). https://doi.org/10.3389/fpls.2014.00629

217. **Voss, I., Sunil, B., Scheibe, R., & Raghavendra, A. S.** (2013). Emerging concept for the role of photorespiration as an important part of abiotic stress response. Plant Biology, 15(4), 713–722. https://doi.org/10.1111/j.1438-8677.2012.00710.x

218. **Vranic, M., Perochon, A., Benbow, H., & Doohan, F. M.** (2022). Comprehensive analysis of pathogen-responsive wheat NAC transcription factors: new candidates for crop improvement. G3 Genes|Genomes|Genetics, 12(11). https://doi.org/10.1093/g3journal/jkac247

219. **Wada, S., Takagi, D., Miyake, C., Makino, A., & Suzuki, Y.** (2019). Responses of the Photosynthetic Electron Transport Reactions Stimulate the Oxidation of the Reaction Center Chlorophyll of Photosystem I, P700, under Drought and High Temperatures in Rice. International Journal of Molecular Sciences, 20(9), 2068. https://doi.org/10.3390/ijms20092068

220. **Wagner, D.** (2004). The Genetic Basis of Singlet Oxygen-Induced Stress Responses of Arabidopsis thaliana. Science, 306(5699), 1183–1185. https://doi.org/10.1126/science.1103178

221. **Wang, P., Sun, X., Jia, X., & Ma, F.** (2017). Apple autophagy-related protein MdATG3s afford tolerance to multiple abiotic stresses. Plant Science, 256, 53–64. https://doi.org/10.1016/j.plantsci.2016.12.003

222. **Wang, P., Wang, T., Han, J., Li, M., Zhao, Y., Su, T., & Ma, C.** (2021). Plant Autophagy: An Intricate Process Controlled by Various Signaling Pathways. Frontiers in Plant Science, 12. https://doi.org/10.3389/fpls.2021.754982

223. **Wang, Y., Cai, S., Yin, L., Shi, K., Xia, X., Zhou, Y., Yu, J., & Zhou, J.** (2015). Tomato HsfA1a plays a critical role in plant drought tolerance by activating ATG genes and inducing autophagy. Autophagy, 11(11), 2033–2047. https://doi.org/10.1080/15548627.2015.1098798

224. **Wang, Z., Li, G., Sun, H., Ma, L., Guo, Y., Zhao, Z., Gao, H., & Mei, L.** (2018). Effects of drought stress on photosynthesis and photosynthetic electron transport chain in young apple tree leaves. Biology Open. https://doi.org/10.1242/bio.035279

225. **Wang, Z.-Y., Li, F.-M., Xiong, Y.-C., & Xu, B.-C.** (2008). Soil-Water Threshold Range of Chemical Signals and Drought Tolerance Was Mediated by ROS Homeostasis in Winter Wheat During Progressive Soil Drying. Journal of Plant Growth Regulation, 27(4), 309–319. https://doi.org/10.1007/s00344-008-9057-4

226. **Washington Association of Wheat Growers**. (2018). Drought impacts on Washington's wheat crop | WAWG. http://www.wawg.org/drought-impacts-on-washingtons-wheat-crop/

227. **Waszczak, C., Carmody, M., & Kangasjärvi, J**. (2018). Reactive Oxygen Species in Plant Signaling. Annual Review of Plant Biology, 69(1), 209–236. https://doi.org/10.1146/annurev-arplant-042817-040322

228. **Wen, W., He, Z., Gao, F., Liu, J., Jin, H., Zhai, S., Qu, Y., & Xia, X.** (2017). A High-Density Consensus Map of Common Wheat Integrating Four Mapping Populations Scanned by the 90K SNP Array. Frontiers in Plant Science, 8. https://doi.org/10.3389/fpls.2017.01389

229. **Wheat Initiative**. (2013). An international vision for wheat improvement.

230. **Xiang, Q., & Rathinasabapathi, B.** (2022). Differential tolerance to heat stress of young leaves compared to mature leaves of whole plants relate to differential transcriptomes involved in metabolic adaptations to stress. AoB PLANTS, 14(4). https://doi.org/10.1093/aobpla/plac024

231. **Xie, Q., Mayes, S., & Sparkes, D. L.** (2016). Early anthesis and delayed but fast leaf senescence contribute to individual grain dry matter and water accumulation in wheat. Field Crops Research, 187, 24–34. https://doi.org/10.1016/j.fcr.2015.12.009

232. **Xiong, H., Yu, J., Miao, J., Li, J., Zhang, H., Wang, X., Liu, P., Zhao, Y., Jiang, C., Yin, Z., Li, Y., Guo, Y., Fu, B., Wang, W., Li, Z., Ali, J., & Li, Z.** (2018). Natural Variation in OsLG3 Increases Drought Tolerance in Rice by Inducing ROS Scavenging. Plant Physiology, 178(1), 451–467. https://doi.org/10.1104/pp.17.01492

233. **Xiong, Y., Contento, A. L., Nguyen, P. Q., & Bassham, D. C.** (2007). Degradation of oxidized proteins by autophagy during oxidative stress in arabidopsis. Plant Physiology, 143(1), 291–299. https://doi.org/10.1104/pp.106.092106

234. **Yadav, M. R., Choudhary, M., Singh, J., Lal, M. K., Jha, P. K., Udawat, P., Gupta, N. K., Rajput, V. D., Garg, N. K., Maheshwari, C., Hasan, M., Gupta, S., Jatwa, T. K., Kumar, R., Yadav, A. K., & Prasad, P. V. V.** (2022). Impacts, Tolerance, Adaptation, and Mitigation of Heat Stress on Wheat under Changing Climates. International Journal of Molecular Sciences, 23(5), 2838. https://doi.org/10.3390/ijms23052838

235. **Yamaguchi, M., & Sharp, R. E.** (2010). Complexity and coordination of root growth at low water potentials: recent advances from transcriptomic and proteomic analyses. Plant, Cell & Environment, 33(4), 590–603. https://doi.org/10.1111/j.1365-3040.2009.02064.x

236. **Yamaguchi, M., Valliyodan, B., Zhang, J., Lenoble, M. E., Yu, O., Rogers, E. E., Nguyen, H. T., & Sharp, R. E.** (2010). Regulation of growth response to water stress in the soybean primary root. I. Proteomic analysis reveals region-specific regulation of phenylpropanoid metabolism and control of free iron in the elongation zone. Plant, Cell & Environment, 33(2), 223–243. https://doi.org/10.1111/j.1365-3040.2009.02073.x

237. **Yang, M., Wang, L., Chen, C., Guo, X., Lin, C., Huang, W., & Chen, L.** (2021). Genome-wide analysis of autophagy-related genes in Medicago truncatula highlights their roles in seed development and response to drought stress. Scientific Reports, 11(1). https://doi.org/10.1038/s41598-021-02239-6

238. **Ye, C., Zheng, S., Jiang, D., Lu, J., Huang, Z., Liu, Z., Zhou, H., Zhuang, C., & Li, J.** (2021). Initiation and Execution of Programmed Cell Death and Regulation of Reactive Oxygen Species in Plants. International Journal of Molecular Sciences, 22(23). https://doi.org/10.3390/ijms222312942

239. **Yin, X. M., Huang, L. F., Zhang, X., Wang, M. L., Xu, G. Y., & Xia, X. J.** (2015). OsCML4 improves drought tolerance through scavenging of reactive oxygen species in rice. Journal of Plant Biology, 58(1), 68–73. https://doi.org/10.1007/s12374-014-0349-x

240. **Yoshimoto, K., Hanaoka, H., Sato, S., Kato, T., Tabata, S., Noda, T., & Ohsumi, Y.** (2004). Processing of ATG8s, Ubiquitin-Like Proteins, and Their Deconjugation by ATG4s Are Essential for Plant Autophagy. The Plant Cell, 16(11), 2967–2983. https://doi.org/10.1105/tpc.104.025395

241. **Yoshimoto, K., Shibata, M., Kondo, M., Oikawa, K., Sato, M., Toyooka, K., Shirasu, K., Nishimura, M., & Ohsumi, Y.** (2014). Organ-specific quality control of plant peroxisomes is mediated by autophagy. Journal of Cell Science, 127(6), 1161–1168. https://doi.org/10.1242/jcs.139709

242. **You, J., & Chan, Z.** (2015). ROS Regulation During Abiotic Stress Responses in Crop Plants. Frontiers in Plant Science, 6, 1092. https://doi.org/10.3389/fpls.2015.01092

243. **Young, P. G., & Bartel, B.** (2016). Pexophagy and peroxisomal protein turnover in plants. Biochimica et Biophysica Acta, 1863(5), 999–1005. https://doi.org/10.1016/j.bbamcr.2015.09.005

244. **Yu, J., Holland, J. B., McMullen, M. D., & Buckler, E. S.** (2008). Genetic Design and Statistical Power of Nested Association Mapping in Maize. Genetics, 178(1), 539–551. https://doi.org/10.1534/genetics.107.074245

245. **Yue, J., Wang, Y., Jiao, J., & Wang, H.** (2021). Silencing of ATG2 and ATG7 promotes programmed cell death in wheat via inhibition of autophagy under salt stress. Ecotoxicology and Environmental Safety, 225, 112761. https://doi.org/10.1016/j.ecoenv.2021.112761

246. **Yue, W., Nie, X., Cui, L., Zhi, Y., Zhang, T., Du, X., & Song, W.** (2018). Genome-wide sequence and expressional analysis of autophagy Gene family in bread wheat (Triticum aestivum L.). Journal of Plant Physiology, 229, 7–21. https://doi.org/10.1016/j.jplph.2018.06.012

247. **Zampieri, M., Ceglar, A., Dentener, F., & Toreti, A.** (2017). Wheat yield loss attributable to heat waves, drought and water excess at the global, national and subnational scales. Environmental Research Letters, 12(6). https://doi.org/10.1088/1748-9326/aa723b

248. **Zandalinas, S. I., Fritschi, F. B., & Mittler, R.** (2021). Global Warming, Climate Change, and Environmental Pollution: Recipe for a Multifactorial Stress Combination Disaster. Trends in Plant Science. https://doi.org/10.1016/j.tplants.2021.02.011

249. **Zeng, Y., Li, B., Huang, S., Li, H., Cao, W., Chen, Y., Liu, G., Li, Z., Yang, C., Feng, L., Gao, J., Lo, S. W., Zhao, J., Shen, J., Guo, Y., Gao, C., Dagdas, Y., & Jiang, L.** (2023). The plant unique ESCRT component FREE1 regulates autophagosome closure. Nature Communications, 14(1), 1768. https://doi.org/10.1038/s41467-023-37185-6

250. **Zhai, Y., Guo, M., Wang, H., Lu, J., Liu, J., Zhang, C., Gong, Z., & Lu, M.** (2016). Autophagy, a conserved mechanism for protein degradation, responds to heat, and other abiotic stresses in Capsicum annuum L. Frontiers in Plant Science, 7(FEB2016). https://doi.org/10.3389/fpls.2016.00131

251. **Zhang, G., Zhang, M., Zhao, Z., Ren, Y., Li, Q., & Wang, W.** (2017). Wheat TaPUB1 modulates plant drought stress resistance by improving antioxidant capability. Scientific Reports, 7(1), 7549. https://doi.org/10.1038/s41598-017-08181-w

252. **Zhang, H., & Ling, Q.** (2023). NBR1-mediated selective chloroplast autophagy is important to plant stress tolerance. Autophagy, 1–2. https://doi.org/10.1080/15548627.2023.2251324

253. **Zhang, X., & Hu, J.** (2009). Two small protein families, DYNAMIN-RELATED PROTEIN3 and FISSION1, are required for peroxisome fission in Arabidopsis. The Plant Journal, 57(1), 146–159. https://doi.org/10.1111/j.1365-313X.2008.03677.x

254. **Zhang, X., & Hu, J.** (2010). The Arabidopsis Chloroplast Division Protein DYNAMIN-RELATED PROTEIN5B Also Mediates Peroxisome Division. The Plant Cell, 22(2), 431–442. https://doi.org/10.1105/tpc.109.071324

255. **Zhang, X.-C., & Hu, J.-P.** (2008). FISSION1A and FISSION1B Proteins Mediate the Fission of Peroxisomes and Mitochondria in Arabidopsis. Molecular Plant, 1(6), 1036–1047. https://doi.org/10.1093/mp/ssn056

256. **Zhang, Y., Min, H., Shi, C., Xia, G., & Lai, Z.** (2021). Transcriptome analysis of the role of autophagy in plant response to heat stress. PLOS ONE, 16(2), e0247783. https://doi.org/10.1371/journal.pone.0247783

257. **Zhao, C., Liu, B., Piao, S., Wang, X., Lobell, D. B., Huang, Y., Huang, M., Yao, Y., Bassu, S., Ciais, P., Durand, J.-L., Elliott, J., Ewert, F., Janssens, I. A., Li, T., Lin, E., Liu, Q., Martre, P., Müller, C., … Asseng, S.** (2017). Temperature increase reduces global yields of major crops in four independent estimates. Proceedings of the National Academy of Sciences of the United States of America, 114(35), 9326–9331. https://doi.org/10.1073/pnas.1701762114

258. **Zhao, J., Lu, Z., Wang, L., & Jin, B.** (2020). Plant Responses to Heat Stress: Physiology, Transcription, Noncoding RNAs, and Epigenetics. International Journal of Molecular Sciences, 22(1), 117. https://doi.org/10.3390/ijms22010117

259. **Zheng, H., Yang, Z., Wang, W., Guo, S., Li, Z., Liu, K., & Sui, N.** (2020). Transcriptome analysis of maize inbred lines differing in drought tolerance provides novel insights into the molecular mechanisms of drought responses in roots. Plant Physiology and Biochemistry, 149, 11–26. https://doi.org/10.1016/j.plaphy.2020.01.027

260. **Zhou, C., Dong, Z., Zhang, T., Wu, J., Yu, S., Zeng, Q., Han, D., & Tong, W.** (2020). Genome-Scale Analysis of Homologous Genes among Subgenomes of Bread Wheat (Triticum aestivum L.). International Journal of Molecular Sciences, 21(8), 3015. https://doi.org/10.3390/ijms21083015

261. **Zhou, J., Ma, J., Yang, C., Zhu, X., Li, J., Zheng, X., Li, X., Chen, S., Feng, L., Wang, P., Ho, M. I., Ma, W., Liao, J., Li, F., Wang, C., Zhuang, X., Jiang, L., Kang, B.-H., & Gao, C.** (2023). A non-canonical role of ATG8 in Golgi recovery from heat stress in plants. Nature Plants, 9(5), 749–765. https://doi.org/10.1038/s41477-023-01398-w

262. **Zhou, J., Wang, J., Cheng, Y., Chi, Y. J., Fan, B., Yu, J. Q., & Chen, Z.** (2013). NBR1-Mediated Selective Autophagy Targets Insoluble Ubiquitinated Protein Aggregates in Plant Stress Responses. PLoS Genetics, 9(1). https://doi.org/10.1371/journal.pgen.1003196

263. **Zhou, J., Wang, J., Yu, J. Q., & Chen, Z.** (2014). Role and regulation of autophagy in heat stress responses of tomato plants. Frontiers in Plant Science, 5(APR). https://doi.org/10.3389/fpls.2014.00174

264. **Zhou, J., Zhang, Y., Qi, J., Chi, Y., Fan, B., Yu, J. Q., & Chen, Z.** (2014). E3 Ubiquitin Ligase CHIP and NBR1-Mediated Selective Autophagy Protect Additively against Proteotoxicity in Plant Stress Responses. PLoS Genetics, 10(1). https://doi.org/10.1371/journal.pgen.1004116

265. **Zhu, T., Zou, L., Li, Y., Yao, X., Xu, F., Deng, X., Zhang, D., & Lin, H.** (2018). Mitochondrial alternative oxidase-dependent autophagy involved in ethylene-mediated drought tolerance in Solanum lycopersicum. Plant Biotechnology Journal, 16(12), 2063–2076. https://doi.org/10.1111/pbi.12939

266. **Zientara-Rytter, K., Łukomska, J., Moniuszko, G., Gwozdecki, R., Surowiecki, P., Lewandowska, M., Liszewska, F., Wawrzyńska, A., & Sirko, A.** (2011). Identification and functional analysis of Joka2, a tobacco member of the family of selective autophagy cargo receptors. Autophagy, 7(10), 1145–1158. https://doi.org/10.4161/auto.7.10.16617